The Thesis Committee for Tarek Rafic Hariz
Certifies that this is the approved version of the following thesis:

Nanoparticle-Stabilized CO_2 Foams for Potential Mobility Control Applications

APPROVED BY

SUPERVISING COMMITTEE:

Supervisor:

Steven L. Bryant

Chun Huh

Nanoparticle-Stabilized CO$_2$ Foams for Potential Mobility Control Applications

by

Tarek Rafic Hariz, B.S.C.E

Thesis

Presented to the Faculty of the Graduate School of

The University of Texas at Austin

in Partial Fulfillment

of the Requirements

for the Degree of

Master of Science in Engineering

The University of Texas at Austin

December 2012

Dedication

To my parents, Rafic and Suzy, and my brother, Atif.

Acknowledgements

I would like to thank my advisor, Dr. Steven Bryant, for his guidance and support throughout this research. I would also like to thank Dr. Chun Huh for his insight and advice during our regular technical meetings, and for providing me with numerous papers to improve my knowledge. I am also thankful to Dr. Keith Johnston, Andrew Worthen, and Ki Youl Yoon for our helpful discussions and for supplying me with nanoparticles. Special thanks to Professor Hee-Chan Cho, of the Seoul National University, for his expertise on fly ash and for providing us with fly ash samples.

I would also like to thank Glen Baum for being an incredibly resourceful lab supervisor and for helping me with my experimental set-up. Dr. Paul Bommer for allowing me to use his cement lab to prepare and fracture cores. Gary Miscoe for helping me calibrate my equipment and providing me with cores. Sophia Ortiz for being so helpful in ordering materials and equipment. Scott Gabel for his hard work and for helping me run experiments during his summer internship.

In addition, I would like to thank my lab mates: Doo Hyun Chung, David Espinosa, Matt Roberts, and Nicolas Huerta for their input and company. Thanks to Mazen Abdulbaki, Natalia Salies, and Sean Murray for their friendship throughout my undergraduate and graduate studies.

Abstract

Nanoparticle-Stabilized CO_2 Foams for Potential Mobility Control Applications

Tarek Rafic Hariz, M.S.E.

The University of Texas at Austin, 2012

Supervisor: Steven L. Bryant

Carbon dioxide (CO_2) flooding is the second most common tertiary recovery technique implemented in the United States. Yet, there is huge potential to advance the process by improving the volumetric sweep efficiency of injected CO_2. Delivering CO_2 into the reservoir as a foam is one way to do this. Surfactants have traditionally been used to generate CO_2 foams for mobility control; however, the use of nanoparticles as a foam stabilizing agent provides several advantages. Surfactant-stabilized foams require constant regeneration to be effective, and the surfactant is adsorbed onto reservoir rocks and is prone to chemical degradation at harsh reservoir conditions. Nanoparticle-stabilized foams have been found to be tolerant of high temperature and high salinity environments. Their nano size also allows them to be transported through reservoir rocks without blocking pore throats.

Stable CO_2-in-water foams were generated using 5 nm silica nanoparticles with a short chain polyethylene glycol surface coating. These foams were generated by the co-injection of CO_2 and a nanoparticle dispersion through both rock matrix and fractures. A

threshold shear rate was found to exist for foam generation in both fractured and non-fractured Boise sandstone cores. The ability of nanoparticles to generate foams only above a threshold shear rate is advantageous; in field applications, high shear rates are associated with high permeability zones, where the presence of foam is desired. Reducing CO_2 mobility in these high permeability zones diverts CO_2 into lower permeability regions containing not yet swept oil. Nanoparticles were also found to be able to stabilize CO_2 foams by co-injection through rough-walled fractures in cement cores, demonstrating their ability to stabilize foams without matrix flow.

Experiments were conducted on the ability of fly ash, a waste product from burning coal in power plants, to stabilize oil-in-water emulsions and CO_2 foams. The use of fly ash particles as a foam stabilizing agent would significantly reduce material costs for potential tertiary oil recovery and CO_2 sequestration applications. Nano-milled fly ash particles without surface treatment were able to generate stable oil-in-water emulsions when high frequency, high energy vibrations were applied to a mixture of fly ash dispersion and dodecane. Oil-in-water emulsions were also generated by co-injecting fly ash and dodecane, a low pressure analog to CO_2, through a beadpack. Emulsions generated by co-injection, however, were unstable and coalesced within an hour. A threshold shear rate was required for the emulsion generation. Fly ash particles were found to be able to stabilize CO_2 foam in a high pressure batch mixing cell, but not by co-injection through a beadpack. Dispersions of fly ash particles were found to be stable only at low salinities (<1 wt% NaCl).

Table of Contents

List of Tables

List of Figures

xiii

Chapter 1: Introduction

In the past decade, nanotechnology has been the subject of intensive research. As a result, it has had a large impact on numerous industries, from healthcare and pharmaceuticals to electronics and aerospace. Nanotechnology could potentially have a similar positive impact on the oil and gas industry, where it is already being used to a certain extent. The use of nanoparticles in petroleum industry dates back several decades- natural clay nanoparticles have been used in drilling fluids, mesoporous silica catalysts have been used in downstream processing. However, it is only recently that we have been able to better understand how nanoparticles work. Recent advances in nanotechnology also allow for the synthesis and coating of nanoparticles to obtain desired properties. These engineered nanoparticles are being studied for several potential applications in the upstream oil and gas industry. This thesis primarily investigates the potential use of such engineered nanoparticles to generate stable carbon dioxide (CO_2) foams for enhanced oil recovery (EOR) and CO_2 sequestration. The thesis also investigates the use of natural fly ash particles to stabilize oil-in-water emulsions and CO_2 foams.

The first chapter of this thesis will discuss the practical applications and the motivation behind foam stabilization. The second chapter will cover the recent work done using nanoparticles for enhanced oil recovery applications, as well an overview of fly ash particles. The third chapter discusses the materials used, experimental procedures, and the apparatuses used for experiments. The fourth chapter includes the results and discussion of the experiments run. The final chapter presents the conclusions reached from the experiments, as well as recommendations for future work.

1.1   FOAM FOR ENHANCED OIL RECOVERY

Carbon dioxide flooding is the second most widely used EOR method in the United States today, second to steam flooding. CO_2 EOR provides approximately 280,000 barrels of oil per day, which accounts for over 5 percent of the total U.S oil production (Enick and Olsen 2011). Despite its domestic success in recovering additional oil, there is still much room for improvement. Some of the main problems associated with CO_2 flooding are poor volumetric sweep efficiency, viscous fingering, and early CO_2 breakthrough. These problems are due to the low viscosity of injected CO_2 compared to the displaced reservoir fluids, which yields an unfavorable (high) mobility ratio. The presence of fractures in reservoirs exacerbates these problems by providing a very high permeability path for the injected CO_2 to channel through, bypassing low permeability regions that may contain oil.

Mobility ratio is the ratio of the mobility of the injected fluid to that of the displaced fluid. The equation for mobility ratio is shown below, where λ is mobility, μ is viscosity, and k_r is relative permeability.

$$\lambda_{ratio} = \frac{\lambda_{CO_2}}{\lambda_{oil}} = \frac{k_{r_{CO_2}}/\mu_{CO_2}}{k_{r_{oil}}/\mu_{oil}} = \frac{k_{r_{CO_2}} * \mu_{oil}}{k_{r_{oil}} * \mu_{CO_2}}$$

Since the viscosity of CO_2 is considerably lower than that of the displaced oil and brine, CO_2 floods have an unfavorable mobility ratio that is greater than 1. Mobility control is the process of reducing the mobility ratio to improve the volumetric sweep efficiency and reduce CO_2 cycling (Enick and Olsen 2011). To reduce the mobility ratio, the effective viscosity of the injected CO_2 must be increased and/or the relative permeability of the CO_2 phase decreased. Figure 1.1 illustrates the effect of mobility ratio on the displacement front and sweep efficiency at different pore volumes injected. As the mobility ratio M decreases, there is a more uniform displacement, less viscous fingering, and a delayed CO_2 breakthrough.
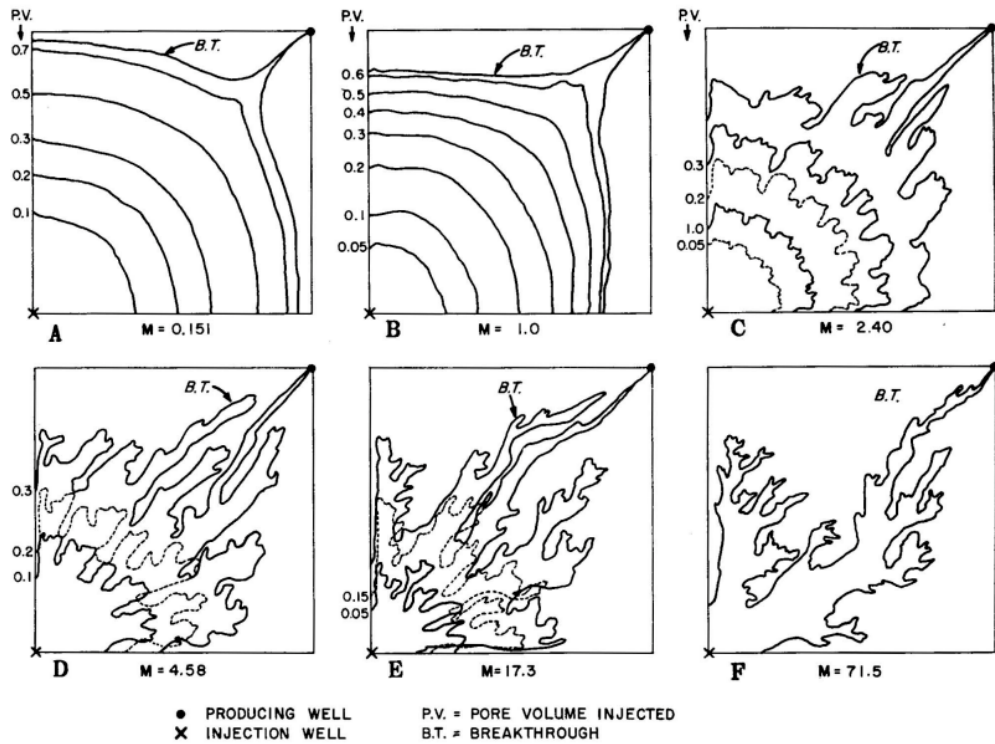
Figure 1.1 - Displacement fronts for different mobility ratios, and injected pore volumes until breakthrough. Quarter of an inverted 5-spot pattern shown. (Habermann 1960)

Water alternating gas (WAG) injection is the most common form of mobility control that is used in CO_2 flooding. WAG injection reduces the mobility ratio by reducing CO_2 saturation, which in turn reduces its relative permeability (Bennion and Bachu 2005). The use of CO_2 foams for mobility control has been shown to be a more effective mobility control method than WAG (Li et al. 2010). For the purpose of this thesis, the term "foam" is used to describe both liquid and supercritical CO_2-in-water emulsions. CO_2 foams reduce the mobility ratio by increasing the effective viscosity of the CO_2 phase and reducing the CO_2 relative permeability. The foams in this study consist of dispersed CO_2 bubbles that are separated by thin liquid films, called lamellae. The presence of lamellae leads to increased drag forces on the CO_2 as it flows through porous media, resulting in an increased *apparent* viscosity (i.e. increased resistance to flow). The actual viscosity of the CO_2 gas remains unchanged (Hirasaki and Lawson

3

1985). The presence of foam also results in increased gas trapping, which reduces CO_2 relative permeability by blocking off some of the pore networks to the flowing CO_2 phase. While CO_2 relative permeability is decreased, the water relative permeability function is not affected by the presence of foam, as illustrated in Figure 1.2. Foam only decreases the permeability to water by establishing a higher trapped gas saturation. (Friedmann et al. 1988, Renkema and Rossen 2007).
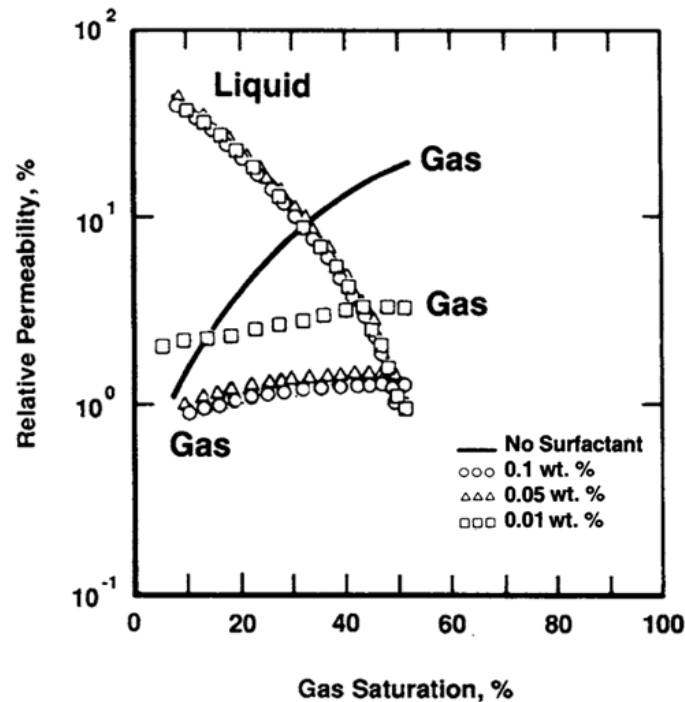
Figure 1.2 - Effect of surfactant concentration on gas/brine relative permeabilities in a sandstone core (Friedmann et al. 1991).

Traditionally, surfactants have been used to generate CO_2 foams for mobility control. However, surfactant-stabilized foams lack long term stability, and their success is dependent on the constant generation of lamella in the porous media (Rossen 1996). In addition, injected surfactants are lost due to adsorption onto reservoir rocks and to chemical degradation, particularly under harsh reservoir conditions. The use of nanoparticles as a foaming agent could help overcome the limitations associated with surfactants. Furthermore, the generation of nanoparticle-stabilized foams have been

4

shown to require a threshold shear rate by co-injection experiments through beadpacks (Espinosa et al. 2010). This property of nanoparticles can be very beneficial in heterogeneous reservoirs containing high permeability regions and fractures. Fluids flowing through such high permeability regions experience a high shear rate, which would trigger the formation of CO_2 foam and reducing the mobility of the CO_2. This would help divert CO_2 to less permeable regions that may still contain oil.

1.2   FOAM FOR CO_2 SEQUESTRATION

This study is primarily focused on the use of CO_2 foam for mobility control in EOR. However, the use of CO_2 foams can also be beneficial to CO_2 sequestration. Geologic sequestration of CO_2 is one of the options available to reduce the amount of greenhouse gases in the atmosphere. Deep saline aquifers are attractive geologic storage sites since they offer the largest potential storage capacities (IPCC 2007), as well as the required depth to have desirable CO_2 properties, such as a high density (Benson and Cole 2008). Under deep aquifer conditions, we can expect the mobility ratio of injected CO_2 to the formation brine to range from around 5 to 20 (Okwen et al. 2010), carrying the potential of CO_2 channeling through the native brine. Just as mobility control helps to improves sweep efficiency for EOR, it can improve storage efficiency in CO_2 sequestration. CO_2 Volumetric storage efficiency is generally estimated to be the fraction of the total pore volume available for sequestration. With a more favorable mobility ratio, a larger pore volume becomes accessible to the injected CO_2, allowing for more CO_2 storage per acre of pore space rights acquired.

1.3   RESEARCH OBJECTIVES

The primary motivation behind this research is reducing the mobility of the injected CO_2 to improve volumetric sweep efficiency and oil recovery in reservoirs. Surface treated nanoparticles have been shown to stabilize CO_2 foams by co-injection through a beadpack. The objectives of this thesis are to investigate the ability of such nanoparticles to stabilize foam by co-injection through rock matrix and through fractures.

The presence of a critical shear rate, below which a foam is not generated, is also investigated for co-injection through cores.

The thesis also investigates the possibility of using nanoparticles that have an in-house surface coating, as well as fly ash particles without surface treatment. Fly ash is a waste product produced by burning coal at power plants, and its use for EOR/sequestration would significantly improve process economics. A preliminary study using dodecane, a low pressure analog to CO_2, was carried out to test fly ash emulsion stability. The presence of a critical shear rate to generate oil-in-water emulsions using fly ash by co-injection through a beadpack was also investigated. Finally, the CO_2 foam stabilizing ability of fly ash is investigated by mixing in a pressure cell and by co-injection.

Chapter 2: Background

2.1 PARTICLE-STABILIZED EMULSIONS/FOAMS

In 1907, S.U. Pickering described a phenomenon whereby fine solid particles were able to stabilize emulsions in the absence of surfactants (Pickering 1907). These particle-stabilized emulsions, since known as Pickering emulsions, have been of great interest to researchers due to their remarkable stability. Solid particles stabilize emulsions by adsorbing onto the interface between two phases, forming a rigid protective barrier that prevents droplet coalescence (Binks 2002). Particle-stabilized oil-in-water (o/w) and water-in-oil (w/o) emulsions have been found to be stable over long periods of time (>2 years) and are able to remain stable at high temperatures and salinities (Zhang et al. 2009, 2010). Particles have also been found to be capable of generating stable CO_2-in-water (c/w) foams at 8 wt% NaCl brine and 50 °C (Worthen et al. 2013). For this reason, the use of particles to stabilize c/w foams is being investigated as an alternative to surfactants for high-salinity and high-temperature reservoirs.

Emulsion stability is affected by the particle size, shape, concentration, wettability, and particle-particle interactions (Tambe and Sharma 1994; Binks 2002). The adsorption energy, E, is the energy required to remove the particle from the interface, and is given by the following equation:

$$E = \pi r^2 \gamma_{\alpha\beta} (1 \pm \cos\theta)^2$$

r is the radius of the particle, $\gamma_{\alpha\beta}$ is the interfacial tension, and θ is the contact angle of the particle at the interface as measured through the aqueous phase. For a 100 nm particle stabilizing a CO_2-in-water foam ($\gamma_{CO2\text{-}Water} \approx 30$ mN/m (Bachu and Bennion 2009)), we see an adsorption energy of ~50,000 kT at θ=90° and 60 °C. This high adsorption energy of the particles to the CO_2-water interface makes the adsorption effectively irreversible. Most surfactant molecules have adsorption energies of several kT due to their relatively small size, making them less effective at stabilizing emulsions than particles (Binks 2002).

For surfactants, the HLB (hydrophilic-lipophilic balance) and HCB (hydrophilic-CO_2-philic balance) determine the internal phase and external phase of the emulsion and foam generated, respectively. For nanoparticles, the critical parameter is the contact angle that the particle makes with the interface, which is determined by the particle's wettability. The wettability is in turn determined by HLB and HCB. In the case of hydrophilic particles, the contact angle (θ) is less than 90° and results in an o/w emulsion or c/w foam. Hydrophobic particles result in a θ>90°, and typically a w/o or w/c emulsion (Dickson et al. 2004). Figure 2.1 illustrates the effect of the particle's contact angle with the interface on the type of emulsion or foam formed.
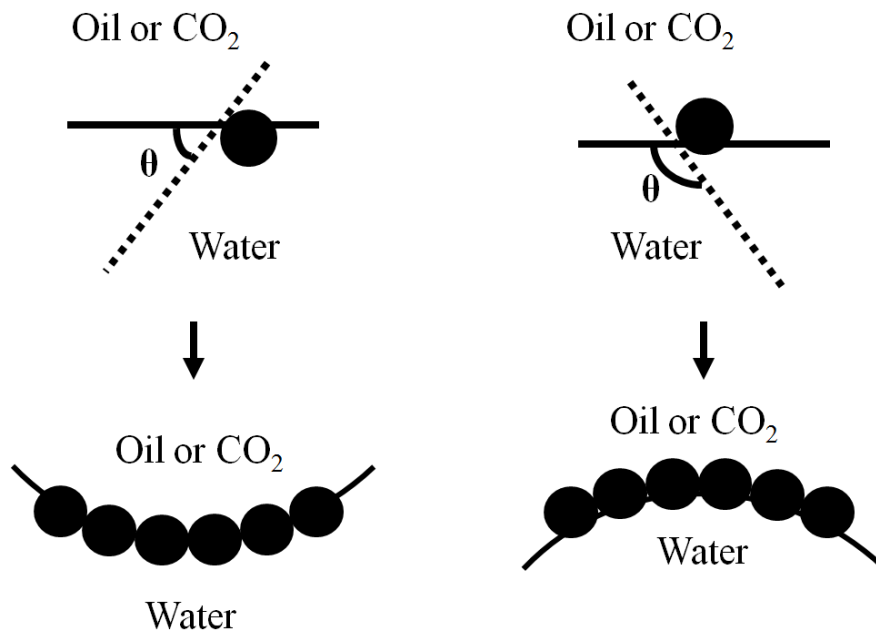
Figure 2.1 - Effect of the contact angle (θ) on the type of emulsion or foam formed. (Adapted from Binks 2002)

The particles used for this thesis include surface treated silica nanoparticles, bare silica nanoparticles, as well as uncoated fly ash particles. These particles are hydrophilic, which result in the formation of emulsions/foams with an aqueous external phase. The next two sections provide some background information on these particles and their abilities to stabilize c/w foams and o/w emulsions.

8

2.2   SILICA NANOPARTICLE-STABILIZED EMULSIONS/FOAMS

Bare colloidal silica nanoparticles and polyethylene glycol (PEG) coated silica nanoparticles were examined in this study. For these nanoparticles to be able to stabilize emulsions[1], mechanical energy must be introduced to the mixture for the formation of droplets and for the adsorption of particles onto the interface of the two phases present. The presence of solid nanoparticles at the interface prevents droplet coalescence, resulting in a stable emulsion. The surface treatment of nanoparticles alters their wettability, which affects their ability to stabilize emulsions and determines whether the emulsions generated will have an internal or external aqueous phase. Both the bare colloidal silica nanoparticles and PEG-coated nanoparticles are hydrophilic and favor the formation of emulsions with an external aqueous phase. The PEG-coated nanoparticles consist of a silica core with covalently bonded PEG polymer chains. PEG-coated nanoparticles were the only particles found to stabilize of c/w foams by Espinosa (2011). Surface treatment of particles also affects the ability of the particles to be dispersed. Bare colloidal silica nanoparticles are electrostatically stabilized, and flocculate in the presence of salt. The PEG coating provides a steric repulsive force, which improves their stability in the presence of salt.

Recent work by Espinosa (2011) showed that polyethylene glycol coated silica nanoparticles were able to generate c/w foams with viscosities up to 18 times that of the fluid mixture without nanoparticles. These foams were generated by co-injecting CO_2 and a nanoparticle dispersion through a beadpack filled with glass beads. Espinosa investigated the effect of shear rate, temperature, phase ratio, particle concentration, and salinity on the performance of PEG-coated nanoparticles. Espinosa used PEG-coated 5 nm silica nanoparticles provided by 3M (St. Paul, MN); this study includes work done using the same nanoparticles as Espinosa's work.

One of Espinosa's key findings was the presence of a 'critical' shear rate, below which a foam will not be generated by the co-injection of CO_2 and nanoparticle

---

[1] The term 'emulsion' in this context refers to both CO_2-in-water foams and oil-in-water emulsions.

dispersion through a beadpack. For liquid CO_2 experiments run at ambient temperature and 1,350 psi, the critical shear rate was found to be less than 720 s^{-1} (exact value was not found). For supercritical CO_2 experiments, which were run at higher temperatures, the critical shear rate was found to be higher (~2,750 s^{-1} at 75 °C, ~4,000 s^{-1} at 90 °C). At these high temperatures, CO_2 density is significantly lower than at ambient temperature as shown in Table 2.1. This leads to a larger difference in density between the dispersed CO_2 phase and the external water phase. The higher density difference results in increased buoyant forces on the CO_2 droplets, which promotes foam destabilization (Dickson et al. 2004). This destabilizing effect may explain the higher shear rate required to stabilize c/w foams at higher temperatures. The critical shear rate was also found to be independent of the injected phase ratio. For the purpose of this thesis, phase ratio is defined as the volumetric flow rate of the CO_2 divided by that of the aqueous phase at the pressure and temperature of the experiment. Unless otherwise noted, experimental work done in this thesis using the 3M particles was carried out with a phase ratio of 1 at high pressures (~2,000 psia) and ambient temperature, where CO_2 density is approximately 0.87 g/cm^3.

Table 2.1 - Foam generation results from Espinosa (2011). Foam generation by co-injection of CO_2 and 3M 5 nm PEG-coated nanoparticles through a beadpack. Fluid densities are from NIST database.

	25 °C	75 °C	90 °C
CO$_2$ phase	Liquid	Supercritical	Supercritical
Critical shear rate, s^{-1}	< 720	~ 2,750	~ 4,000
Pressure (psia)	1,350	1,350	1,350
ρ_{CO_2}**, g/cm^3**	0.806	0.208	0.184
ρ_{Water}**, (at 1,350 psi), g/cm^3**	1.001	0.982	0.965

Espinosa also investigated the effect of nanoparticle concentration on the viscosity of foams generated. The threshold concentration for foam generation was found

to be between 0.025 wt% and 0.05 wt%. The optimal concentration, based on the foam viscosity, was found to be approximately 0.5 wt%. These tests were done using the 3M PEG-coated nanoparticles at 1,350 psia, 1430 s^{-1}, and ambient temperature. As a result, most of the experiments done in this work using the 3M particles were run at a slightly higher concentration of 1 wt%.

Roberts (2011) showed that o/w emulsions can be generated by co-injecting decane and a nanoparticle dispersion through a fracture. Decane was used as a low pressure analog fluid to CO_2 in these experiments. The nanoparticles used included the 3M 5 nm PEG-coated silica nanoparticles and Nyacol DP9711 20 nm silica nanoparticles. The Nyacol DP9711 nanoparticles are believed to be surface-modified with OH-functionality. Roberts concluded that there exists a critical shear rate required to stabilize emulsions by co-injection through a fracture. Extending the Roberts' work to CO_2 systems, this thesis investigates the ability of PEG-coated silica nanoparticles to stabilize c/w foams by co-injection through fractures.

Recent work (Mo et al. 2012) has shown that silica nanoparticles can stabilize foams by co-injection through Berea sandstone cores. The paper does not specify whether the nanoparticles are surface treated. Their results indicate that the maximum foam resistance occurs between 40% and 60% foam quality, which is the CO_2/nanoparticle dispersion phase ratio. Foams generated were stable and remained unchanged after 48 hours. Based on their results, a shear rate of approximately 200 s^{-1} was required to generate stable lamellae with a foam quality of 20% (gas fraction), and 5,000 ppm concentration of nanoparticles. These coreflood experiments were run at ambient temperature, and 1200 psig, where CO_2 density is 0.83 g/mL.

2.3   FLY ASH PARTICLES

In an effort to find a emulsifying agent that does not need to be synthesized or surface-treated, fly ash particles were investigated in this study. Fly ash is one of the waste products generated by burning coal in power plants; almost 60% of fly ash produced in the United States ends up in landfills (ACAA 2009a). Therefore, its use would be a more economic option than engineered particles, especially for CO_2 sequestration where a waste product (fly ash) could be used to sequester another (CO_2).
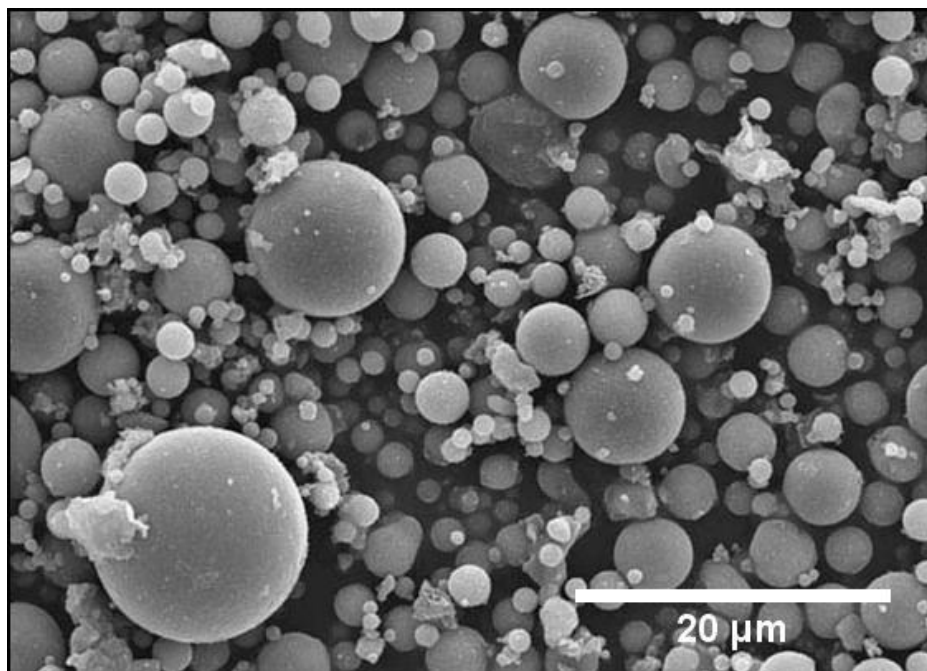
Figure 2.2 - SEM view of Class F fly ash at 2,000× magnification. (Center for Applied Energy Research, University of Kentucky).

Fly ash composition is largely dependent on the mineralogy of the coal used, but the primary components are SiO_2, Al_2O_3, CaO, and Fe_2O_3 (Cho et al. 2001). It is formed from the inorganic matter, such as quartz and clay, present in the coal used to generate electricity in power plants. These inorganic minerals melt in the furnace, and are then rapidly cooled as they exit the furnace into the post-combustion zone. This rapid cooling of the molten minerals results in the formation of spherical, amorphous particles that

range from less than a micron to several hundred microns in size. The expansion of volatile matter that may be trapped inside these molten particles affects their shape and size (Kutchko and Kim 2006). Figure 2.2 shows an SEM view of fly ash particles at 2,000× magnification.

Golomb et al. (2004) showed that c/w and w/c emulsions can be formed using several different fine particles in a high-pressure batch reactor. Unprocessed fly ash was found to be able to stabilize a c/w foam with droplet sizes ranging from 80 μm to 150 μm. The composition of fly ash particles makes them hydrophilic in nature; therefore, they are preferentially wetted by the aqueous phase and promote the formation of c/w emulsions. The fly ash particles used in this study were nano-milled to reduce particle size.

Chapter 3: Experimental Methods and Materials

This chapter describes the materials used, experimental setup, and procedures used in obtaining the data presented in this thesis. There are three main groups of experiments done in this thesis: coreflood experiments, beadpack experiments, and batch emulsion experiments. The apparatus used for beadpack experiments was used in building the coreflood apparatus.

3.1   COREFLOOD EXPERIMENTS

This section of Chapter 3 covers the materials, equipment, and procedures used in running coreflood experiments. These experiments were run to investigate the foaming ability of PEG-coated silica nanoparticles by co-injection through fractured and non-fractured cores.

3.1.1   Materials Used

PEG-coated 5 nm Silica nanoparticles (3M)

The nanoparticles used in coreflood experiments were PEG-coated silica nanoparticles which were received from 3M Co., St. Paul, MN. These hydrophilic nanoparticles consist of a 5 nm silica core with PEG chains grafted to the surface, and were received as a dispersion of 19.3 wt% concentration.

Carbon Dioxide

The CO_2 used in these experiments is >99.99% pure and was purchased from Matheson Tri-Gas Inc. (Basking Ridge, NJ). The CO_2 was loaded into an accumulator using a compressor for further pressurization before use.

De-ionized Water

The de-ionized (DI) water used in these experiments was filtered using a Barnstead Nanopure II filtration system.

Boise Sandstone Cores

Boise sandstone cores were used to test the ability of nanoparticles to stabilize CO_2 foams by co-injection through rock matrix. Boise sandstone was selected as the rock type due to its high permeability, low clay content, and availability. Cores used typically had absolute permeabilities of approximately 1.6D. Low clay content provides the advantage of using DI water in corefloods. Each core is initially saturated with DI water, and used to run a baseline experiment where CO_2 and DI water are co-injected. After the baseline experiment, the core is vacuumed and re-saturated with DI water in preparation for CO_2 and nanoparticle co-injection. If brine were used in the baseline experiment, the core cannot be vacuumed to re-saturate, since the salt present will be deposited during the process. Some Boise sandstone cores were also fractured using the procedure described in the appendix.

Cement cores

Cement cores were used in coreflood experiments to test the performance of nanoparticles in stabilizing a foam by co-injection through a fracture. The negligible permeability of the cement matrix ensures that injected fluids travel only through the fracture. Cement cores were prepared using Class H Portland cement in Dr. Paul Bommer's cement lab (University of Texas at Austin, Dept. of Petroleum and Geosystems Eng.). The procedure for making and fracturing used cement cores is described in the appendix.

FEP Shrink Wrap Tubing

1" diameter shrink wrap tubing was used in fracturing cores as well as to protect the core holder rubber sleeve from CO_2 damage. The shrink wrap tubing was obtained from Geophysical Supply Company (Houston, TX).

3.1.2 Coreflood System

Figure 3.1 is a schematic of the setup used, and Section 3.1.3 provides the experimental procedure used to operate and maintain the setup. The coreflood system consists primarily of two pumps used to co-inject CO_2 and a nanoparticle dispersion through a core holder. An ISCO pump, labeled (B) in Figure 3.1, injects nanoparticles into the core holder (A) after passing through a water bath. An HPLC pump (C) brings water into the CO_2 accumulator (D), which displaces the compressed CO_2 into the core holder after passing through the water bath. The fluid mixture then flows through a 10 ft segment of capillary tubing (E), followed by a high pressure view cell (F), and finally into a waste accumulator (G). As the fluid mixture flows into the waste accumulator, it displaces the water through the back pressure relief valve (H). Pressure transducers, (I1) and (I2), measure the pressure drops across the core holder and the capillary tubing respectively. These data are sent to a computer (not shown), where it is recorded over time.

Figure 3.1 - Coreflood setup used to run experiments. The red dotted boxes represent the water bath (left) and oven (right). A) core holder, B) ISCO nanoparticle pump, C) HPLC CO_2 displacement pump, D) CO_2 accumulator, E) capillary tubing, F) view cell, G) waste accumulator, H) back pressure relief valve, I1) and I2) differential pressure transducers.

17
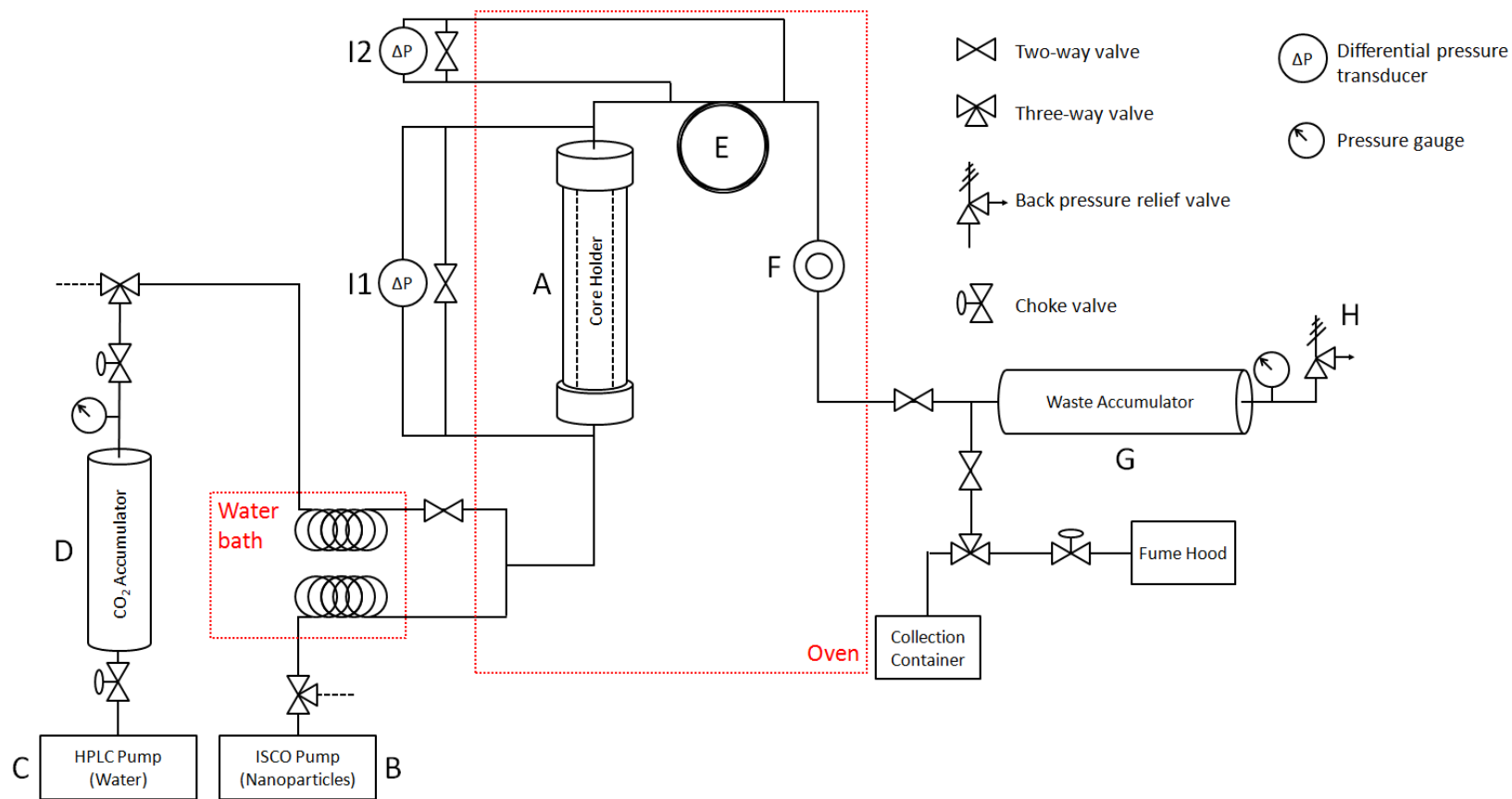
Core Holder

A Hassler type core holder (serial # UTPT-HAS-1x12-5k-27), manufactured by Phoenix Instruments Inc., was used. The core holder is designed for 1" diameter cores up to 12" in length. It has a working pressure of 5,000 psi at ambient temperature. The core holder was mounted vertically inside of an oven on a steel Unistrut frame. The core holder has 5 pressure taps, which were not used in the experiments, and were therefore sealed shut.

The core holder contains a rubber sleeve that provides a seal around the core in order to prevent leak-around flow, i.e. flow of injected fluids past the core instead of through the core. The seal is achieved by injecting hydraulic pump oil or mineral oil into the annular space between the rubber sleeve and the core holder outer wall. The oil is injected using a manual hand pump, and provides a confining pressure that can be read off the mounted pressure gauge. The hand pump used is an Enerpac P-392 hydraulic hand pump with a maximum working pressure of 10,000 psi.

The rubber sleeves initially used with the core holder set-up were made of Viton, a brand of synthetic rubber. Injected high pressure CO_2 can dissolve into the rubber and may rupture it upon depressurization and expansion. CO_2 exposure can also lead to the cracking and damaging of the rubber sleeve. For this reason, the Viton rubber sleeve and O-rings were replaced with Aflas 80 Durometer rubber material, which provides better resistance to CO_2.

Some modifications to the core holder platens were done in order to be able to use a core that has been coated with heat shrink tubing. A portion of the platens was machined down from 1.04" in diameter to approximately 1.00". This allows the machined down segment to be inserted into the heat shrink tubing so that the injected fluid, including CO_2, does not contact the rubber sleeve.

In order to use shorter cores of around 6" in length, spacers were used. These spacers consist of an aluminum cylinder 3" in length, 1" diameter, with a 1/8" diameter hole drilled through the center. Both ends of the spacers were also grooved in order to allow the fluid to flow more evenly across the face of the core.

Nanoparticle Injection Pump

A Teledyne ISCO 500D syringe pump was used to inject nanoparticle dispersions or de-ionized water into the core holder. The syringe pump has a maximum capacity of approximately 500 mL and can pump at pressures up to 3,750 psi. The pump can be operated to inject at constant pressure or at a constant flow rate. For the purpose of this experimental work, the pump was operated at constant flow rate.

CO_2 Displacement Pump

A Model 1500 HPLC dual piston pump, manufactured by Scientific Systems Inc., was used to pump DI water into an accumulator to displace the CO_2. The pump used has a maximum pressure rating of 6,000 psi and a maximum operating flow rate of 12 mL/min. The HPLC pump has a self-flushing mechanism to keep it operating smoothly. The flushing fluid used is a solution of 80% DI water and 20% isopropyl alcohol that must be replaced frequently. It is important to avoid getting any air in the inlet line of this pump.

CO_2 Accumulator

A large capacity floating-piston accumulator donated by Occidental Petroleum was used to store CO_2 at high pressure and to inject CO_2 into the system by displacing it with water. The accumulator consists of a pressure vessel with a piston that provides a seal, dividing the vessel into two compartments. CO_2 is loaded into the top compartment and pressurized using a Haskel air-driven compressor. Water can then be pumped into the bottom of the accumulator to further pressurize the CO_2 and to displace the CO_2 during experiments.

The accumulator uses several O-rings: one at each end, and three around the piston. Aflas rubber O-rings are used due to their CO_2 resistance. Since these O-rings will have to be replaced often, it is recommended to have spare O-rings in order to avoid down time.

Temperature Control - Oven and Water Bath

A 24 ft^3 Blue M oven was used as needed to maintain the setup at a desired temperature. The oven also provides some safety by housing a lot of the high pressure components and the core holder. A water bath is available to preheat the injected fluids before entering the oven. The inlet lines are coiled and immersed in the water bath to provide longer heat transfer time. No high temperature coreflood experiments were run in the coreflood apparatus in this study.

Capillary Tubing

A 10 ft long segment of capillary tubing with an internal diameter of 0.03" (1/16" OD) was used in order to measure the apparent viscosity of fluid mixtures. The capillary tubing is coiled in order to save space and consists of two separate 5 foot segments joined with a straight union of 0.05" internal diameter. The pressure drop is measured across the capillary tubing and is used to calculate apparent viscosity of the fluids flowing through it.

View Cell

An in-house high pressure vessel with sapphire windows was used to qualitatively observe the foam and foam bubble size during experiments. The view cell window is approximately 1.5 cm in diameter. The sapphire view cell windows are manufactured by Swiss Jewel Company and have a 1" diameter and a thickness of 3/8".

Waste Accumulator

A 400 mL floating-piston accumulator was used at the outlet of the system to collect the effluent of the experiments. The waste accumulator is loaded with DI water at the end that is connected to the back pressure regulator. Effluent from experiments flows into the other end, moving the piston and displacing the water. This protects the back pressure relief valve from solids that can clog the orifice.

Back Pressure Relief Valve

A spring loaded back pressure relief valve (model SS-4R3A), manufactured by Swagelok, is used to keep the system at a desired pressure during experiments. The back pressure relief valve maintains an almost constant pressure by preventing flow until the upstream pressure becomes greater than the set pressure. The operating pressure range can be changed by using different springs of different stiffness. For best performance, the back pressure relief valve should not be used in the presence of solids. A waste accumulator is used to prevent the flow of nanoparticles and displaced sand from cores into the back pressure relief valve. It is also recommended to use DI water in the waste accumulator to avoid scale deposition in the relief valve orifice. If the relief valve becomes stuck open, it will be necessary to remove it and flush it with water at high flow rates to clean it out.

Pressure Transducers and Data Acquisition

Rosemount differential pressure transducers (model 3051CD5A22A1A) are used to measure the pressure drops across the core holder and the capillary tubing. These pressure transducers have a maximum operating pressure of 3,600 psia and can read pressure drops up to 2,000 psia. The pressure transducers are connected to a power supply unit and a data acquisition card which sends the data to a computer. The pressure transducer data are then displayed and recorded on a computer using a LabVIEW program. For better accuracy, these pressure transducers have to be calibrated to operate in the intended range. Readings from the pressure transducers also have to be normalized in order to eliminate any offset in the data.

CO_2 Compressor

A Haskel ASF-B32 pneumatic driven pump is used to fill up and pressurize the CO_2 accumulator. The pump has an inlet that takes in lower pressure CO_2 directly from a liquid CO_2 cylinder and compresses it into the accumulator. The pump is powered

pneumatically by a line of compressed air. Note that the compressed air should be supplied using tubing of at least 1/4" diameter.

3.1.3 Coreflood Procedure

This section contains a detailed procedure for running coreflood experiments with both fractured and non-fractured cores. Detailed instructions on preparing cores are included in the appendix. After preparing a core, it is loaded into the core holder, where the permeability of the core is first measured. The baseline experiment is then run, whereby DI water and CO_2 are co-injected into the core. The core is then removed from the core holder, vacuumed and saturated with water in preparation for the foam experiment. The core is then loaded back into the core holder, where the permeability is measured again to ensure that there has been no change to the core. The foam experiment can then be run, where a nanoparticle dispersion and CO_2 are co-injected into the core. After each CO_2 experiment, the system will have to be vented and the waste accumulator reloaded. After several experiments, the CO_2 accumulator may have to be refilled.

3.1.3.1 Preparing Cores

One inch diameter cores were used in the coreflood experiments. For sandstone cores, a drill fitted with a core barrel is used to cut out one foot long cores from blocks. This procedure results in wet cores, which were dried by baking in an oven at ~110 °C for at least a day. After drying out, the core can then be cut to the desired length. A hacksaw was used to cut the core, which resulted in an artificially smoothed end. A coarse file was then used on the ends of the core to shave off the smoothed face, and restore its original rough texture. The cores will then have to be prepared using the procedure included in the appendix for non-fractured cores and fractured cores. Cement cores were also used in some experiments to test the foaming ability of PEG-coated silica nanoparticles by co-injection through fractures. The procedure for preparing cement cores is also included in the appendix.

3.1.3.2 Loading a Core into the Core Holder

After preparing and saturating a core using the steps described in the appendix, the core can then be loaded into the core holder. The heat shrink tubing coated core (and spacers) should be slipped into the top of the core holder gently. If there is too much resistance, it may be necessary to evacuate some of the confining fluid. This can be done by opening valve (2) shown in Figure 3.2. The core should never be loaded into the core holder with force, as that may cause the rubber sleeve to slip out of place and spill the confining fluid.

The bottom platen should be placed into the extended portion of the heat shrink tubing. The bottom end cap, which as a clover-leaf bayonet mechanism, should then be fastened in place. The hand-screw located at the bottom of the core holder should also be tightened to secure the bottom end cap. The top platen should then be placed into the top extended portion of the heat shrink tubing and pushed down. A retainer with a hand-screw is then used to secure the top end cap in place and provide axial confinement. The inlet and outlet flow lines can then be connected to the core holder using the 'quick-connect' fittings from Swagelok. 'Quick-connect' fittings are tubing fittings that do not require nuts and threads, and are used for frequently connected and disconnected lines.

In order to form a seal around the core, it is necessary to provide a confining pressure. A net confining pressure (confining fluid pressure – pore pressure) of at least 600 psi should be loaded on the core. This was done using a hydraulic hand pump connected to the core holder annulus. With only valves (1) and (2) open, the hydraulic pump should be operated until hydraulic oil exits from valve (2). This is done to ensure there is minimal air trapped in the annulus. Valve (2) can then be shut, and the hydraulic pump can be operated until the desired confining pressure is achieved. After which, valve (1) can be shut in order to trap the confining fluid. Valve (3) should only be open when running high temperature experiments. It is used to keep the confining pressure constant by allowing some oil to flow out a back pressure relief valve due to thermal expansion.
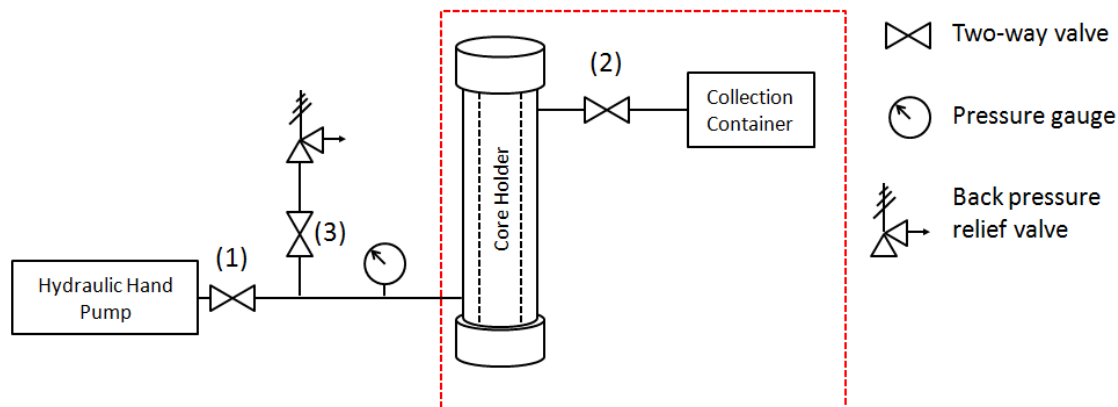
Figure 3.2 - Schematic of core holder confining fluid system. The red dashed box represents the oven.

3.1.3.3 Measuring Core Permeability

The next step after loading a core into the core holder, and applying confining pressure, is to measure the core absolute permeability. This is done by injecting de-ionized water through the core at several flow rates while measuring the pressure drop across the core holder. Detailed steps of the procedure and the corresponding diagram (Figure 3.3) are below.

The system should be started with all two-way valves closed, except for valves (8) and (9). Three-way valve (10) should be open in the direction of the collection container. This allows us to inject water through the system, and out to a collection container at atmospheric pressure. De-ionized water to be injected should be loaded into the ISCO pump. This is done by switching valve (4) to a container filled with DI water (not shown), running the pump on 'Refill' mode until the pump's column is full. The pump should then be run in order to pump out any air that may have entered the column. Three-way valve (4) can then be switched to direction of the flow system. All the lines in the system should also upstream of the core holder must be initially filled with de-ionized water. This prevents air from being pumped into the core, which would affect the permeability measurements. This can be achieved by opening the core bypass valve (6) and disconnecting the 'quick-connect' connections of the core holder. The pump can then

be operated for a few minutes until no air is seen exiting the effluent. After clearing the lines of any air, bypass valve (6) should be shut, and the core holder reconnected to the system.

To measure the core permeability, pressure drop data recording should be started using the LabVIEW software on the desktop computer. DI water can then be injected at a constant flow rate using the ISCO pump. After the pressure drop across the core has reached steady state, a new flow rate should be set. This step should be repeated until enough data are collected; it is recommended to get at least three data points. Before using the collected data to calculate core permeability, it may be necessary to normalize the pressure drop data to eliminate any offset. The steps for normalizing pressure data and calculating permeability are included in the Section 3.1.4. After core permeability measurement, the baseline experiment can be run using the procedure in the next section. The core does not have to be unloaded between the permeability measurement experiment and the baseline experiment.
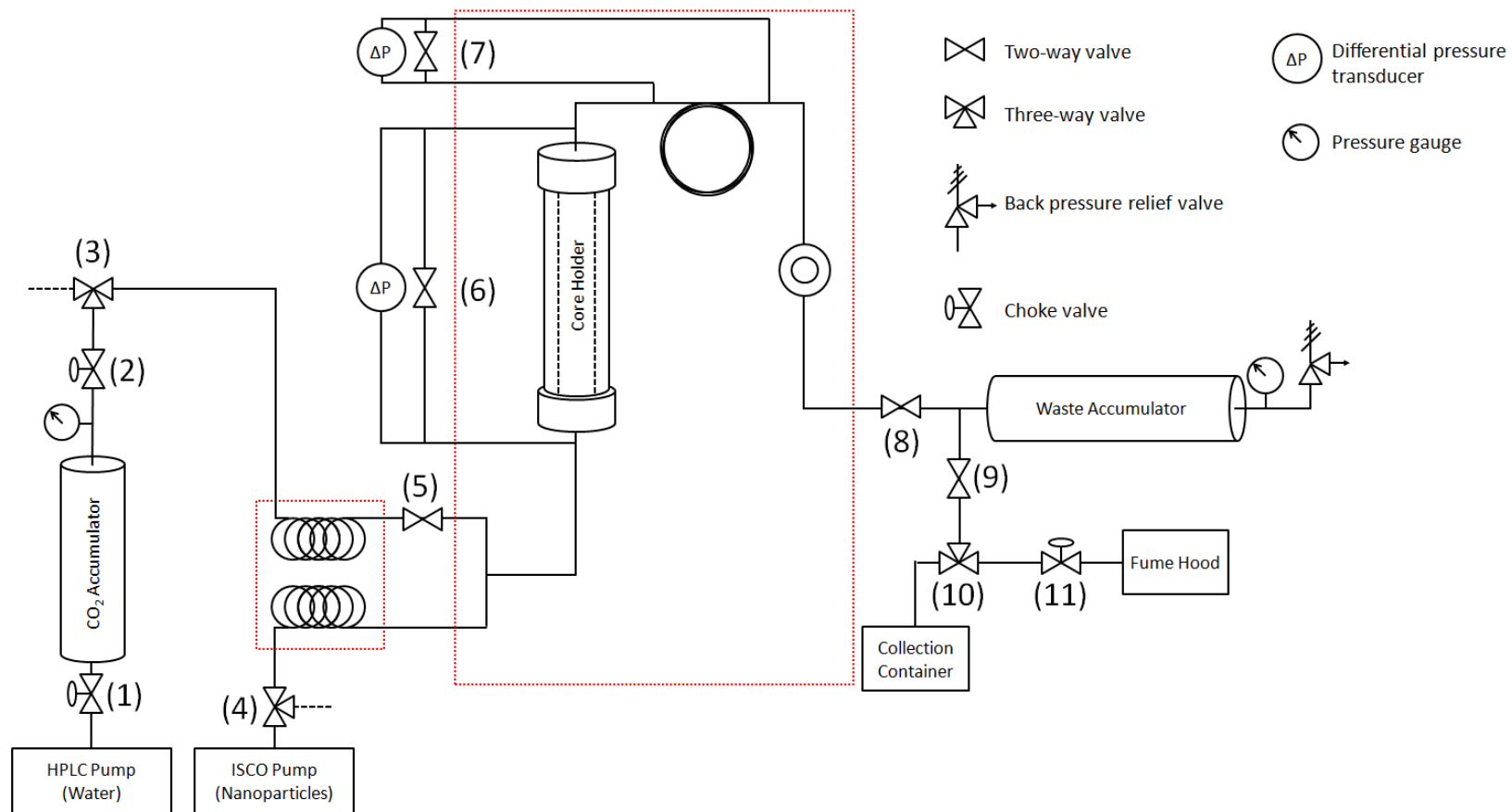
Figure 3.3 - Schematic of coreflood flow system. The red dashed boxes represent the water bath (L) and the oven (R).

3.1.3.4 Co-injecting through Non-fractured Cores

The procedure used for running the baseline experiment and the foam experiment are the same. The baseline experiment is run using DI water and CO_2, while the foam experiment is run using nanoparticle dispersion and CO_2. The data from the baseline experiment is used to evaluate the effects of nanoparticles on mobility reduction and the apparent viscosity of the fluid mixture. The baseline experiments are run using the same core, temperature, pressure, salinity, and phase ratio as its corresponding foam experiment. It is not recommended to change the phase ratio during an experiment since it may take several pore volumes of injected fluid to reach a steady state saturation in the core.

After running the baseline experiment and venting the system, the core should be removed from the core holder to be vacuumed and saturated with water before running the foam experiment. This is done in order for the core to have the same starting saturation during the baseline experiment and the foam experiment. If brine is used instead of DI water in these experiments, vacuuming the core will result in salt deposition that may alter the permeability of the core. If the baseline experiment was run using brine, the core should be flushed with many pore volumes of DI water before vacuuming.

After the core's permeability has been measured, the baseline/foam experiment can be run using the following procedure and the corresponding diagram, Figure 3.3:

1. Ensure that there is enough compressed CO_2 in the accumulator to run the experiment. If not, the CO_2 accumulator must be refilled using the procedure listed in Section 3.1.3.8.
2. Ensure that the waste accumulator has been emptied out and reloaded with water on the back pressure relief valve side. The procedure for reloading the waste accumulator is described in Section 3.1.3.7.
3. Load the water/nanoparticle dispersion to be injected into the ISCO pump.

4. All the lines in the system should be initially filled with water. The lines should be free of air if the permeability measurement was carried out prior to this procedure.

5. The system should be started with all two-way valves shut except for valves (1), (2), and (8). Three-way valves (3) and (4) should both be open in the direction of the flow system.

6. The HPLC pump should then be operated to compress the CO_2 in the accumulator to the desired pressure. This pressure should approximately match the aqueous phase injection pressure to prevent water from flowing into the CO_2 accumulator during the experiment. Once the desired pressure is obtained, the HPLC pump should be turned back off.

7. The screw-top of the back pressure relief valve should be tightened to prevent flow until high pressures.

8. Confining pressure should be placed on the core using the hydraulic hand pump. The net confining pressure should be at least 600 psi at all times.

9. Pressure drop data recording should be started using the LabVIEW software on the desktop.

10. The ISCO pump, containing the de-ionized water or nanoparticle dispersion, should then be operated at a constant flow rate to build up pressure against the back pressure relief valve.

11. As the pressure builds up, it is necessary to increase the confining pressure on the core so that the net confining pressure is at least 600 psi. Failing to do so may damage the sleeve or cause confining fluid leakage into the core.

12. Once the system pressure reaches the desired value, the back pressure relief valve can be adjusted slowly to open. Once open, it is recommended to flow water/nanoparticle dispersion through the system for a few minutes to make sure the flow rate is constant. This can be determined by whether the pressure drop across the capillary tubing is constant. If the pressure drop data is oscillating, the back pressure relief valve may need further adjustment.

28

13. The HPLC pump can then be run at constant flow rate to begin CO_2 injection. After the pump is run, valve (5) will need to be opened to allow the CO_2 into the system.

14. Continue CO_2 and water co-injection until the CO_2 breaks through in the view cell, and the pressure drop data reaches a steady value. If both pressure drop readings (across the core and the tubing) change simultaneously, this is most likely due to fluctuations in the flow rate caused by the back pressure relief valve.

15. The CO_2 and water injection flow rates can then be changed to get as many data points as necessary.

16. The experiment can be run until the waste accumulator is filled. At that point, the pressure drop reading should fall to zero since there is no flow. The water and CO_2 pumps must be shut immediately to prevent over-pressurization.

17. Valves (1), (2), and (5) should then be shut to disconnect the CO_2 accumulator from the flow system.

18. Pressure data recording can then be stopped.

19. The system should then be vented using the procedure listed in Section 3.1.3.6.

3.1.3.5 Co-injecting through Fractured Cores

The overall procedure for running fractured core experiments is slightly different than the procedure used for non-fractured cores. Fractured cores can be prepared using the procedures described in the appendix. After the core is prepared and loaded into the core holder, the following procedure should be carried out before the co-injection experiment.

This procedure is done to minimize the change in fracture aperture during an experiment or between the baseline and foaming experiment. The fractured core is placed under two compression cycles, as shown in the examples in Figure 3.4. During the first cycle, the confining pressure on the fractured core is increased gradually using the

hydraulic hand pump. As the net confining pressure[2] is increased from 400 psia to 1,2000 psia, the average fracture width decreases from ~66 μm to ~40 μm. The confining pressure is then relieved temporarily, and then re-applied in the second cycle. During the second compression cycle, the confining pressure does not affect the average fracture width significantly. The first compression cycle leads to some inelastic deformation of the core, where the fracture aperture is significantly reduced as the confining pressure is increased. During the second compression cycle, the fracture aperture does not vary considerably as the confining pressure is increased.
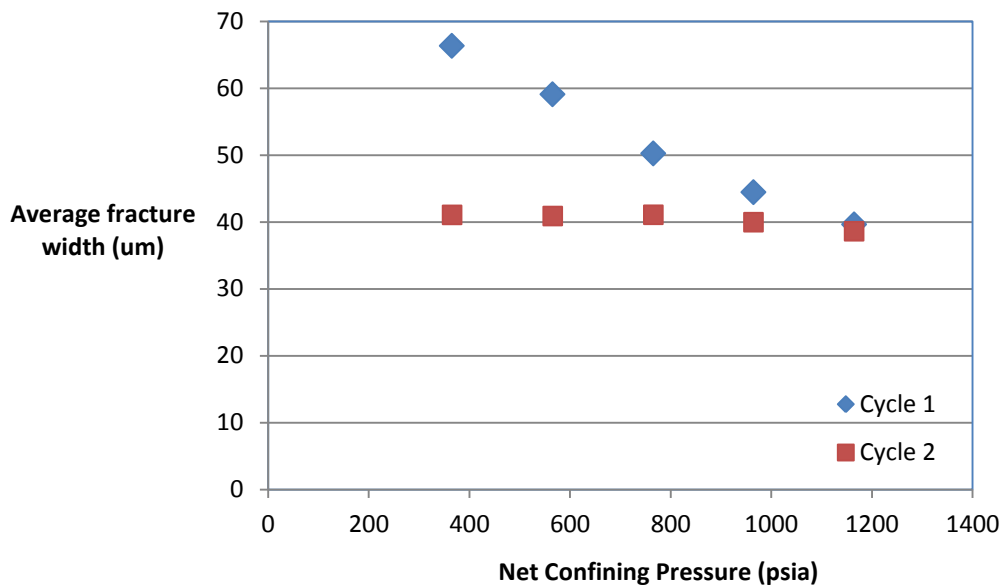
Figure 3.4 - Plot showing the average fracture width in microns at different net confining pressures.

The procedure used in placing the core in these compression cycles is as follows:

1. The system shown in Figure 3.3 should start with all valves closed except for valves (8) and (9), and three way valve (10) open towards the collection container.

2. Load the ISCO pump with DI water and make sure there is no air in the pump column.

---

[2] Net confining pressure on the core is confining pressure - pore pressure.

3. Load the fractured core into the core holder, and apply some confining pressure-typically 400 psia or 600 psia. This can be done by operating the hydraulic hand pump. With valves (1) and (2) open, in Figure 3.2, operate the hand pump until confining fluid exits into the collection container. Close valve (2), and operate the hand pump until the desired confining pressure is achieved. Close valve (1) after using the hand pump to trap the confining fluid.

4. Begin differential pressure data recording on the computer.

5. Start DI water injection, typically at a high flow rate such as 20 mL/min in order to have a more accurate measurement. Fractured cores will have a higher permeability, and would require a large flow rate for the pressure drop to be large enough to record accurately.

6. Continue DI water injection at the set flow rate until a constant pressure drop across the core is obtained.

7. Increase the confining pressure by opening valve (1) in Figure 3.2 and operating the hand pump until the desired confining pressure is achieved. Close valve (1) after using the hand pump.

8. Repeat the above steps until the first cycle is complete. It is not recommended to apply too large of a confining pressure (>2,000 psia) on the core to prevent any possible damage to the sleeve/core.

9. Relieve the confining pressure on the core by opening valve (1) and the hand pump relief valve (not shown) in Figure 3.2 and letting the confining fluid drain until the pressure is atmospheric. Close the relief valve and valve (1).

10. Allow the core some time, typically 15 minutes, to rest before starting the second compression cycle.

11. For the second compression cycle, repeat steps 5-8. At the end of the second compression cycle, the baseline experiment can be run using the procedure in Section 3.1.3.4.

3.1.3.6 Venting the System

After running an experiment that involves CO_2 injection, the system must be vented. It is important to vent the system carefully for safety reasons and to prevent any damage to the equipment. Use the following procedure and Figure 3.3 to vent the system:

1. At the end of a CO_2 experiment, all pumps must be stopped and valves (1), (2), and (5) must be shut.

2. Open the bypass valves (6) and (7) to protect the pressure transducers from large, sudden changes in pressure drop that may affect their calibration.

3. If the waste accumulator was not filled during the experiment, it is recommended to adjust the back pressure relief valve so that it opens and the remaining water is drained from the accumulator. This allows us to reduce the system pressure before venting.

4. With choke valve (11) shut, three-way valve (10) must be open to the direction of the choke valve and fume hood.

5. Slowly open choke valve (11) to begin venting the system. It is recommended to vent the system as slowly as possible to prevent freezing of water in the lines and to protect the core holder rubber sleeve and O-rings. In the event that some CO_2 has dissolved into the rubber sleeve, decompressing rapidly may cause damage to the sleeve and other rubber components.

6. As system pressure is reduced, the confining pressure should also be gradually reduced. This can be done by opening the two-way valve to the hydraulic hand pump, and using the built-in release valve. Confining pressure should always be at least 600 psi greater than the system pressure to prevent leakage in the core holder.

7. Continue venting the system slowly until the system pressure falls down to atmospheric pressure.

8. The confining pressure can then be completely relieved, and the core can be removed from the core holder. This is done by disconnecting the 'quick-connect'

fittings and then unscrewing the top retainer and the bottom screw of the core holder.

9. The waste accumulator can then be disconnected using the 'quick-connect' fittings and reloaded using the procedure in Section 3.1.3.7.

10. If nanoparticles were used in the experiment, it is recommended to flush the system with DI water to prevent nanoparticles from being deposited in the lines.

3.1.3.7 Reloading the Waste Accumulator

A waste accumulator consisting of a high pressure vessel with a movable piston was used to collect the effluent of high pressure experiments. During an experiment, the waste fluids, usually liquid CO_2 and nanoparticle dispersion, flow into the accumulator displacing water through a back pressure relief valve that keeps the system under a set pressure. This also prevents solids from going into the back pressure relief valve, which could be damaging. The water displaced is collected in a large 5 gallon container. The back pressure relief valve used is spring-loaded and can be adjusted to allow flow at a desired pressure within the spring's limit. The spring can be changed to allow for a different operating pressure range.

After each experiment, the waste accumulator should be properly vented and reset. The experimental set-up should first be vented slowly of any CO_2 by following the steps in previous section. Once the CO_2 has been vented, the waste accumulator can then be removed by disconnecting the 'quick-connect' connections. The accumulator ends should then be screwed off carefully as to not damage the O-rings. The DI water/nanoparticle dispersion should then be disposed of safely (waste container for dispersions). After the disposal, the internal piston should be reset to its original position by pushing it down using a metal bar or rod. DI water can then be filled into the void end of the accumulator and the end caps screwed back on carefully. Re-connect the waste accumulator to the setup using the 'quick-connect' lines ensuring that the piston is facing the apparatus.

The waste accumulator has O-rings surrounding the end-caps as well as the internal piston. AFLAS material O-rings were used to provide some corrosion resistance to the CO_2 present. These CO_2 resistant O-rings will still need to be replaced when they begin to crack and can no longer hold a seal. When replacing O-rings, it is recommended to apply some silicone lubricant to the piston O-ring in order to reduce mechanical damage.

3.1.3.8 Charging CO₂ Accumulator

A floating piston accumulator was used to store the CO_2 used in experiments. The accumulator consists of a pressure vessel with a piston that provides a seal, dividing the vessel into two compartments. CO_2 is loaded into the top compartment and pressurized using a Haskel air-driven compressor. Water can then be pumped at the bottom of the accumulator to further pressurize the CO_2 or to displace the CO_2 during experiments. The accumulator will need to be filled up with CO_2 whenever it is depleted or whenever it is vented for maintenance. The following procedure, along with Figure 3.5, is used to empty out the water and refill the accumulator with CO_2 when necessary.

To empty out any water present in the accumulator:

1. Close all valves shown in Figure 3.5.
2. Disconnect the tubing running from valve (8) to the HPLC pump
3. Gradually open choke valve (8) at the bottom of the accumulator to drain the water present. This step should be done carefully since the water may be at high pressure and may contain CO_2 if the O-rings around the piston have not maintained a seal.
4. Once the water has been drained, close valve (8) and reconnect the tubing running from the valve to the bottom of the HPLC pump.

Once the water has been drained from the bottom of the accumulator, the CO_2 can then be loaded into to the accumulator. The following procedure is used:

1. All valves shown in Figure 3.5 should be shut, and three-way valve (6) should be open towards the pneumatic compressor.

34

2. Open valve (7) connecting the accumulator to the compressor.

3. Open choke valve (4) on the liquid CO_2 cylinder.

4. Open the compressed air choke valve (1) and valve (2) to provide the high pressure air required to run the compressor.

5. Immediately open valves (3) and (5) providing the compressor with the CO_2 that is to be compressed into the accumulator.

6. Monitor the pressure of the accumulator using the mounted pressure gauge. Continue running the compressor until the pressure reaches around 1,500 psia.

7. Close valve (2) to turn off the compressor, and then close all other valves.

8. Redirect three-way valve (6) to flow system.

If the pressure is too low in the CO_2 accumulator, it may be necessary to drain the water and reset the piston manually. This should only be done when the CO_2 is depleted from the accumulator. With all the valves in Figure 3.5 shut, disconnect the flow line connecting valve (7) to (6), and replace it with a line that extends to the fume hood. Slowly open choke valve (7) to vent any remaining CO_2. Disconnect the tubing running from valve (8) to the HPLC pump, and replace it with a 1/4" tubing that extends to a large waste container, then open choke valve (8). Remove the top end cap of the accumulator, and use a large rod to push the piston down, forcing the water out of the bottom of the accumulator. It is recommended to connect a 1/4" tubing at the bottom of the accumulator to reduce the time necessary to empty out the water.
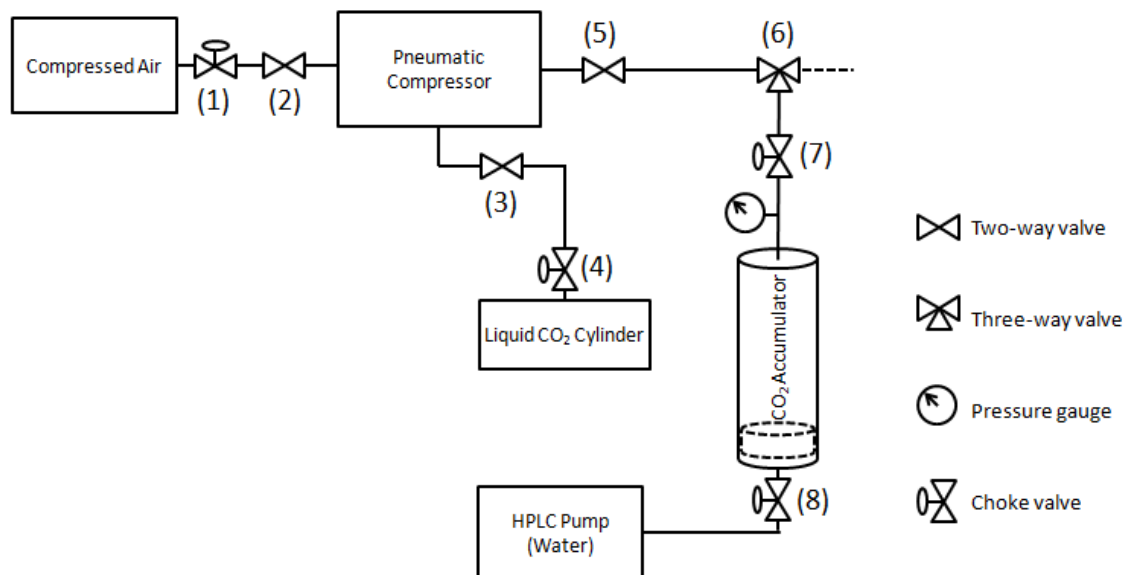
Figure 3.5 - Schematic of CO_2 infrastructure used.

CO_2 Accumulator Maintenance

The CO_2 accumulator used has an O-ring at each end. It also has a Teflon piston that separates the CO_2 and water inside the accumulator. Three O-rings provide a seal around the piston. The presence of CO_2 causes the O-rings to crack over time and eventually fail in holding an effective seal. In order to provide some resistance to CO_2 corrosion, the O-rings used are made of thermoset synthetic rubbers such as Viton, Buna N, or AFLAS. Over time, these O-rings will need to be replaced, especially the piston O-rings since they undergo mechanical damage in addition to corrosion. The O-rings should be replaced every few months whenever the accumulator does not hold pressure over time.

To replace the O-rings in the accumulator, the accumulator should first be disconnected from the experimental set-up and safely vented of any remaining CO_2. If water is present at the bottom of the accumulator, it should also be drained using the instructions provided. Once the cylinder has been emptied out, the end caps can then be screwed off and the piston pushed out of the vessel using a long bar. The O-rings around

the piston and at the ends of the accumulator can then be removed and replaced. It is recommended that the O-rings on the piston be coated with some silicone lubricant to reduce the mechanical damage to the O-rings. The piston can then be set back at the bottom of the accumulator. It is also recommended that some graphite anti-seize be placed on the threads of the accumulator ends. The end caps can then be screwed on and the accumulator can then be reconnected to the system.

3.1.4 Data Analysis

3.1.4.1 Normalizing Pressure Drop Data

The pressure drop data is typically offset by a certain value that is dependent on the absolute pressure of the experiment. Therefore, the pressure drop data from every experiment must be normalized before being used for calculations. This applies to both the pressure drop measurements across the core and the across capillary tubing.

In order to normalize the pressure drop data, the injected flow rate must be varied in order to get at least two pressure drop vs. flow rate data points. When plotted, the data should be linear and should intersect the origin since at a flow rate of 0 mL/min, the pressure drop across the core should be 0 psi. The data is normalized by subtracting or adding an offset value such that the y-intercept of the resulting line is zero. This should also cancel out the effects of hydrostatic pressure, which are almost negligible.

In the following example (Figure 3.6), a 1 wt% nanoparticle dispersion in DI water was injected into a 1" diameter, 6" long, Boise sandstone core at several flow rates. The system was at a pressure of 1,950 psia and ambient temperature. The measured data is linear, however the fitted line does not intersect the origin as expected. The pressure drop data must then be normalized by subtracting an offset value of 3.035 psia. The resulting line intersects the origin.

38

$$y = 0.5027x + 3.035$$

$$y = 0.5027x$$
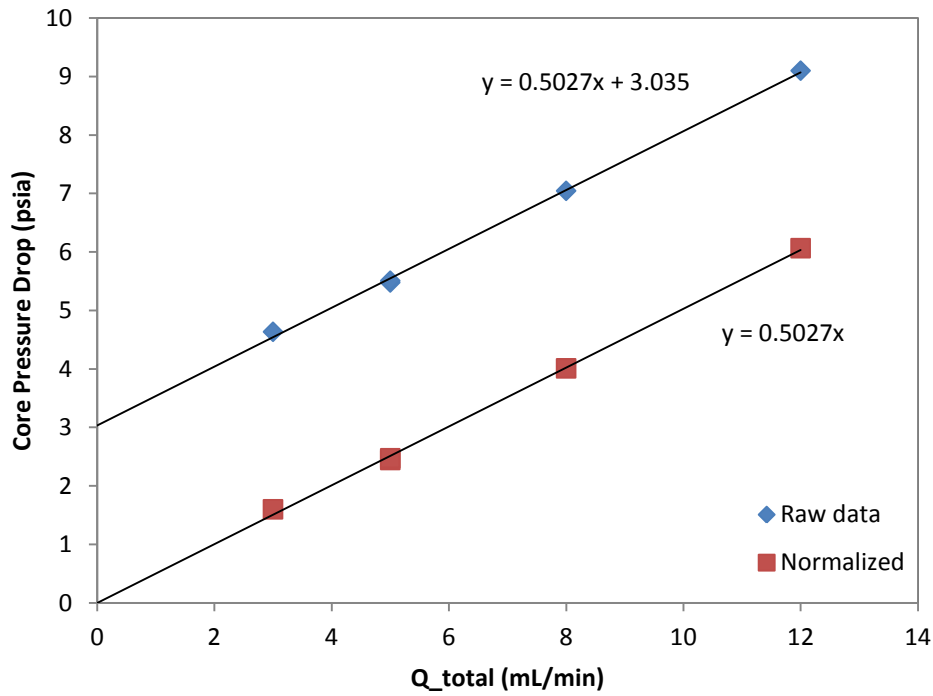
Figure 3.6 - Example of normalizing pressure drop data. Plot shows pressure drop across core vs. total injected flow rate before and after normalization.

3.1.4.2 Core Permeability

The permeabilities of the cores used in experiments were calculated using Darcy's law:

$$k = \frac{Q\mu L}{A\Delta P}$$

$k = permeability\ of\ the\ core\ (cm^2)$

$Q = volumetric\ flow\ rate\ (cm^3/s)$

$\mu = viscosity\ of\ injected\ fluid\ (Pa*s)$

$L = length\ of\ core\ (cm)$

$A = cross\ sectional\ area\ of\ core\ (cm^2)$

$\Delta P = pressure\ drop\ across\ core\ (Pa)$

3.1.4.3 Mobility

The mobility of the fluid mixture, λ, was calculated for some coreflood experiments using Darcy's law, using pressure drop data:

$$\lambda = \frac{QL}{\Delta PA}$$

$Q = volumetric\ flow\ rate\ (cm^3/s)$

$A = cross\ sectional\ area\ of\ core\ (cm^2)$

$L = length\ of\ core\ (cm)$

$\Delta P = pressure\ drop\ across\ core\ (Pa)$

3.1.4.4 Shear Rate through Core Matrix

The shear rate on the fluids flowing through a non-fractured core was calculated using the following equation (Lake 1989):

$$\dot{\gamma} = \frac{4Q}{\left(A\sqrt{8k\emptyset}\right)}$$

$\dot{\gamma} = shear\ rate\ (s^{-1})$

$Q = volumetric\ flow\ rate\ (cm^3/s)$

$A = cross\ sectional\ flow\ area\ (cm^2)$

$k = permeability\ (cm^2)$

$\emptyset = porosity\ (dimensionless)$

3.1.4.5 Mobility Reduction Factor

The mobility reduction factor is the ratio of the pressure drop across the core for the experiment with nanoparticles to that of the baseline experiment. The term 'mobility reduction factor' is used instead of normalized viscosity since the difference in pressure drops may also be a result of changes in relative permeability.

$$MRF = \frac{\Delta P_{foam}}{\Delta P_{baseline}}$$

$\Delta P_{foam} = pressure\ drop\ across\ the\ core\ for\ the\ foam\ experiment\ (psia)$

$\Delta P_{baseline} = pressure\ drop\ across\ the\ core\ for\ the\ baseline\ experiment\ (psia)$

3.1.4.6 Apparent Viscosity

The apparent viscosity of the fluid mixture flowing through the capillary tubing can be calculated using the Hagen-Poiseuille equation:

$$\mu_{app} = \frac{\pi \Delta P r^4}{8LQ}$$

$\mu_{app.} = apparent\ viscosity\ (Pa * s)$

$\Delta P = pressure\ drop\ across\ capillary\ tubing\ (Pa)$

$r = inner\ radius\ of\ capillary\ tubing\ (cm)$

$L = length\ of\ capillary\ tubing\ (cm)$

$Q = volumetric\ flow\ rate\ (cm^3/s)$

3.1.4.7 Normalized Viscosity

The normalized viscosity in the capillary tubing is calculated as the ratio of the apparent viscosity of the experiment run with nanoparticles to that of the baseline experiment. It is the same as the pressure drop ratio of the foam experiment to the baseline experiment.

$$\mu_{norm.} = \frac{\mu_{app.\ foam}}{\mu_{app.\ baseline}}$$

$\mu_{norm.} = normalized\ apparent\ viscosity\ (dimensionless)$

$\mu_{app.\ foam} = apparent\ viscosity\ of\ fluid\ mixture\ for\ the\ foam\ expt.(cP)$

$\mu_{app.\ baseline} = apparent\ viscosity\ of\ fluid\ mixture\ for\ the\ baseline\ expt.(cP)$

3.1.4.8 Shear Rate in Capillary Tubing

The shear rates on the fluid flowing in the capillary tubing were calculated using the equation for wall shear rate in a capillary tube. This equations assumes laminar and single phase flow.

$$\dot{\gamma} = \frac{4Q}{\pi r^3}$$

$\dot{\gamma} = shear\ rate\ (s^{-1})$

$Q = volumetric\ flow\ rate\ (cm^3/s)$

$r = tubing\ radius\ (cm)$

3.1.4.9 Net Confining Pressure

The net confining pressure is the difference between the pressure of the confining fluid and the pore pressure. During coreflood experiments, the confining pressure can be set to a desired value by controlling a hydraulic hand pump. In order to ensure a good seal around a core, it is recommended to have a net confining pressure no less than 600 psia.

$$P_{net\ confining} = P_{confining} - P_{pore}$$

The confining pressure is read off a pressure gauge attached to the confining fluid annulus of the core.

The pore pressure used is the average pressure inside the core, which can be estimated from the injection and exit pressures. Since the core is the main contributor to the pressure drop seen across the system (from injection to exit), it is assumed that the pore pressure is the average of injection and exit pressures:

$$P_{pore} = \frac{P_{in} + P_{exit}}{2}$$

3.1.4.10 Fracture Aperture, Permeability, and Flow Rate

Fracture permeability, k_f, is given by:

$$k_f[cm^2] = \frac{H^2}{12}$$

$$k_f[md] = 8.44 \times 10^9 H^2$$

where H is the fracture aperture or height in cm, as shown in Figure 3.7.

If the permeability of the fractured core has been measured, the fracture height can be calculated using a parallel permeability model as follows:

$$\bar{k} = \frac{\sum_{i=1}^{n}(k_i * A_i)}{\sum_{i=1}^{n} A_i}$$

where $\bar{k}$ is the average permeability, which corresponds to the value calculated from the measured pressure drop across the core.

$$\bar{k} = \frac{k_m * (A_{Core} - WH) + k_f WH}{A_{core}}$$

where k_m is the matrix permeability, A_{core} is the cross sectional area of the core, k_f is the fracture permeability, W is the fracture width, and H is the fracture height or aperture. Solving for k_f, we get:

$$k_f = \frac{\bar{k} * A_{core} - k_m(A_{core} - WH)}{WH}$$

Substitute the equation for fracture permeability into the above equation to get:

$$WH^3 - 12(\bar{k} * A_{core} + k_m * (A_{core} - WH)) = 0$$

Fracture aperture, H, can now be solved for.

To compute the fraction of the fluids flowing through the fracture, F_f, the following equation was derived from Darcy's law for flow in parallel media:

$$F_f = \frac{A_f * k_f}{\overline{k} * A_{core}} = \frac{A_f * k_f}{A_f * k_f + A_m * k_m}$$

$$A_f = H * W$$

$$A_m = A_{core} - A_f$$

where A_f is the cross sectional area of the fracture, and A_m is the cross sectional area of the core matrix.

The fraction of flow through the core matrix, F_m can then be calculated:

$$F_m = 1 - F_f$$
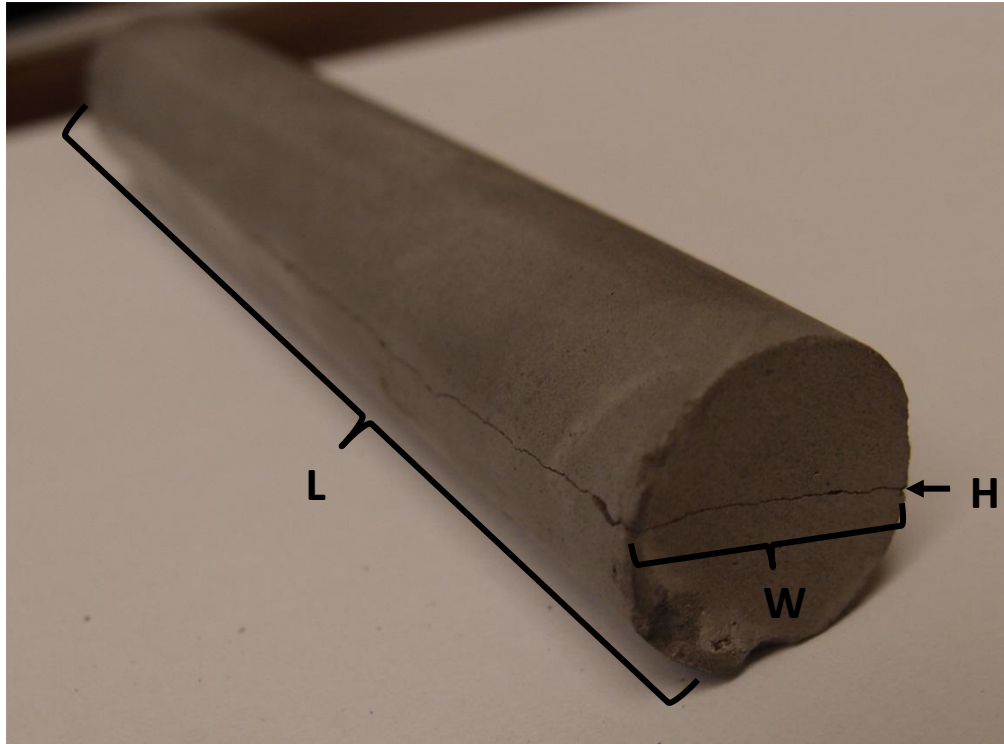
Figure 3.7 - Fractured cement core showing relevant parameters used in calculating fracture properties.

3.1.4.11 Shear Rate through Fracture and Reynolds Number

To calculate the shear rate in the fracture, we assume the fracture to be a rectangular duct with a negligible height-to-width ratio. The shear stress at the slit wall is given by:

$$\tau_w = \left(\frac{H}{2}\right)\left(\frac{\Delta P}{L}\right)$$

where H is the slit height, ΔP is the pressure drop across the slit, and L is the length of the slit.

For Newtonian fluids experiencing laminar flow,

$$\frac{H\Delta P}{2L} = \mu\left(\frac{6Q}{WH^2}\right)$$

where Q is the volumetric flow rate through the fracture, W is the slit width, and μ is the viscosity of the fluid. The shear rate can be derived from the two above equations to be:

$$\dot{\gamma}_a = \frac{6Q}{WH^2}$$

where $\dot{\gamma}_a$ is the shear rate through the slit.

To use this equation, we are assuming that the fluid flowing through the slit is a Newtonian fluid undergoing laminar flow. For experiments involving CO_2 and water mixtures, we are assuming that the flow is Newtonian in order to calculate the apparent shear rate.

The Reynolds number within the fracture can be calculated using the following equation:

$$Re = \frac{\rho Q D_H}{\mu A}$$

where ρ is the density, Q is the volumetric flow rate, D_H is the hydraulic diameter of the fracture, μ is the dynamic viscosity, and A is the cross-sectional area of the fracture. For a slit where $W \gg H$, the hydraulic diameter, D_H, becomes equal to double the fracture aperture ($=2*H$). Fractured core experiments run in this study are all within laminar flow regime, with $Re < 1500$ (Son 2006, Parrish 1963).

3.2   BEADPACK EXPERIMENTS

3.2.1   Materials Used

NexSil 20 and NexSil 6 Aqueous Colloidal Silica Nanoparticles

Bare colloidal silica nanoparticles were used in some beadpack experiments. These 6 nm and 20 nm diameter nanoparticles were received as 17 wt% and 40 wt% dispersions respectively from Nyacol Nano Technologies, Inc. (Ashland, MA). These nanoparticles do not have any surface coating and have a negatively charged surface.

NexSil 20 and NexSil 6 with PEG Coating

NexSil 20 bare colloidal silica nanoparticles were coated with PEG polymer of different chain lengths. These nanoparticles were surface treated by Ki Youl Yoon, from the Chemical Engineering department of the University of Texas at Austin.

Carbon Dioxide and DI Water

As described in Section 3.1.1.

3.2.2   Beadpack System

Figure 3.8 is a schematic of the setup used, and Section 3.2.3 provides the experimental procedure used to operate and maintain the setup. This setup was used before the coreflood setup (Section 3.1.2) was built. The apparatus consists primarily of two pumps that inject CO_2 and nanoparticle dispersion though a beadpack, which is submerged in a water bath. An ISCO pump, labeled (B) in Figure 3.8, injects the nanoparticle dispersion or water into the beadpack (A). An HPLC pump (C) injects DI water into the bottom of the CO_2 accumulator (D), displacing CO_2 into the beadpack. The fluid mixture then flows through a segment of capillary tubing (E), followed by a high pressure view cell (F), and finally into a waste accumulator (G). As it flows into the

46

waste accumulator, it displaces the resident water through the back pressure relief valve (H). A differential pressure transducer (I) measures the pressure drop across the capillary tubing. This data is then transmitted to a computer (not shown), where it is recorded over time.

The primary differences between the beadpack setup and the coreflood setup are as follows:

- The beadpack setup uses a beadpack filled with glass beads instead of a core holder as porous media.
- Pressure drop is measured across the core holder and the capillary tubing in the coreflood setup. Pressure drop is only measured across the capillary tubing in the beadpack setup.
- The core holder setup is rated to a higher pressure due to upgraded valves.
- Only the beadpack and some coiled tubing for heat transfer were placed in the water bath for the beadpack setup; capillary tubing was insulated but not submerged in the water bath. Most of the components of the core holder setup are housed in an oven or water bath, which allows for better temperature control.
- The length of capillary tubing used to measure apparent viscosity is 125 cm in the beadpack setup, and 305 cm in the coreflood setup.

This system used the same nanoparticle injection pump, CO_2 displacement pump, CO_2 accumulator, water bath, capillary tubing, view cell, waste accumulator, back pressure relief valve as the coreflood setup. Refer to Section 3.1.2 for detailed equipment description for the above components.

Beadpack Column

A high pressure column (HiP, Erie, PA) was filled with 180 μm spherical glass beads and was used as a beadpack. The HiP column has an ID of 0.386 cm and is 10.2 cm in length. Pieces of mesh were placed at the ends of the beadpack to prevent glass beads from exiting into the flow system.
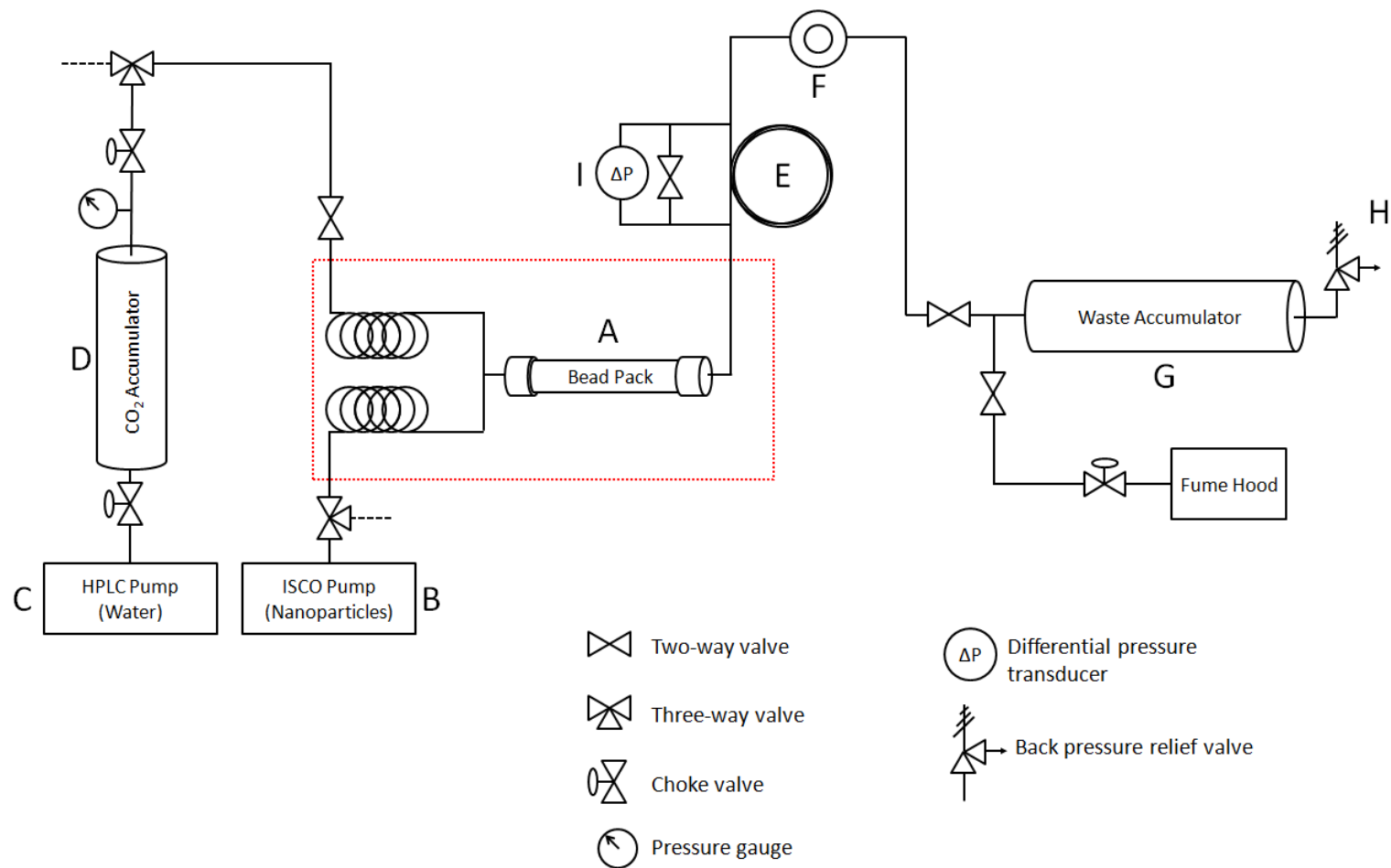
Figure 3.8 - Beadpack experimental set up. The dotted red box represents the water bath. A) beadpack, B) ISCO nanoparticle pump, C) HPLC CO_2 displacement pump, D) CO_2 accumulator, E) capillary tubing, F) view cell, G) waste accumulator, H) back pressure relief valve, I) differential pressure transducer.

3.2.3　Beadpack Experimental Procedure

This section contains a detailed procedure for running beadpack experiments. After loading the beadpack column with glass beads, it can be connected to the system and placed in the water bath. Similar to coreflood experiments, a baseline experiment is first run where CO_2 and DI water are co-injected into the beadpack. The foam experiment can then be run by co-injecting CO_2 and a nanoparticle dispersion. These experiments can be run successively without having to re-prepare the beadpack; whereby for coreflood experiments, the core must be removed and re-saturated with water before running the foam experiment. After each CO_2 experiment, the system will have to be vented and the waste accumulator reloaded.

The procedures for refilling the CO_2 accumulator, reloading the waste accumulator, and venting the system are the same as those of the coreflood setup, and were therefore not repeated.

3.2.3.1 Preparing Beadpack

In order to prepare a beadpack, the column must first be opened using a vise. The column should then be cleaned out and dried. Mesh with the appropriate mesh size to hold back the beads must then be placed at both ends of the column. In order to do this, several small pieces of mesh can be rolled up and stuffed into the column end caps. Another option is to epoxy a piece of mesh to the end caps, however this must be done frequently since the epoxy fails over time.

After securing pieces of mesh in both end caps, attach one end cap to the beadpack column. Beads can then be poured into the open until full. The beadpack should then be tapped along its side in order to pack the sand better. This should be done until the sand level remains constant. The other end of the beadpack can then be attached and fastened using a vise. It is recommended to coat the column end cap threads with anti-seize lubricant when necessary. Before connecting the beadpack to the flow system, it is recommended to test the integrity of the mesh by flowing water through the beadpack on

its own and inspecting the effluent for beads. This is done to ensure that beads are not injected into the flow system, which would require extensive cleaning.

3.2.3.2 Co-injection through Beadpack

The following procedure and diagram (Figure 3.9) describe the steps involved in running a high pressure co-injection experiment. The procedure is the same for both baseline and foam experiments. The baseline experiment is run using DI water and CO_2, while the foam experiment is run using a nanoparticle dispersion and CO_2. The data from the baseline experiment are used to evaluate the effect of the nanoparticles on the apparent viscosity of the fluid mixture.

1. Ensure that there is enough compressed CO_2 in the accumulator to run the experiment. If not, the CO_2 accumulator must be refilled using the procedure listed in Section 3.1.3.8.
2. Ensure that the waste accumulator has been emptied out and reloaded with water on the back pressure relief valve side. The procedure for reloading the waste accumulator is described in Section 3.1.3.7.
3. Load the water/nanoparticle dispersion to be injected into the ISCO pump.
4. The system should start with all two-way valves shut, except for valves (1), (2), and (8). Three-way valve (3) should be open towards the flow system.
5. The HPLC pump should then be operated to compress the CO_2 in the accumulator to the desired pressure. This pressure should approximately match the aqueous phase injection pressure to prevent water from flowing into the CO_2 accumulator during the experiment. Once the desired pressure is obtained, the HPLC pump should be turned back off.
6. The screw-top of the back pressure regulator should be tightened to prevent flow until high pressures.
7. Pressure drop data recording should be started using the LabVIEW software on the desktop.

8. The ISCO pump, containing the de-ionized water or nanoparticle dispersion, should then be operated at a constant flow rate to build up pressure against the back pressure regulator.

9. Once the system pressure reaches the desired value, the back pressure regulator can be adjusted slowly to open. Once open, it is recommended to flow water/nanoparticle dispersion through the system for a few minutes to make sure the flow rate is constant. This can be determined by whether the pressure drop across the capillary tubing is constant. If the pressure drop data is oscillating, the back pressure relief valve may need further adjustment.

10. The HPLC pump can then be run at constant flow rate to begin CO_2 injection. After the pump is run, valve (5) will need to be opened to allow the CO_2 into the system.

11. Continue CO_2 and water co-injection until the CO_2 breaks through in the view cell, and the pressure drop data reaches a steady value.

12. The CO_2 and water injection flow rates can then be changed to get as many data points as necessary.

13. The experiment can be run until the waste accumulator is filled. At that point, the pressure drop reading should fall to zero since there is no flow. The water and CO_2 pumps must be shut immediately to prevent over-pressurization.

14. Valves (1), (2), and (5) should then be shut to disconnect the CO_2 accumulator from the flow system.

15. Pressure data recording can then be stopped.

16. The system should then be vented using the procedure listed in Section 3.1.3.6.
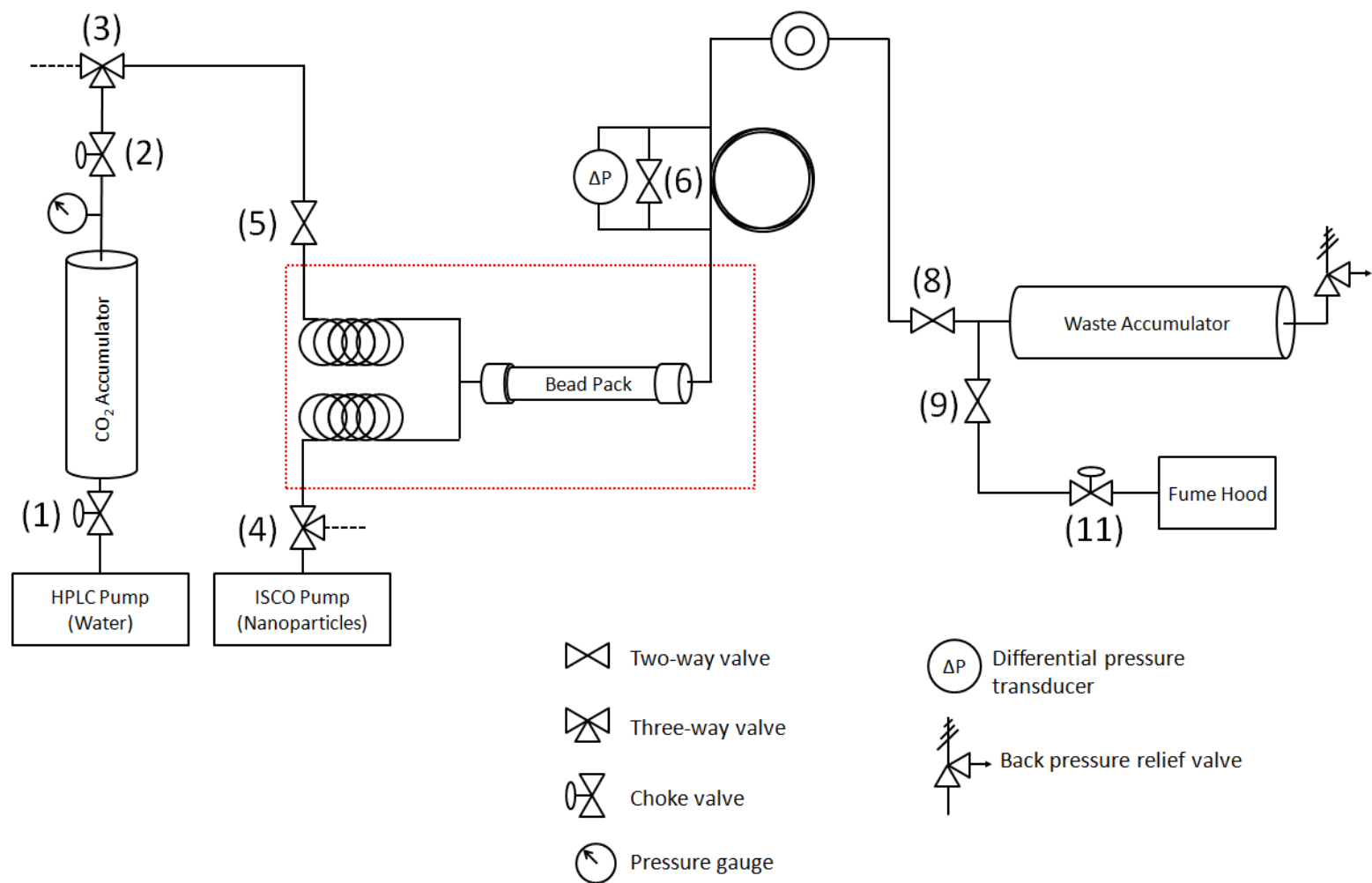
Figure 3.9 - Beadpack experimental set up. The dotted red box represents the water bath

3.2.4   Data analysis

Methods for normalizing pressure data, and calculating apparent viscosity, normalized viscosity, and capillary tubing shear rate can be found in Section 3.1.5. In addition to those calculations, the beadpack permeability will have to be estimated based on bead size since there was no differential pressure drop measurement across the beadpack.

3.2.4.1 Beadpack Permeability

In order to calculate the shear rate through the beadpack, the permeability of the beadpack must first be estimated. The permeability, k, of the beadpack used was estimated using the following equation (Lake 1989):

$$k = \frac{1}{72\tau} \frac{\o^3 D_p^3}{(1 - \o)^2}$$

where τ is the tortuosity, $\o$ is porosity, and D_p is bead diameter. Tortuosity is assumed to be 25/12, which is determined empirically for regularly packed spheres (Lake 1989). Porosity is assumed to be 38% for dense disordered packing of spherical grains in a tube.

3.2.4.2 Shear Rate through Beadpack

The calculation of the shear rate on the fluids flowing through a beadpack is the same as described in Section 3.1.4.4. The permeability used to calculate the shear rate is estimated using the above equation (3.2.4.1).

3.3   FLY ASH EMULSION EXPERIMENTS

The emulsifying ability of natural fly ash particles was investigated by preparing o/w emulsions primarily in batches. These emulsions were prepared using a sonifier, which provides high frequency vibration that emulsifies the two phases. Dodecane oil was used as an analog to the non-wetting CO_2 phase. The presence of a critical shear rate for o/w emulsification was investigated by co-injecting dodecane oil and the fly ash dispersion through a beadpack. The foam generation ability of fly ash was also tested by

mixing in a pressure cell and by co-injection through a beadpack. The experimental procedures used in preparing fly ash emulsions are detailed in this section.

3.3.1 Materials Used

Dodecane

Dodecane was used as a low pressure analog fluid to represent the non-wetting CO_2 phase due to dodecane's comparable density at room temperature and pressure to that of CO_2 at reservoir conditions. Relevant properties of CO_2 and dodecane are shown in Table 3.1. Reagent grade n-dodecane from Fisher Chemical was used in preparing the emulsions studied in this work.

Table 3.1 - Density, ρ, viscosity, μ, and interfacial tension with respect to DI water, σ, of relevant fluids. (Abdallah et al. 2011, NIST, Kvamme et al. 2007)

	DI Water	Dodecane	CO_2
	at 25 °C and 1 atm	at 25 °C and 1 atm	at 50 °C and 2,500 psi
$\rho\ (g/cm^3)$	0.997	0.746	0.745
$\mu\ (cP)$	0.890	1.36	0.0627
$\sigma\ (mN/m)$	N/A	52.5	29.6

Fly Ash Particles

Several batches of fly ash particles (see Table 3.2) were received from Professor Hee-chan Cho of the School of Civil, Urban & Geosystems Engineering of the Seoul National University, Korea. The fly ash particles are received after undergoing nano-milling to reduce particle size. For some of the batches received, chemical additives were added during the grinding process. Sodium hexametaphosphate (SHMP), which is a commercial compound used as a water softener, was added as a deflocculant to batches A, B, and C. Polyethylene glycol was added to batch E during wet grinding. No chemical additives were added to batch D or F. Note that the exact concentration of the chemical additives present in the fly ash samples received is unknown due to the wet grinding process; approximate concentrations are presented in Table 3.2. The first few batches of samples received, A and B, had high unburned carbon content of approximately 2-7%. Samples C, D, E, and F were received with lower carbon content; excess carbon was removed by burning it off in an oven at approximately 900 °C. Pictures of the samples as received are shown in Figure 3.10. Samples C, D, E, and F also have smaller particle size than batches A and B. The size distribution of batches A through E are included in the appendix; no size distribution data was received for batch F, however average particle size should be comparable to that of batches C, D and E.

Table 3.2 - Summary of fly ash batches received and used in this experimental work.

Batch	Size Dist.	Peaks	Dispersant	Fly Ash wt%	Carbon content
A	Appx B.A	~0.2-4 μm	~2 wt% SHMP	~15	High (2-7%)
B	Appx B.B	~1 μm	~2 wt% SHMP	~15	High (2-7%)
C	Appx B.C	~125 nm	~2 wt% SHMP	~2.5	Low
D	Appx B.D	~115 nm	DI water	~2.5	Low
E	Appx B.E	~130 nm	~2 wt% PEG	~2.5	Low
F	Unknown	-	N/A	N/A	Low

Figure 3.10 - Fly ash batches as received after mixing; from left to right: batch A, B, C, D, and F in powder form. Batch E not shown.

3.3.2 Preparing Fly Ash Dispersions

Some of the fly ash batches received were not colloidally stable (batches A and B), and had to be shaken before use. Fly ash particles in batches C through E were remained in dispersion for extended periods of time, but were still shaken before using to ensure more uniform samples were taken. To prepare a fly ash dilution, the equation in appendix was used to calculate the quantity of fly ash dispersion and water to be mixed. The samples were then shaken before using to prepare o/w batch emulsions.

In order to use the fly ash dispersions with high carbon solid content (batches A and B) in co-injection experiments, it was necessary to remove the solid content to avoid plugging the beadpack or the flow system used. This was achieved by diluting the fly ash dispersion in DI water, and then sonifying the dispersion for ~30 minutes. The dispersion was then centrifuged at 10,000 rpm for 15 minutes to separate the larger carbon solids. After centrifuging, the supernatant was then extracted using a syringe. The resulting supernatant is a clear dark dispersion that is more stable than the original dispersion; it does not settle out of solution over time as fly ash batches A and B do. The increased stability is most likely due to a lower fly ash concentration, lower carbon solids content, and sonification. Figure 3.11 compares the fly ash dispersion prepared using this procedure (right) to the original received dispersion (left) after 24 hours of settling.
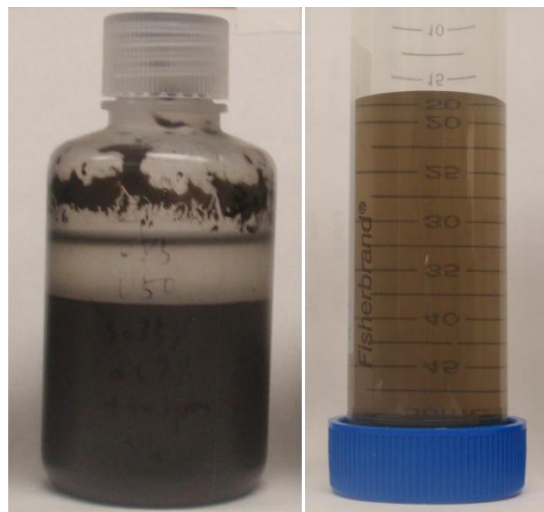
Figure 3.11 - Comparison of fly ash batch B as received (left) to the supernatant extracted after sonification and centrifuging.

3.3.3 Preparing o/w Batch Emulsions

Batch samples of fly ash-stabilized o/w emulsions were prepared using a Branson Sonifier 250 with a 1/8" tapered sonifying microtip, shown in Figure 3.12. The sonifier provides a local high frequency, high energy vibrations to emulsify the two phases. The same procedure was used to prepare the o/w emulsions in this study; equal volumes of dodecane and fly ash dispersion were placed in a vial and sonified for 2 minutes. The total volume of the fluid mixture used per sample was approximately 4 mL. The sonifying microtip was immersed in the mixture and placed at the interface of the two fluids. During sonification, the sonifying tip and the vial were not moved in order to maintain reproducibility of experimental results. The sonifier was run at ambient conditions at 50% output level, with 50% duty cycles. After sonification, the sample was removed and capped.

The sonifier tip should be rinsed with de-ionized water and isopropyl alcohol after every sample prepared. Caution should be taken to avoid contacting the tip of the operational sonifier with any solid surface, such as the container walls or bottom, as this may damage the sonifier tip.

Figure 3.12 - Branson Sonifier 250 (L) and 1/8" tapered microtip (R) used to prepare o/w emulsions.

3.3.4 Measuring Fly Ash Critical Shear Rate

The presence of a critical shear rate, below which o/w emulsions are not generated, was investigated for fly ash particle-stabilized emulsions using the apparatus shown in Figure 3.13. The experimental set-up consists of two HPLC pumps, two accumulators, and a beadpack. One HPLC pump injects water into an accumulator displacing dodecane into the beadpack at a set flow rate. The second HPLC pump injects water into the second accumulator, displacing a fly ash dispersion into the beadpack at a set flow rate.

The beadpack consists of a 3" long piece of tubing, with an ID of 0.43", that has been packed with 45 μm - 63 μm spherical glass beads using the same procedure described in Section 3.2.3.1. Dodecane and a fly ash dispersion are then co-injected through the beadpack to generate an emulsion. The total injected flow rate was varied to increase the shear rate; the phase ratio of injected fluid can also be modified.

59

The effluent was then collected separately for each flow rate or phase ratio used. The collected samples were visually inspected for the presence of any emulsion. Some of the generated emulsions were inspected under a microscope to determine emulsion droplet size. Refer to Section 3.2.4 for the calculation of beadpack permeability and the shear rate through the beadpack.
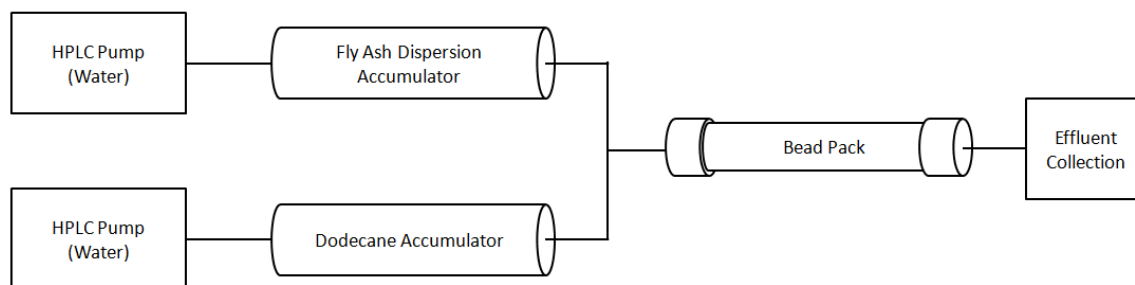
Figure 3.13 - Schematic of apparatus used to generate o/w emulsions by co-injecting dodecane and fly ash dispersion through a beadpack.

3.3.5   Foam Generation in Batch Mixer

The ability of fly ash particles and bare colloidal silica to generate stable c/w foams was also investigated using a high pressure batch mixer in Dr. Keith Johnston's laboratory (University of Texas at Austin, Chemical Engineering Dept.). The apparatus consists of a high pressure view cell with a stir bar used for agitation. CO_2 and a dispersion are loaded into the cell and then stirred for 30 minutes. The presence of a foam is determined visually in these experiments. Any generated foam was observed over time for stability.

Chapter 4: Results and Discussion

4.1 FOAM GENERATION IN CORE MATRIX

Several experiments were run using Boise sandstone cores to investigate the ability of PEG-coated silica nanoparticles to stabilize CO_2-in-water foams by co-injection through rock matrix. The presence of a critical shear rate required for foam generation through rock matrix was also investigated. The results presented in this section were obtained using the coreflood apparatus and procedure described in Section 3.1. The experiments were run by co-injecting a nanoparticle dispersion and liquid CO_2 through a core, while measuring the pressure drop across the core and across a piece of capillary tubing downstream of the core. A corresponding baseline (nanoparticle-free) experiment was run for each coreflood, where DI water and liquid CO_2 are co-injected through the core. The data from the baseline experiment are used to show the effect of the presence of nanoparticles on the fluid mixture. A view cell was also used to make qualitative observations of the foam based on droplet size. The non-fractured Boise coreflood experiments were carried out at the experimental conditions listed in Table 4.1. A complete presentation of the results of this experiment is in Appendix C.

Table 4.1 - Summary of experimental conditions used for non-fractured Boise sandstone corefloods.

Experimental Conditions used for Non-fractured Boise Sandstone Cores	
Nanoparticles dispersion	1 wt% 3M 5 nm PEG-coated silica nanoparticles in DI water
Temperature	23 °C
Pressure	~2,000 psia
CO_2 density	~0.87 g/mL
Volumetric phase ratio	1 (mL/min CO_2)/(mL/min NP)
Total flow rate	Varied
Net confining pressure*	~1,000 psia

* Net confining pressure is the difference between the pressure of the confining fluid and the pore pressure of the core.

The total injected flow rate is varied at a constant phase ratio of 1. Increasing the injected flow rate increases the shear rate on the fluid mixture as it pass through the core matrix. For the purpose of coreflood experiments in this work, the critical shear rate is considered to be the minimum shear rate required to generate a foam within the core. To determine whether a foam has been generated in the core, a mobility reduction factor (MRF) is calculated, as given in 3.1.4.5, by dividing the core pressure drop of the nanoparticle experiment by that of the baseline experiment. Three corefloods were run using non-fractured Boise cores, whose properties are listed in Table 4.2. Core permeability was calculated by measuring the pressure drop across the core while injecting DI water at varying flow rates. A baseline experiment was carried out for each core used.

Table 4.2 - Properties of the Boise sandstone cores used in co-injection experiments.

Experiment	Core Diameter (in.)	Core Length (in.)	Permeability (mD)
B1	1.0	11.8	1,650
B2	1.0	5.9	1,650
B3	1.0	6.0	1,720

The results obtained from the non-fractured coreflood experiments suggest the presence of a critical shear rate, below which the presence of nanoparticles does not affect the pressure drop measurement across the core. Figure 4.1 shows the MRF values for the three corefloods plotted against the core shear rate. At lower shear rates (<475 s^{-1}), the MRF is approximately 1, which means that the pressure drop measured in the nanoparticle experiment is the same as that of the baseline experiment. As the shear rate through the core is increased, the MRF value increases. For coreflood B1, MRF increases by a factor of 1.9 between 470 and 780 s^{-1}. MRF of coreflood B2 increases by more than a factor of 2 between 470 and 930 s^{-1}. MRF of coreflood B3 increases by a factor of 2.3

between 460 and 1140 s^{-1}. For the three experiments using non-fractured Boise sandstone cores, there seems to be a threshold shear rate where the foam begins to reduce the mobility of the fluid mixture flowing through the core. For comparison, the critical shear rate for the PEG-coated silica nanoparticles used was reported as low as 720 s^{-1} by co-injection through a beadpack at a similar CO_2 density (Espinosa 2011).
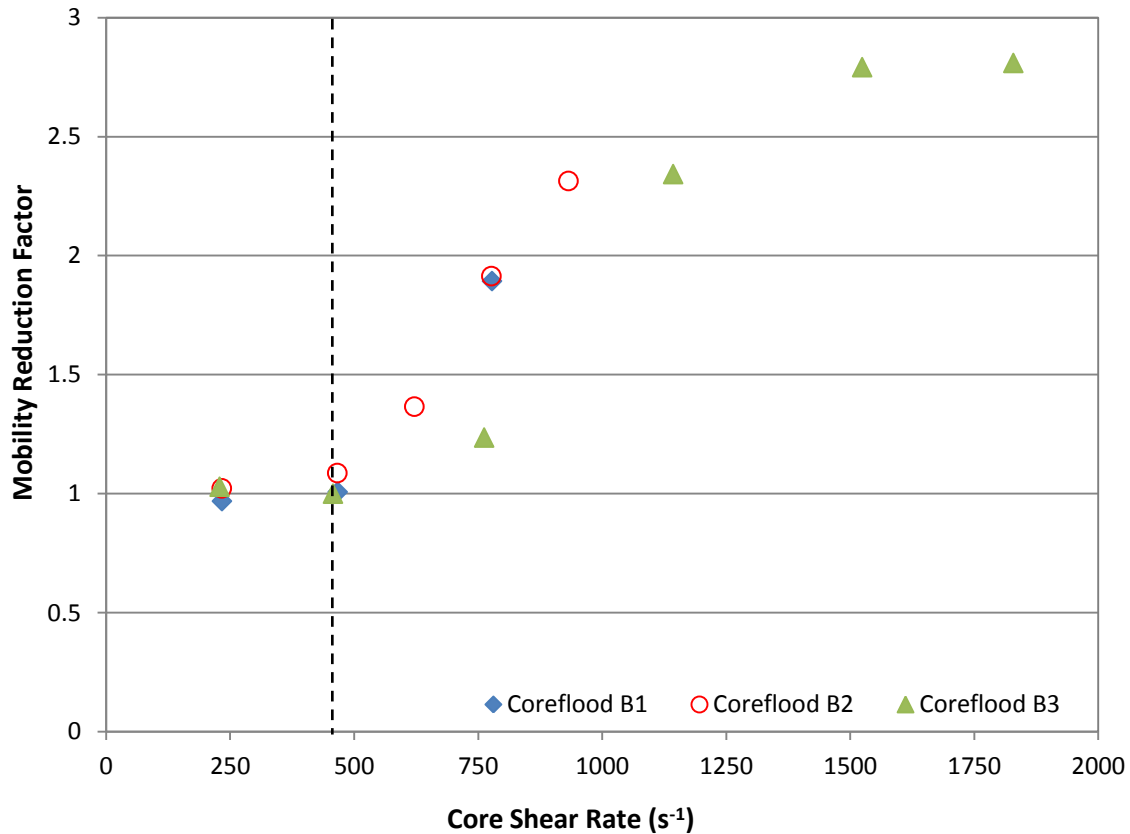
Figure 4.1 - Mobility reduction factor for non-fractured Boise corefloods. Core B1 was 11.8" long, while cores B2 and B3 were approximately 6" long.

Figure 4.2 shows the normalized viscosity of the fluid mixture as measured in the capillary tubing. The normalized viscosity is calculated by dividing the pressure drop of the fluid mixture in the nanoparticle experiment to that of the baseline without nanoparticles. The secondary horizontal axis shows the shear rate of the fluid mixture through the capillary tubing at the different flow rates (see 3.1.4.8). The results of coreflood B2 and B3 indicate a more flow-resistant foam at lower flow rates, which

63

corresponds to lower shear rates through the core matrix. On the other hand the core pressure drop data suggests that a more flow-resistant foam is generated at the higher flow rates. By inspecting the foam flowing through the view cell Figure 4.5, we can see that a more uniform foam with a finer texture (smaller droplet size) is generated at higher flow rates. Foams with finer textures result in a larger resistance to flow through a matrix, as tested by Ettinger and Radke (1989) using Berea sandstone cores. It is likely that the coarse-textured foams observed at low flow rates in the capillary viscometer and view cell were generated via snap-off mechanism as the fluid mixture was moving from the core matrix to the open tubing or spacer. This would explain why the pressure drop across the core does not seem to be affected by it. This phenomenon is described as "exit" foam by Radke and Ransohoff (1986), where coarse foams are generated at the exit face of a porous media. They conducted visual experiments showing the generation of coarse gas bubbles at the exit of a beadpack with no evidence of foam generation within the beadpack. Figure 4.3 shows a coarse foam being generated at low velocities at the outlet of the beadpack (right of the dark line). Figure 4.4 shows a fine textured foam, generated at high velocities within the beadpack, exiting the system (Radke and Ransohoff 1986).
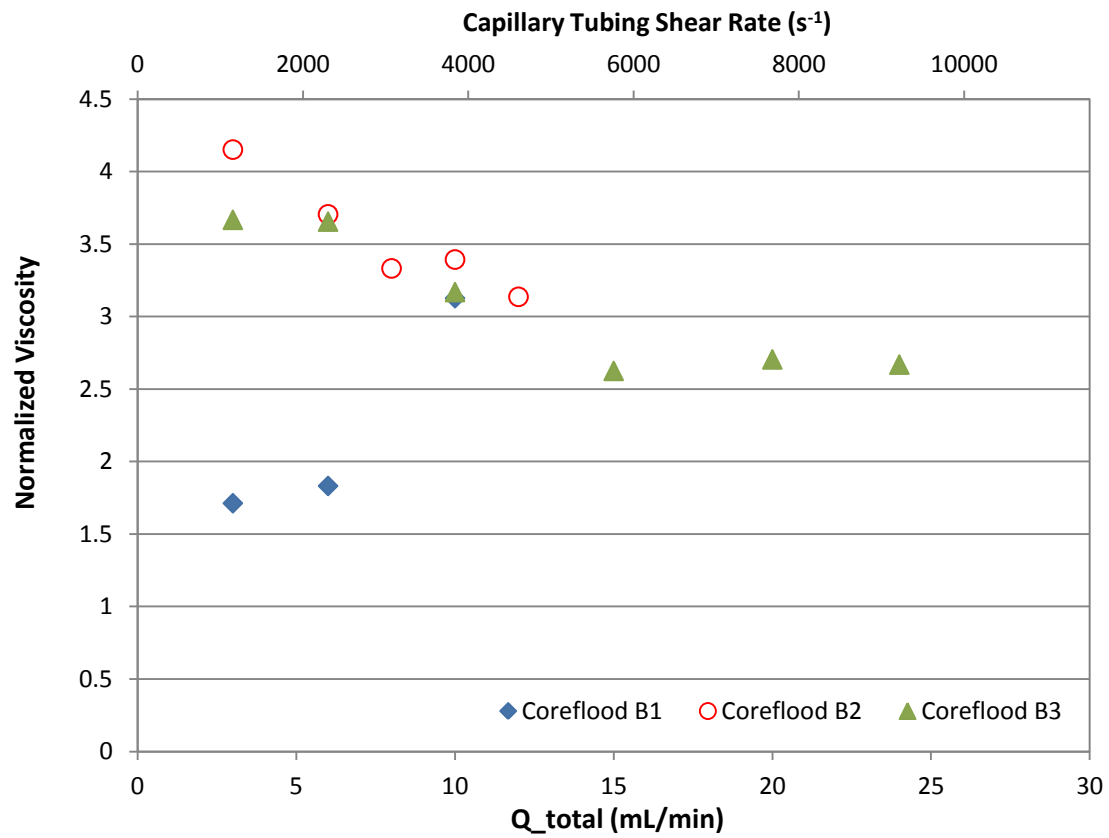
Figure 4.2 - Normalized viscosity as measured in the capillary tubing. Core B1 was 11.8" long, while cores B2 and B3 were approximately 6" long.
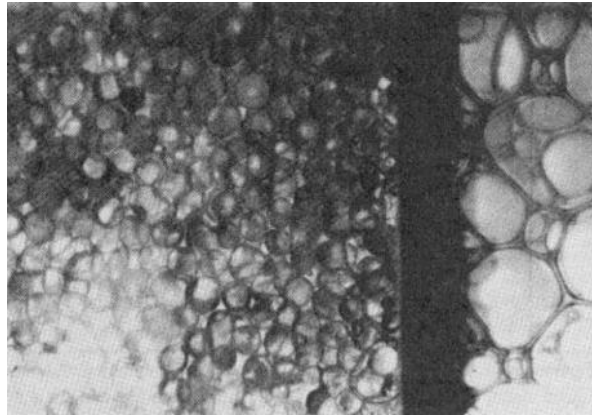
Figure 4.3 - At low velocities, coarse gas bubbles are generated at the exit of the beadpack. Beadpack is to the left, exit is to the right of the dark vertical line. (from Radke and Ransohoff 1986)
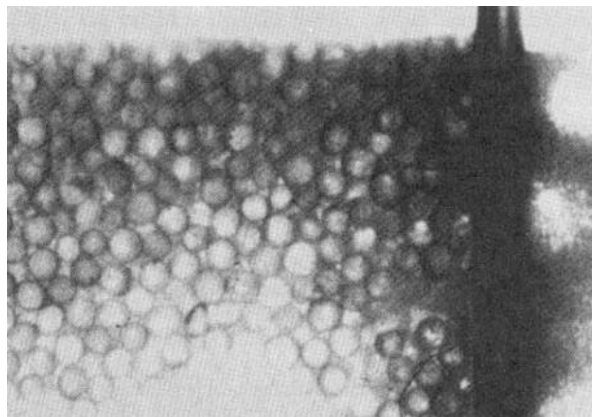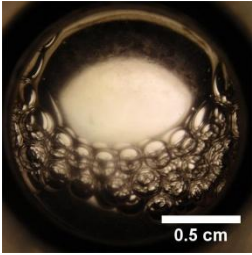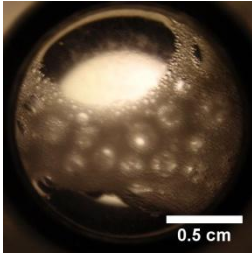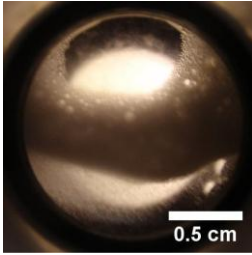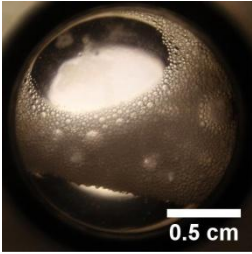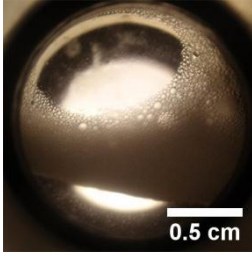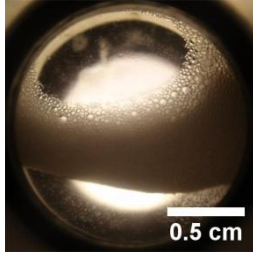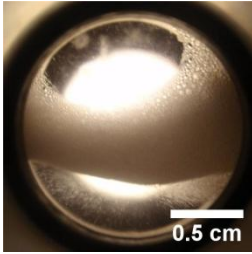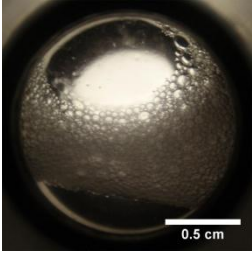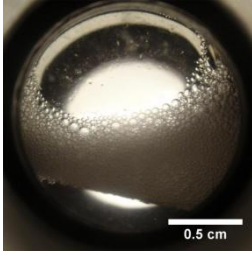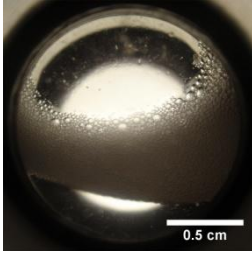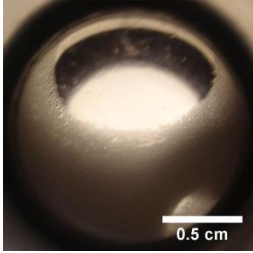
Figure 4.4 - At high velocities, fine-textured foam is generated within the beadpack. Beadpack is to the left, exit is to the right of the dark vertical line. (from Radke and Ransohoff 1986)

The presence of an "exit" foam at lower flow rates explains why the normalized viscosity values as measured in the capillary tubing are not 1. The coarser "exit" foams generated at low flow rates have are measured to have a larger normalized viscosity in the capillary tubing than the fine textured foam that is generated within the core matrix. The rheology of foam flowing through porous media is different than that through a capillary tube, therefore it is difficult to compare the pressure data across the core to that of the capillary tubing. With that in mind, possible reasons for a reduced normalized

viscosity in the capillary tubing at higher flow rates are the effects of shear thinning and a different flow regime for the larger coarse droplets than for the fine-textured foam.

The lack of additional data points makes the normalized viscosity of coreflood B1 difficult to interpret. However, the different trend seen in coreflood B1 than that of B2 and B3 could be a result of the use of spacers in the core holder. Since coreflood B1 was run using a 11.8" core, no spacers were used in the core holder. The presence of two spacers in corefloods B2 and B3 may be responsible for some additional agitation resulting in finer textured, or a larger quantity of, "exit" foam as shown in the view cell photographs at 3 mL/min (Figure 4.5).

Figure 4.5 - Photographs of the fluid mixture passing through the view cell at different flow rates for Boise corefloods

Q_{total}:	3 mL/min	6 mL/min	8 mL/min	10 mL/min	24 mL/min
Core $\dot{\gamma}$ (s⁻¹):	230	470		780	
Coreflood B1					
Core $\dot{\gamma}$ (s⁻¹):	230	470	620	780	
Coreflood B2					
Core $\dot{\gamma}$ (s⁻¹):	230	460		760	1830
Coreflood B3					

4.2   FOAM GENERATION IN FRACTURED CORES

The ability of PEG-coated silica nanoparticles to stabilize c/w foam by co-injection was also investigated in this study. Experiments were run with two types of fractured cores: fractured Boise sandstone cores, and fractured cement cores. Boise sandstone cores have a relatively high permeability (~1.6 D), which results in both matrix and fracture flow in the experiments. In order to isolate the effects of fracture flow on foam generation, a coreflood using a fractured cement core was run.

4.2.1   Fractured Sandstone Cores

Two experiments were run using fractured Boise sandstone cores to investigate the ability of PEG-coated silica nanoparticles to stabilize CO_2-in-water foams by co-injection through fractures. The presence of a critical shear rate that may be required for foam generation in the fractured cores was also investigated. The results were obtained using the apparatus and procedure described in Section 3.1. The experiments were run by co-injecting a nanoparticle dispersion and liquid CO_2 through a fractured core, while measuring the pressure drop across the core and a piece of capillary tubing downstream of the core. A corresponding baseline was run for each core; however, there were some difficulties in maintaining the same fracture aperture for both baseline and nanoparticle experiment. As a result, the data in this section are presented in the form of mobility, as opposed to a mobility reduction factor. A view cell was used to make qualitative observations of the foam based on droplet size. The fractured Boise sandstone corefloods were carried out at the experimental conditions listed in Table 4.3, which are the same as those of the non-fractured Boise cores.

Table 4.3 - Summary of experimental conditions used for fractured Boise sandstone
corefloods.

Experimental Conditions used for Fractured Boise Sandstone Cores	
Nanoparticles dispersion	1 wt% 3M 5 nm PEG-coated silica nanoparticles in DI water
Temperature	23 °C
Pressure	~2,000 psia
CO_2 density	~0.87 g/mL
Volumetric phase ratio	1 (mL/min CO_2)/(mL/min NP)
Total flow rate	Varied

In these corefloods, the total injection flow rate is varied at a constant volumetric phase ratio of 1. Increasing the flow rate increases the shear rate through the core matrix and fracture. The critical shear rate is considered to be the minimum shear rate required to generate a foam in the core. The mobility of the fluid mixture passing through the core is can be calculated using Darcy's law with the pressure drop data and the volumetric flow rate. This allows us to present the pressure drop data in a way that accounts for the different flow rates used. The properties of the two fractured Boise cores used in the experiments are listed in Table 4.4. Both cores have a 1" diameter and are 6" in length. The matrix permeability of the non-fractured Boise cores is ~1,650 mD. Both cores were fractured using a load frame with approximately 20 kN of force. Fracture properties were calculated assuming we have a uniform rectangular slit along the length of the core. Based on the fracture permeability, we can also estimate the fractions of injected fluid flowing through the fracture, $F_{fracture}$, and through the matrix based on a parallel permeability model.

Table 4.4 - Properties of the fractured Boise sandstone cores used in co-injection
experiments.

Experiment	L_{core} (in.)	$\bar{k}$ (mD)	H (μm)	Net P_{conf} (psia)	$F_{fracture}$ (%)
F1	6	6425	105	1400	76.7
F2	6	2830	66	950	42.1

Figures 4.6 and 4.7 show the mobility of the fluid mixture flowing through the core at different injection flow rates. The fracture shear rate is calculated using the fraction of flow through the fracture and the geometry of the fracture. The matrix shear rate was calculated using the fraction of flow through the core matrix and known matrix permeability for Boise sandstone cores (~1,650 mD). The fracture shear rate and the matrix shear rate calculations are based on the assumption that the fracture is an open slit running through the length of the core. With the application of a large confining pressure, the fracture in a sandstone core may behave more as a high permeability streak, as opposed to an open slit. For this reason, the average core shear rate was also estimated from the average permeability of the core, as measured using the pressure drop data. This assumes a homogenous core permeability.

Figure 4.6 shows the mobility of the fluid mixture in the nanoparticle experiment F1. As the injection flow rate is increased, the different shear rate representations also increase. At low flow rates, the mobility seems to be constant at approximately 3000 mD/cP. Between 14 and 20 mL/min, the mobility of the fluid mixture is reduced by a factor of 2. Results from experiment F2, shown in Figure 4.7, also show the same trend. The mobility seems to be level at approximately 1400 mD/cP at lower flow rates, and then decreases to approximately 900 mD/cP from 13 to 16 mL/min. The results of these two experiments suggest the presence of a threshold shear rate to generate a foam. Photographs of the fluid mixture flowing through the view cell at different flow rates are shown in Figure 4.10. The results are comparable to that of the non-fractured core, where the mobility of the fluid mixture passing through the core is reduced after a certain shear rate. Since decoupling the contributions for foam generation from the matrix and the fracture under confining pressure is difficult, at present it is unknown whether the shear rate required for mobility reduction in the fractured core is the same as that of the non-fractured core; and this aspect warrants further examination.
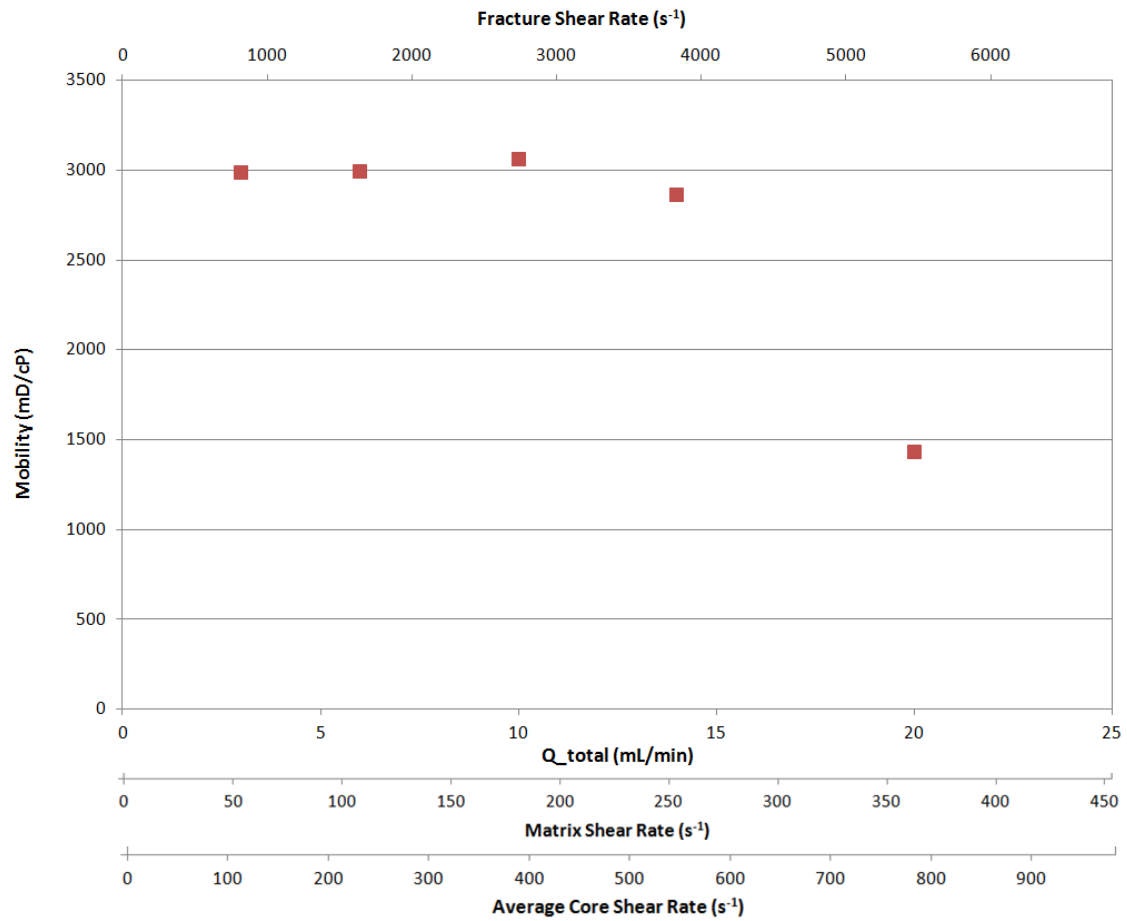
Figure 4.6 - Mobility of the fluid mixture vs. flow rate, fracture shear rate, matrix shear rate, and average core shear rate, for experiment F1.
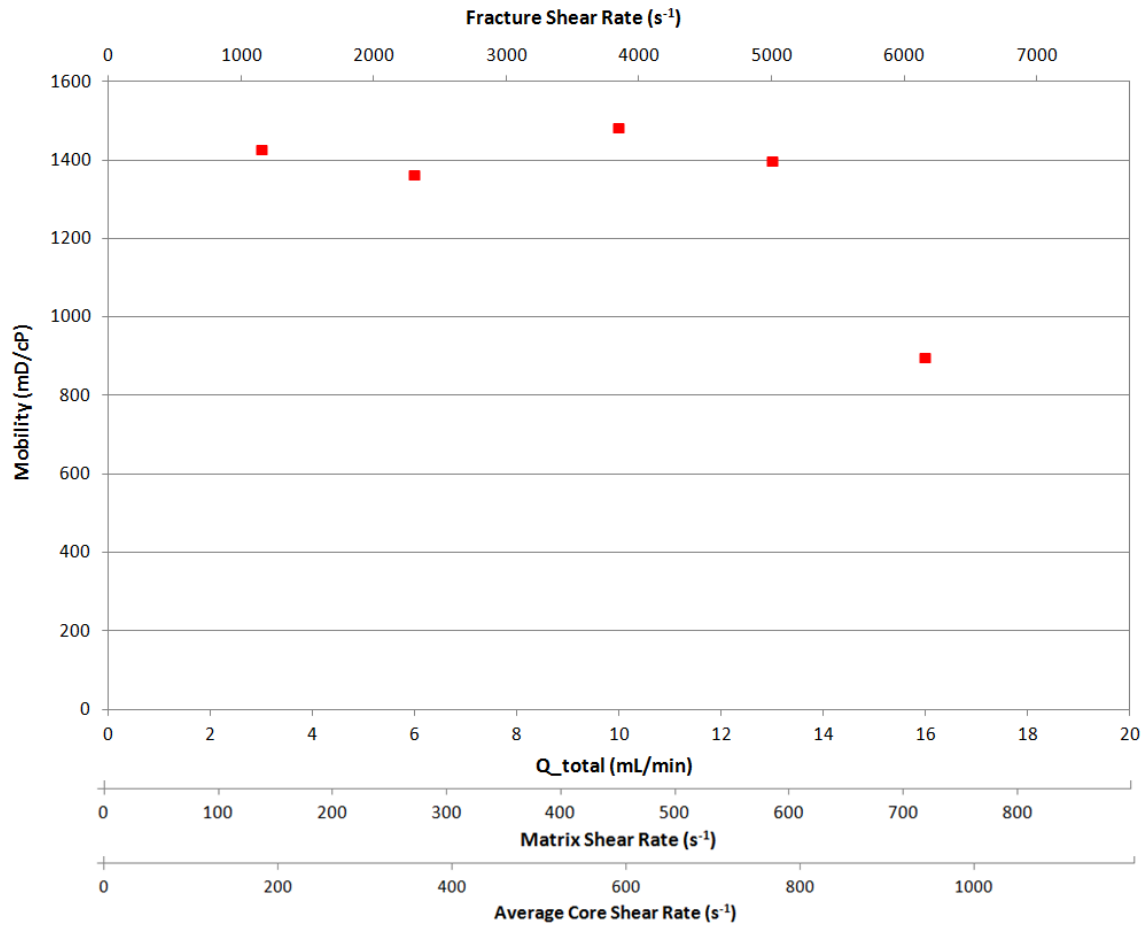
Figure 4.7 - Mobility of the fluid mixture vs. flow rate, fracture shear rate, matrix shear rate, and average core shear rate, for experiment F2.

Figures 4.8 and 4.9 show the normalized viscosity from the capillary tubing pressure drop data for the above corefloods. In both corefloods, the normalized viscosity in the capillary tubing starts off greater than 1, even though the mobility of the core does not change until higher flow rates. A possible explanation is that the foams generated at the lower flow rates are "exit" foams as described above and shown in the Section 4.1. For fractured sandstone cores under confining pressure, it is unlikely to have an open fracture channeling throughout the length of the core. This means that the generation of an "exit" foam can still occur at the exit face of the core.
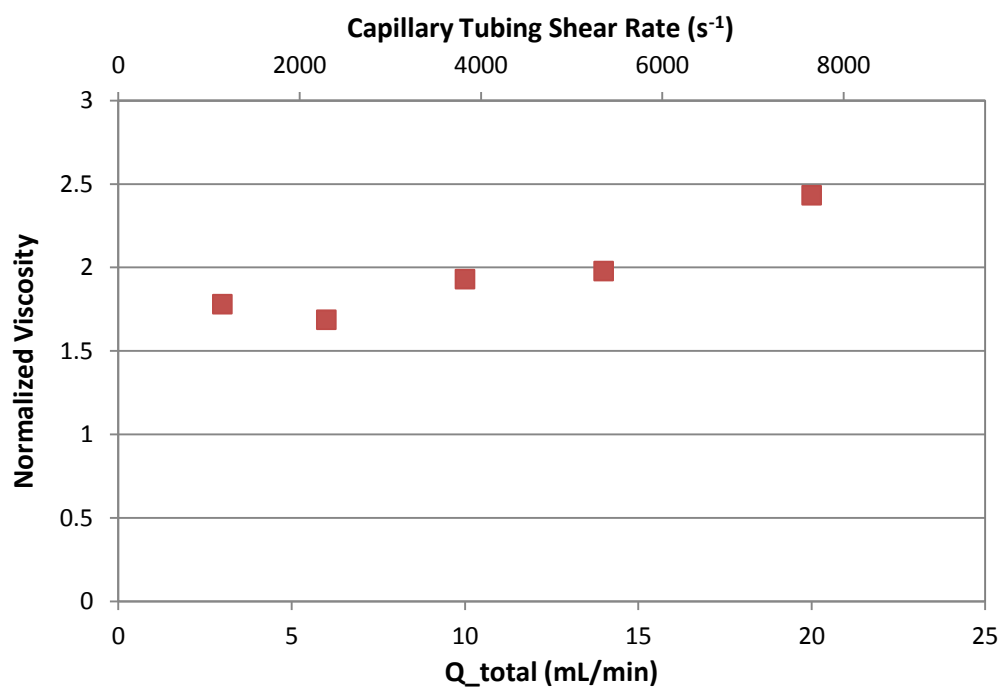
Figure 4.8 - Normalized viscosity measured in the capillary tubing, for experiment F1.
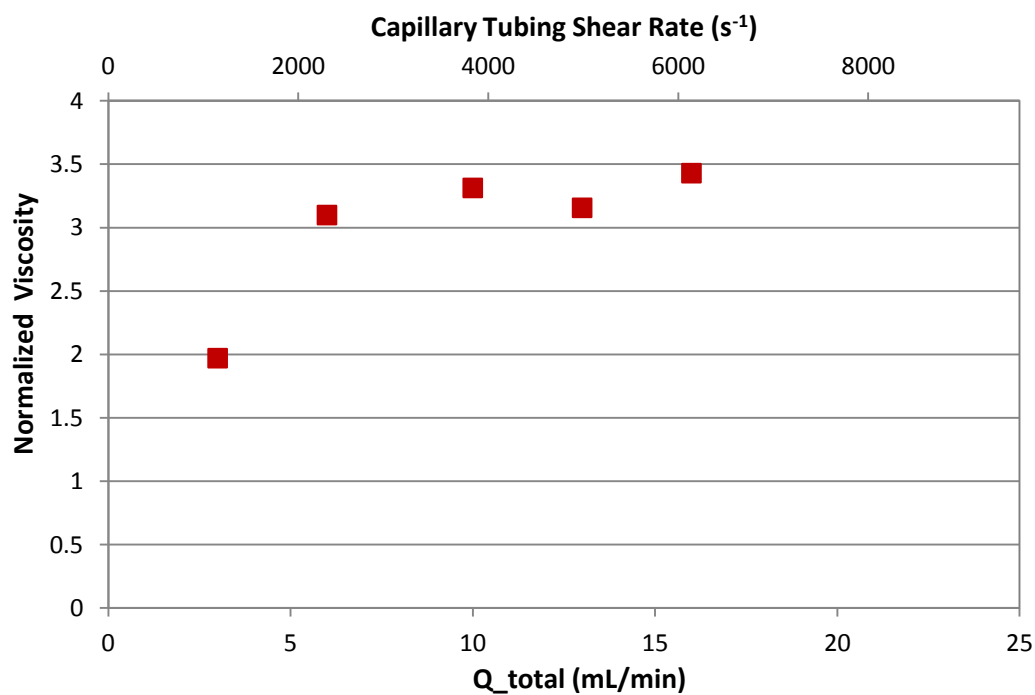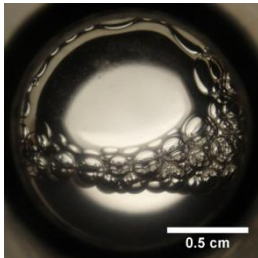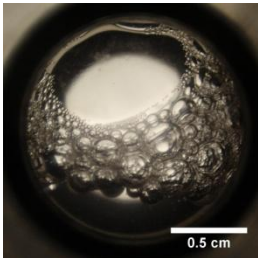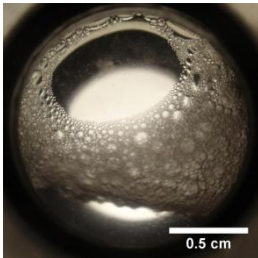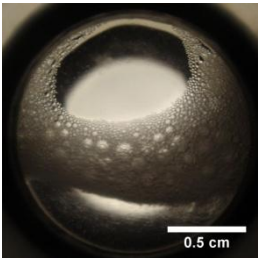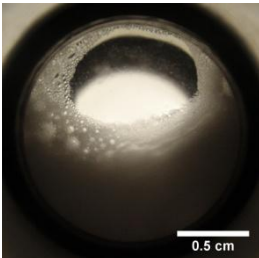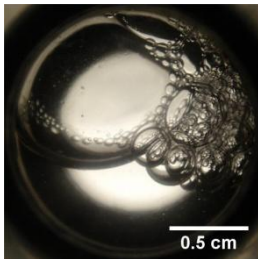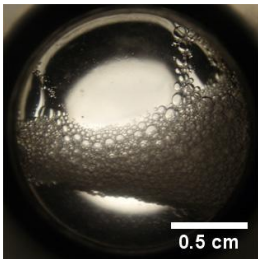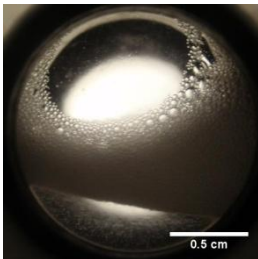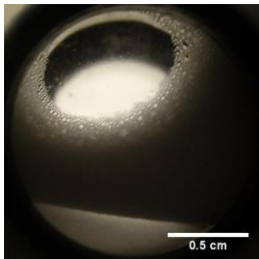
Figure 4.9 - Normalized viscosity measured in the capillary tubing, for experiment F2.

Figure 4.10 - Photographs of the fluid mixture passing through the view cell at different flow rates for fractured Boise corefloods.

Q$_{total}$:	3 mL/min	6 mL/min	10 mL/min	14 mL/min	20 mL/min
Coreflood F1					

				16 mL/min	
Coreflood F2					

4.2.2 Fractured Cement Cores

Fractured cement cores were used to investigate the ability of PEG-coated silica nanoparticles to stabilize a foam by co-injection through a fracture. The permeability of cured cement is in the order of microdarcies, ensuring that the injected fluid flows almost exclusively through the fracture. A 0.96" diameter cement core was prepared using Class H Portland cement and fractured using a load frame at ~14 kN of force. The cement core was then offset vertically by ~0.25" and the extruding ends removed. A 1 wt% dispersion of 3M 5 nm PEG-coated silica nanoparticle was then co-injected with CO_2 at room temperature and 2,040 psia. Tables 4.5 and 4.6 list the experimental conditions and the properties of the fractured cement core used, respectively. A baseline experiment was run using the fractured cement core, whose average permeability was measured to be ~1,640 mD, corresponding to a 72 μm fracture aperture. However, when running the nanoparticle experiment, the measured permeability was reduced to ~956 mD, with an effective fracture aperture of 60.5 μm. This is due to the unloading and loading of the confining pressure that must be done between experiments. For this reason, the mobility reduction factor could not be calculated using the baseline data. Instead, a normalized viscosity with respect to the nanoparticle dispersion is calculated for the fluid mixture passing through the core. This normalized viscosity is calculated by dividing the core pressure drop during the foam experiment by the core pressure drop when injecting only the nanoparticle dispersion (without CO_2); see Appendix C for more details.

Table 4.5 - Summary of experimental conditions used for the fractured cement coreflood
experiment.

Experimental Conditions used for Fractured Cement Cores	
Nanoparticles dispersion	1 wt% 3M 5nm PEG-coated silica nanoparticles in DI water
Temperature	23 °C
Pressure	~2,040 psia
CO_2 density	~0.87 g/mL
Volumetric phase ratio	1 (mL/min CO_2)/(mL/min NP)
Total flow rate	Varied

Table 4.6 - Properties of the fractured cement core used in co-injection experiment, after
loading/unloading cycle.

Experiment	L_{core} (in.)	$\bar{k}$ (mD)	H (μm)	Net P_{conf} (psia)	$F_{fracture}$ (%)
C1	5.24	965	60.5	660	99.9

Figure 4.11 shows the normalized viscosity versus the injected flow rate and shear rate of the fluid mixture flowing through the fracture. At the lowest flow rate tested, a foam can be seen in the view cell (Figure 4.13), with a normalized viscosity of ~1.9 with respect to the nanoparticle dispersion. As the flow rate is increased, a foam with a finer texture is seen in the view cell. However, the measured normalized viscosity in the fracture decreases at the higher flow rates. A possible explanation for the decrease in the normalized viscosity of the fluid mixture is shear thinning of the foam since the shear rates encountered in the fracture are high, as observed with the surfactant-stabilized foams flowing through homogenous fractures (Yan et al. 2006). At present, it is difficult to reach a conclusion regarding this apparent shear-thinning behavior. In addition, foam generation may not be occurring along the entire length of the core, but at certain "low-permeability patches" since a rough walled fracture was used. Figure 4.14 is a photograph

of the disassembled fractured cement core taken 24 h after the coreflood. The dark wetted regions show the flow path of the injected fluid, while the dry regions are most likely the points of contact between the two core halves.
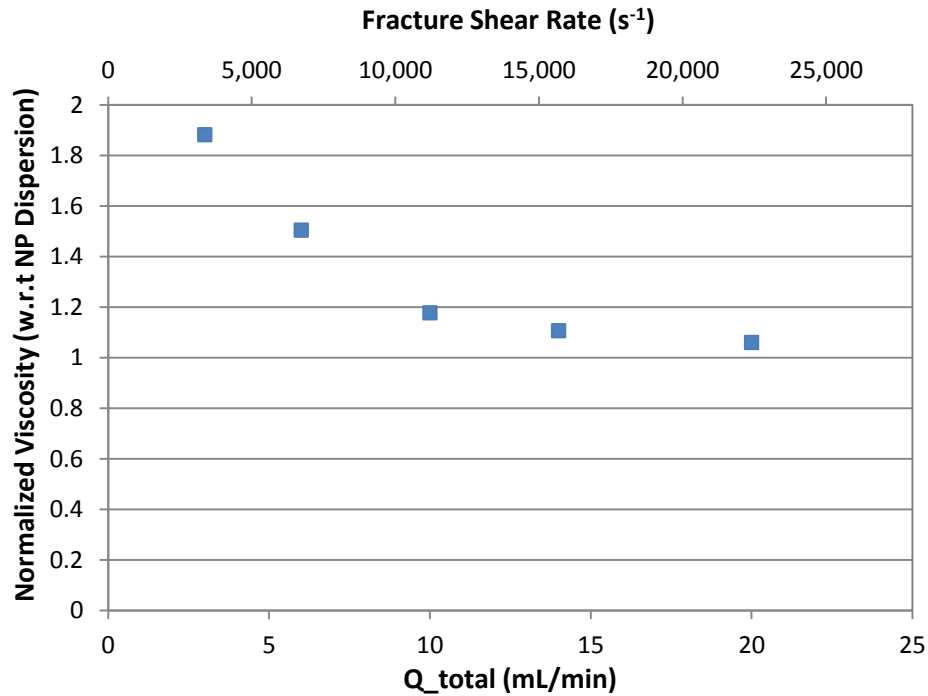
Figure 4.11 - Normalized viscosity of fluid mixture (CO_2 + nanoparticle dispersion) through the fracture vs. injection flow rate and fracture shear rate. The apparent viscosity of the nanoparticle dispersion in the fracture is used to normalize the mixture viscosity.

Figure 4.12 shows the normalized viscosity of the fluid mixture as measured through the capillary tubing downstream of the cement core. The normalized viscosity slightly increases as the flow rate is increased, and then plateaus at approximately 4. This result contrasts from the normalized calculated for the core pressure drop (Figure 4.11). Since it is unclear where along the core's length the foam is generated inside the fracture, the normalized viscosity measurements in the core and in the capillary tubing may not be representing the same type of foam texture. The different trends between the normalized

78

viscosities measured in the fracture and in the capillary tubing could be due to the opposing effects of shear thinning, and improved foam generation at higher shear rates generated in the fracture. The effects of shear thinning may be overcoming the effects of improved foam generation at the higher shear rates through the fracture.
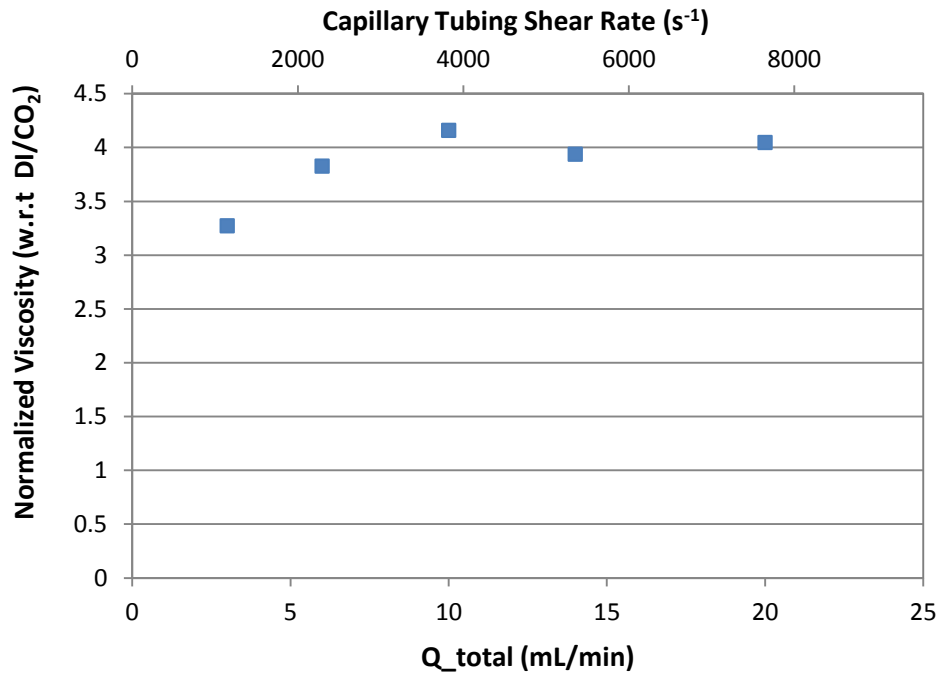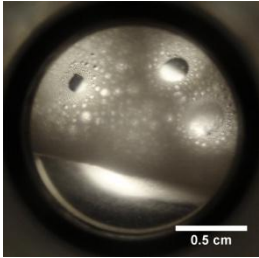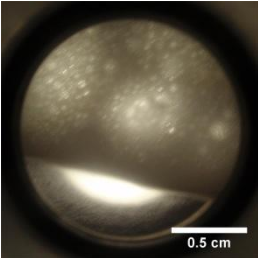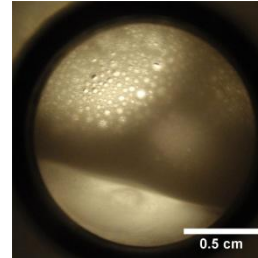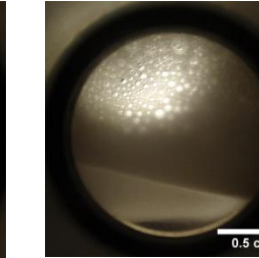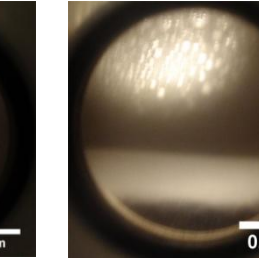
Figure 4.12 - Normalized viscosity of the fluid mixture as measured in the capillary tubing.

Figure 4.13 - Photographs of the fluid mixture passing through the view cell at different flow rates for the fractured cement coreflood.

Q$_{total}$:	3 mL/min	6 mL/min	10 mL/min	14 mL/min	20 mL/min*
Fracture $\dot{\gamma}$ (s^{-1}):	3,360	6,720	11,200	15,670	22,390
Coreflood C1					

*Photograph at 20 mL/min taken at the end of the experiment with no flow.

Figure 4.14 - Fractured cement core C1 showing flow paths (dark regions). Photograph taken after disassembling core less than 24 h after experiment.

4.3 EFFECT OF NANOPARTICLE COATING/SIZE ON FOAM GENERATION

The effects of nanoparticle size and surface coating on CO_2 foam generation was investigated using the beadpack apparatus and procedure described in Section 3.2. In these experiments, a silica nanoparticle dispersion and CO_2 were co-injected into a beadpack filled with 180µm glass beads to generate a foam. The pressure drop measured across a length of capillary tubing attached downstream of the beadpack was used to calculate the normalized viscosity of the fluid mixture, the ratio of the fluid mixture viscosity with and without nanoparticles. A baseline was established by co-injecting CO_2 and DI water through the beadpack and measuring the pressure drop across the capillary tubing. The baseline experiment was run at the same temperature, pressure, flow rate, and phase ratio as the nanoparticle experiments.

Table 4.7 lists the experimental conditions used for supercritical CO_2 beadpack experiments. Most experiments were run at 70 °C and ~1,400 psi, where CO_2 is supercritical. The experiments were run with an injection flow rate of 5 mL/min CO_2, and 1 mL/min dispersion. These flow rates correspond to a shear rate of ~11,000 s^{-1} and a phase ratio of 17.7. The shear rate through the capillary tubing is 7,175 s^{-1} assuming that the temperature of the tubing is the same as that of the submerged beadpack. Table 4.8 summarizes the results of the beadpack experiments using silica nanoparticles.

Table 4.7 - Experimental conditions used in silica nanoparticle/CO_2 co-injection experiments at supercritical conditions.

Experimental Conditions used for scCO$_2$ Beadpack Experiments	
Beadpack temperature	70 °C
Pressure	~1,400 psia
CO_2 density	0.23
Vol. phase ratio*	5 (mL/min CO$_2$)/(mL/min NP)
Vol. phase ratio at beadpack conditions	17.7 (mL/min CO$_2$)/(mL/min NP)
Q_{total}	6 mL/min
Q_{total} at beadpack conditions	18.7 mL/min
Shear rate at beadpack conditions	11,000 s^{-1}

* at accumulator conditions (23.5 °C, 1,400 psia)

Table 4.8 - List of CO_2/ nanoparticle co-injection experiments run through the beadpack. The shear rates shown are for the fluids moving through the beadpack at beadpack conditions. SC: short chain (low molecular weight); LC: long chain (high molecular weight).

Exp.	Nanoparticles	Coating	Conc. (wt%)	T (°C)	P (psia)	Norm. Visc.	Phase Ratio	$\dot{\gamma}$ (s^{-1})
BP1	NexSil 20	None	0.5	70	1400	N/A	17.7	11,000
BP2	NexSil 6	None	0.5	70	1400	N/A	17.7	11,000
BP3	NexSil 20	LC PEG	0.5	70	1400	N/A	17.7	11,000
BP4	NexSil 20	SC PEG	0.5	70	1400	1.45	17.7	11,000
BP5	NexSil 6	SC PEG	0.5	70	1400	2.90	17.7	11,000
BP6	NexSil 6	SC PEG	0.25	70	1450	2.02	17.7	11,000
BP7	NexSil 6	SC PEG	2.0	70	1450	2.45	17.7	11,000
BP8	NexSil 6	SC PEG	0.5	25	1350	1.55	5	3,500
BP9	NexSil 20	SC PEG	0.5	25	1500	1.49	5	3,500

The foam generation abilities of bare silica nanoparticles, NexSil 20 and NexSil 6, were tested. These nanoparticles have a diameter of 20 nm and 6 nm respectively, and are commercially available from Nyacol Nano Technologies Inc. (Ashland, MA). A nanoparticle dispersion of 0.5 wt% in DI water was prepared and co-injected with CO_2 through the beadpack. Pressure drop data is not available for these experiments since a new pressure transducer was being installed. However, no foam was visible in the view cell during the experiments, as shown in Figure 4.15 (NexSil 20 expt., BP1).

Since PEG-coated nanoparticles were found to stabilize CO_2 foams (Espinosa 2011), PEG chains were grafted to the surface of the bare silica nanoparticles by Ki Youl Yoon (University of Texas at Austin, Dept. of Chemical Eng.). The procedure used to coat the nanoparticles yields small volumes of dispersions at low concentrations, which limited the number of experiments and the injection concentrations that can be tested. NexSil 20 bare silica nanoparticles were coated with long chain (LC) PEG polymers (~2,000 g/mol) and were diluted to 0.5 wt% in DI water. The PEG-coated nanoparticle dispersion was co-injected with CO_2 through a beadpack. Pressure drop data is not available for this experiment. However, the view cell shows a poor quality foam with very large bubbles.

The same NexSil 20 bare silica nanoparticles were also coated with short chain (SC) PEG polymers (~350 g/mol). The 0.5 wt% dispersion in DI water was prepared in the same fashion as the LC PEG-coated nanoparticle and the experiment was run at similar conditions. The dispersion co-injected with CO_2 through the beadpack generated a poor foam with a normalized viscosity of ~1.5. Figure 4.15 shows the large droplet size of the generated foam.

The effect of nanoparticle size was investigated by coating NexSil 6 particles, which have a diameter of 6 nm, with the same SC PEG polymers (~350 g/mol). A 0.5 wt% dispersion in DI water was prepared by sonification, and then co-injected with CO_2 at similar conditions as the NexSil 20 experiments. A foam with a normalized viscosity of ~2.9 was generated, and is shown in the view cell in Figure 4.15.

Dispersions of 0.25 wt% and 2 wt% SC PEG-coated NexSil 6 nanoparticles were prepared in DI water and run through the beadpack. These two experiments were run at similar conditions as the above experiments, however with a slightly greater pressure of 1,450 psi. The increase in pressure was not intentional, and is a result of the back pressure relief valve. The 0.25 wt% and 2 wt% dispersions generated foams of ~2.0 and ~2.5 normalized viscosity, respectively. Photographs of the generated foams are shown in Figure 4.15.

Both the NexSil 20 and NexSil 6 bare silica nanoparticles were unable to generate a CO_2 foam by co-injection. However, the PEG-coated version of NexSil 6 particles was able to generate a foam at the same experimental conditions. Bare silica nanoparticles are strongly hydrophilic, and as a result do not have much affinity for the CO_2-water interface. The PEG coating is believed to increase the CO_2-philicity of the particles so that they adsorb onto the interface.

Comparing the results of the experiments run using the SC PEG-coated NexSil 20 and SC PEG-coated NexSil 6, the particle size and wettability have an effect on foam stabilization. The smaller nanoparticles, NexSil 6, stabilize foams with higher normalized viscosity and smaller droplet size. Since the particles were tested at the same wt%, the dispersion with smaller nanoparticles will have a larger number of particles as well as a

83

larger total surface area. This increase in the number of particles and the surface area may explain the better stability seen with smaller particles.

Two experiments, BP8 and BP9, were run with SC PEG-coated NexSil 6 and SC PEG-coated NexSil 20, respectively, at liquid CO_2 conditions. The experimental conditions used in these two experiments are listed in Table 4.9. The two experiments generated a poor foam with large droplet size and a normalized viscosity of ~1.5. Comparing experiments BP8 (supercritical CO_2) and BP5 (liquid CO_2), both of which were run using SC PEG-coated NexSil 6, a more viscous foam with smaller droplets was generated at the supercritical conditions. This is believed to be due to the different shear rates present in the beadpack. At liquid CO_2 conditions, the shear rate in the beadpack is approximately 3,500 s^{-1}, compared to 11,000 s^{-1} at supercritical conditions. The shear rate through the capillary tubing for the experiments done at ambient temperatures is 2,300 s^{-1}.

Table 4.9 - Experimental conditions used in silica nanoparticle/CO_2 co-injection experiments at liquid conditions.

Experimental Conditions used for liquid CO_2 Beadpack Experiments	
Beadpack temperature	23.5 °C
Pressure	~1,400 psia
CO_2 density	~0.83 g/mL
Vol. phase ratio*	5 (mL/min CO_2)/(mL/min NP)
Q_{total}	6 mL/min
Shear rate	3,500 s^{-1}

* at accumulator conditions (23.5 °C, 1,400 psia)

Overall, the *in-house* PEG-coated silica nanoparticles were not able to generate foams with as high normalized viscosity and small droplet size as the PEG-coated 5 nm silica nanoparticles, from 3M, as reported by Espinosa (2011). The length of the PEG chain grafted onto the nanoparticles and the grafting technique seem to be the reason behind the differences seen.

Figure 4.15 - Photographs of fluid mixture flowing through the view cell during beadpack experiments.

BP1	BP3	BP4	BP5

BP6	BP7	BP8	BP9
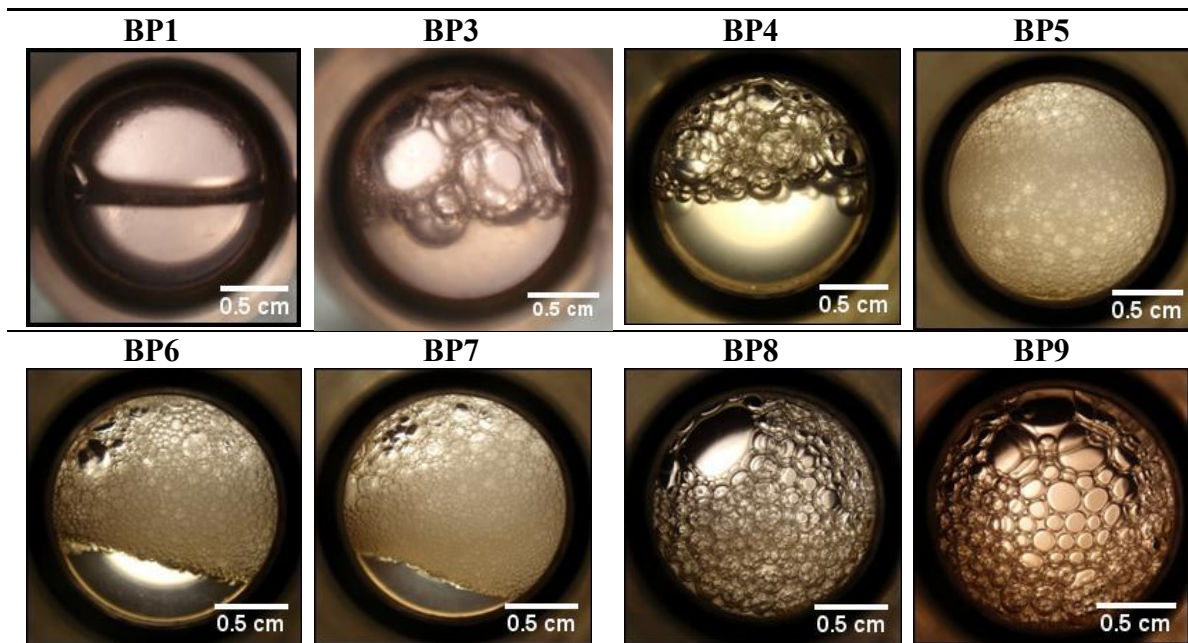
4.4   FLY ASH RESULTS

This section describes the results obtained using fly ash particles to generate emulsions and foams. A series of phase behavior experiments were first carried out using fly ash dispersions and dodecane. These experiments were carried out to test the stability of the emulsions in terms of the fly ash concentration, salinity, and temperature. The existence of a critical shear rate, below which an emulsion is not generated, was investigated by co-injecting fly ash dispersion and dodecane through a beadpack. The ability of fly ash particles to stabilize CO_2-in-water foams by co-injection through a beadpack and by mixing in a high pressure cell was investigated.

4.4.1   Stability of Fly Ash-Stabilized o/w Emulsions

4.4.1.1 Effect of Particle Concentration

The ability of fly ash dispersions to stabilize o/w emulsions was investigated as a preliminary study to CO_2 work. Dodecane was used as a low pressure analog to the CO_2 phase since its density at atmospheric conditions is comparable to that of CO_2 at reservoir conditions. Volumetric phase ratio used is one, unless otherwise specified. Several batches of fly ash samples were received over the time of this study, as described in 3.3.1. Table 3.1 in Chapter 3 highlights the differences between the fly ash batches; particle size distribution data is included in Appendix B.

Batches A and B were received with a high carbon content, relatively large (μm-scale) particle size, and sodium metahexaphosphate as a dispersant. The emulsifying ability of these two batches was investigated by sonifying mixtures of dodecane and the fly ash particles at different particle concentrations. Figure 4.16 shows samples prepared by sonifying 2 mL of dodecane and 2 mL of fly ash dispersion from batches A (top) and B (bottom). The fly ash particles were found to be able to stabilize emulsions with concentrations as low as 500 ppm. At approximately 0.1 wt%, there is a decrease in the volume of emulsion formed, and both dodecane and aqueous excess phases were formed. At low concentrations (<0.2 wt%), there may not be sufficient particles to adsorb onto the

interface to generate the full emulsion phase. For this reason, a concentration of at least 0.2 wt% was used in subsequent experiments.
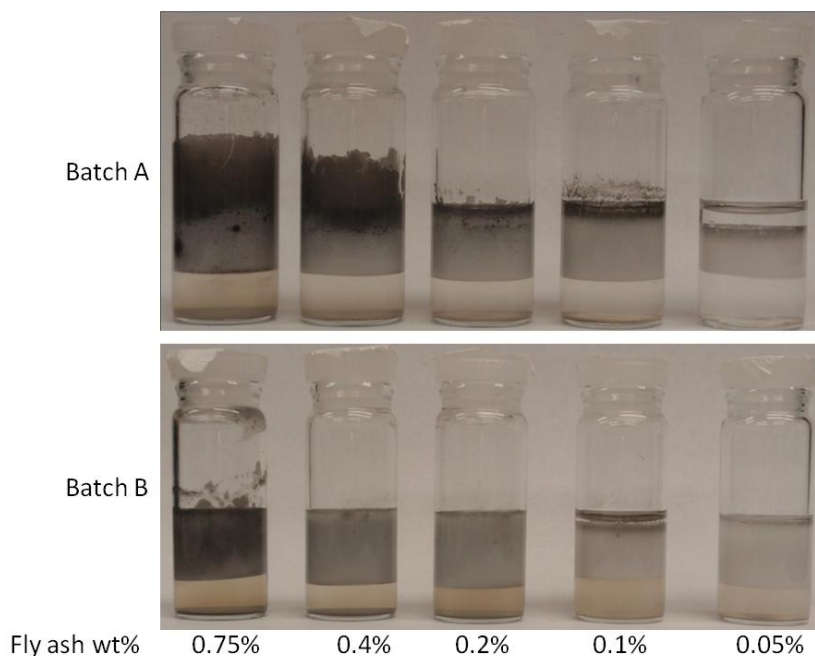
Figure 4.16 - Equal volumes of dodecane and fly ash dispersion of varying concentrations after sonification.

In order to ensure that the sodium hexametaphosphate (SHMP) dispersant used was not responsible for the emulsions observed, a control experiment was carried out. Varying concentrations of SHMP ranging from 0.5 wt% to 10 wt% were dissolved in DI water and placed in a vial with dodecane in a 1:1 volumetric ratio, and sonified for two minutes. Figure 4.17 shows the samples before (top) and after (bottom) sonification. No stable emulsion was formed, demonstrating that the presence of fly ash particles was necessary for emulsion stabilization.
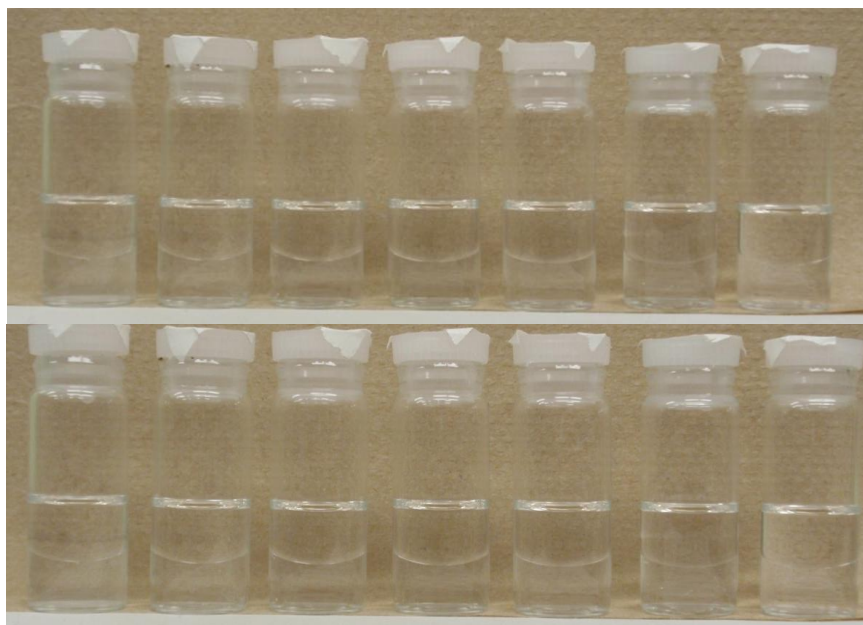
Figure 4.17 - Equal volumes of SHMP solution and dodecane before (top) and after (bottom) sonification. SHMP concentrations range from 0.5 wt% to 10 wt%.

The fly ash particles received in the form of a powder (batch F) were dispersed in DI water at varying concentrations, and then sonified with dodecane. Figure 4.18 shows the samples one day after sonification. The emulsion stabilized at 2.5 wt% was found to be stable over time, and had an average droplet size of approximately 3.8 μm, as shown in Figure 4.19.

0.025%   0.075%   0.25%   2.5%
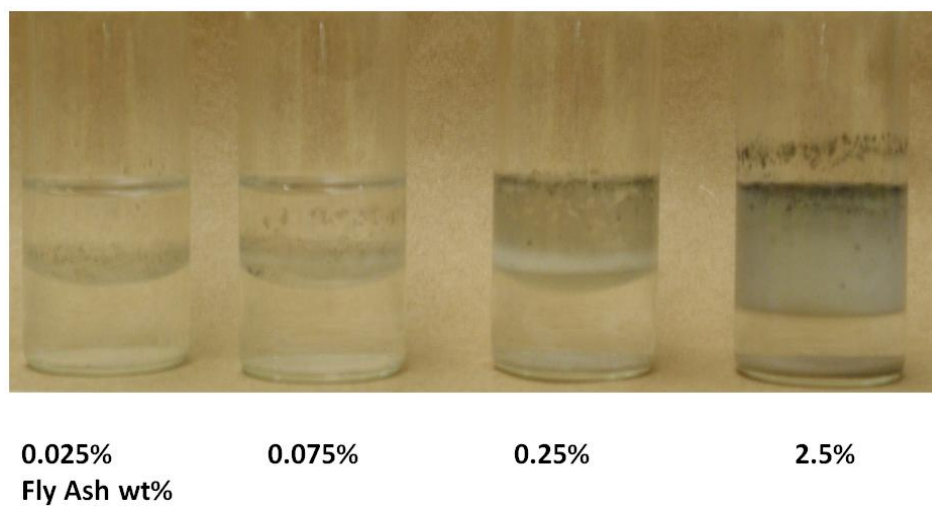
Fly Ash wt%

Figure 4.18 - Concentration scan using fly ash batch F.
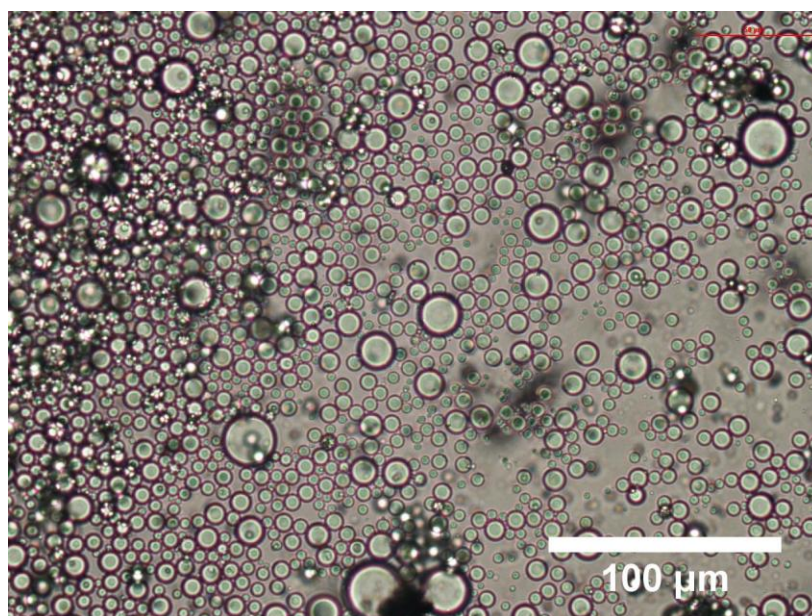
Figure 4.19 - 40× magnification of emulsion extracted from 2.5 wt% fly ash and dodecane emulsion.

4.4.1.2 Effect of Salinity

The fly ash dispersions received were found to be unstable in the presence of salt, suggesting that they are electrostatically stabilized dispersions. At high enough salt concentrations, attractive van der Waals forces overcome charge repulsion and the fly ash particles flocculate and fall out of dispersion. Figure 4.20 shows two 0.75 wt% fly ash (batch B) samples an hour after preparation. The sample on the left was prepared in DI water, while the sample on the right has a salinity of 3 wt% NaCl, which shows flocculation and precipitation in the presence of salt.
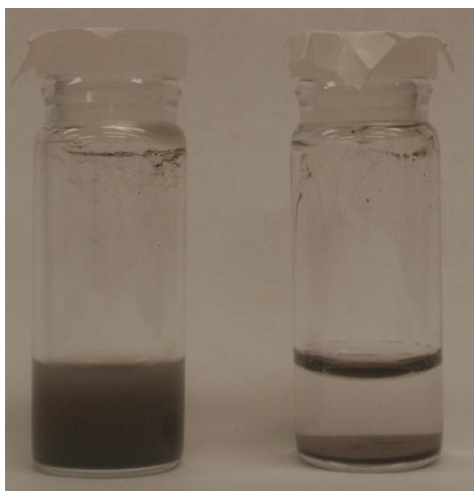
Figure 4.20 - Fly ash particles (0.75 wt% batch B) in DI water (L) and in 3 wt% NaCl brine (R).

The effect of salt on emulsion stability was also investigated. An o/w emulsion was prepared by sonification using 2 mL of dodecane and 2 mL of 0.2 wt% fly ash (batch B) in DI water. 0.5 mL of brine was added to the stable emulsion so that the final salinity was 3 wt% NaCl. The addition of brine destabilized the emulsion almost instantly as shown in Figure 4.21. After some time, the fly ash particles flocculate and fall to the bottom of the aqueous phase. The introduction of salt ions to the emulsion could be causing fly ash particle aggregation, resulting in the removal of particles from the o/w interface. This in turn would cause emulsion destabilization through droplet coalescence.
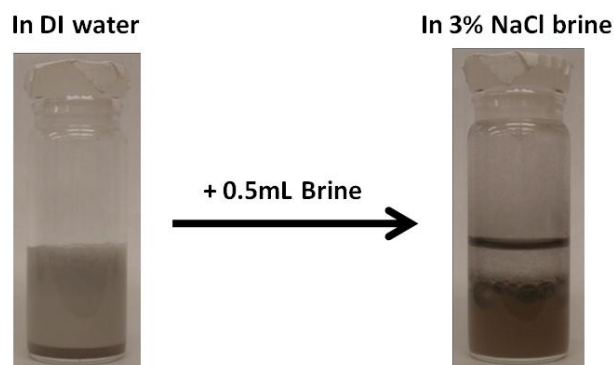
Figure 4.21 - Effect of salt on emulsion stability. Emulsion of 0.2 wt% fly ash and dodecane before and after addition of brine; final aqueous salinity is 3 wt%.

To further investigate the effect of salinity on emulsion stability, a salinity scan was prepared using fly ash particles from batch B, shown in Figure 4.22. These emulsions were prepared by sonifying 2 mL of dodecane and 2 mL of 0.75 wt% fly ash dispersion with varying salinity. A control sample, at the very left of Figure 4.22, was also prepared using DI water. Only the control sample and the sample with 0.1 wt% $CaCl_2$ formed a stable emulsion. Samples of both emulsions were then investigated under a microscope.

| NaCl (%) | 0 | 3 | 1 | 0 | 0 | 3 | 1 |
| CaCl₂ (%) | 0 | 0 | 0 | 0.2 | 0.1 | 0.2 | 0.1 |
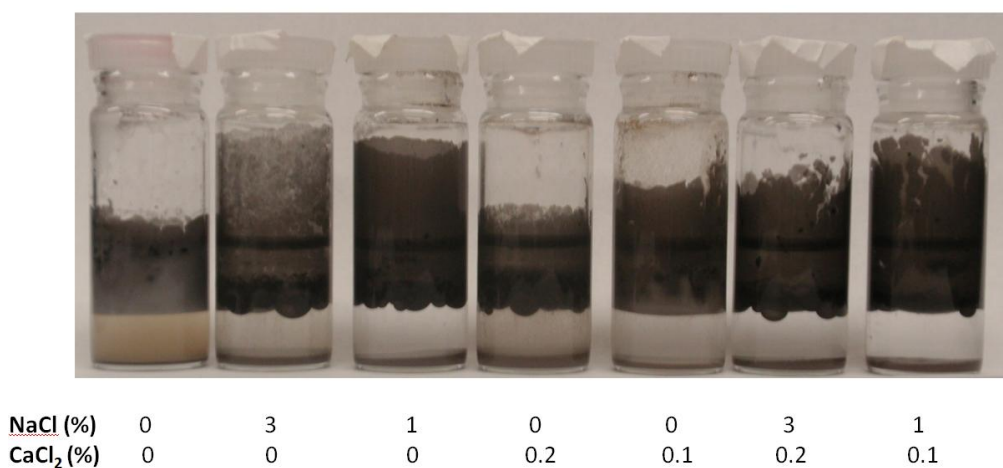
Figure 4.22 - Equal volumes of dodecane and a fly ash dispersion of varying salinity were sonified. Salt concentrations are in weight %.

91

Figure 4.23 compares the emulsion formed in the control experiment (in DI water) to the emulsion formed at 0.1 wt% $CaCl_2$ at 40× magnification. The droplets in the control experiment (0% salinity) are smaller in size and have a more uniform size distribution than those of the emulsion prepared in 0.1 wt% $CaCl_2$. Clumps of what are thought to be fly ash particles can also be seen in the micrograph of the emulsion prepared in 0.1 wt% $CaCl_2$. The presence of salt is believed to be causing fly ash particle flocculation, resulting in less available dispersed particles to adsorb onto the o/w interface. At higher salinities, there is greater particle aggregation resulting in little or no emulsion formation as shown in the salinity scan.
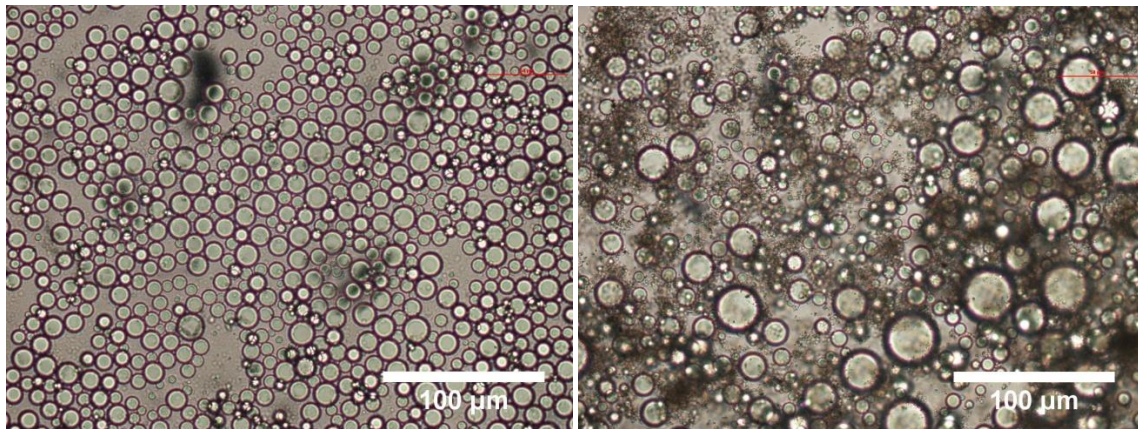
Figure 4.23 - 0.75 wt% fly ash and dodecane emulsion in DI water (L) and in 0.1 wt% $CaCl_2$ brine (R). 40× magnification.

4.4.1.3 Effect of Temperature

The stability of fly ash stabilized o/w emulsions at high temperatures was also tested. Two samples of 0.2 wt% fly ash dispersion (batch B) and dodecane were sonified to generate an emulsion. Both samples, shown side-by-side in each photo of Figure 4.24, were placed in a glass pipettes and sealed using a blow torch to prevent evaporation at high temperature. The control sample (left) was kept at room temperature, while the other sample (right) was placed in a bench top oven for several days at 85 °C. The picture on the left was taken 3 days after sonification. The picture on the right was taken 9 days after sonification. Both emulsions were stable over the 9 day period, however there was some reduction in the volume of emulsion present in both control and experimental samples.
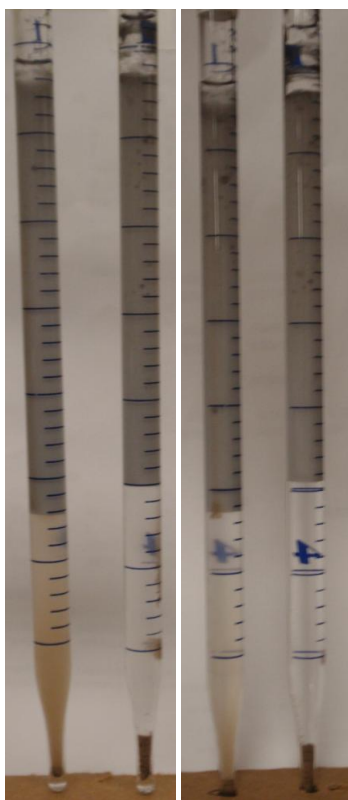
Figure 4.24 - Effect of temperature on fly ash dispersion and dodecane emulsion stability. The control sample (left) was kept at room temperature, while the experimental sample (right) was placed in an oven at 85 °C. From left to right, pictures were taken 3 days, and 9 days after sonification.

93

4.4.2 Fly Ash Critical Shear Rate

Two experiments were carried out to investigate the existence of a critical shear rate to generate fly ash-stabilized o/w emulsions, by co-injection of a fly ash dispersion and dodecane. The first experiment was done using fly ash from batch A, and the second experiment using fly ash from batch C. Both experiments were carried out at ambient temperature and pressure.

Fly ash Batch A was received with a high carbon solid content, and as a result, was not run through the beadpack as received since the large solids particles could plug up the beadpack. A dispersion with lower solid content was prepared using the procedure in Section 3.3.2. 4 mL of fly ash dispersion from batch A was diluted up to 40 mL with DI water, sonified, and then centrifuged to obtain a more stable dispersion with a lower solid content. This process was repeated to get 200 mL of fly ash dispersion, shown in Figure 4.25. The concentration of the fly ash dispersion used is unknown due to the procedure used in preparing the dispersion.

Figure 4.25 - Supernatant obtained after sonifying and centrifuging a fly ash dispersion from batch A.

The prepared fly ash dispersion was then co-injected with dodecane through a beadpack filled with spherical glass beads using the procedure described in Section 3.3.4. During the experiment, the flow rate was gradually increased, and the phase ratio was

varied. The presence of emulsion in the effluent was used to test for the presence of a critical shear rate. Figure 4.26 shows the effluent collected at each flow rate/phase ratio tested. At low shear rates ($<4{,}500$ s^{-1}), there is little or no emulsion in the effluent. At $5{,}250$ s^{-1}, and a phase ratio of 1:1.5 fly ash dispersion to dodecane, some emulsion can be seen in the effluent. As the shear rate is increased to $5{,}850$ s^{-1}, the volume of emulsion in the effluent is increased. The results of this experiment suggest the presence of a critical shear rate that lies between $4{,}500$ s^{-1} and $5{,}850$ s^{-1}.

Figure 4.26 - Effluent collected from a co-injection experiment suggests the presence of a critical shear rate for emulsifying fly ash dispersion and dodecane.

The greatest fraction of emulsion in the effluent was not at the $7{,}000$ s^{-1}, but at $5{,}850$ s^{-1} with a phase ratio of 1:1.5 fly ash dispersion to dodecane. As shown in the emulsions prepared by sonification in the previous section, there is typically an excess aqueous phase suggesting that the optimal phase ratio would have a larger volume fraction of dodecane. This may explain why a larger portion of the effluent is emulsified at the lower flow rate, where a larger volumetric fraction of dodecane to fly ash dispersion is present. Note that the photograph may be deceiving in the quantity of emulsion present; the emulsion tends to form a ring at the interface, which is more apparent in the sample at a shear rate of $5{,}250$ s^{-1}.

95

The emulsions generated in this experiment were not stable over time; the emulsions coalesced within an hour. Before coalescence, a sample of emulsion from the effluent at 5,850 s^{-1} was extracted and studied at 40× magnification. Figure 4.27 shows a comparison between the emulsion generated by co-injection through a beadpack at 5,850 s^{-1} (left) and an emulsion stabilized by sonification (right). Both emulsions were prepared using the same fly ash dispersion and dodecane. The average droplet size of the emulsion generated through the beadpack was ~7.3 μm, while the average droplet size of the sonified emulsion was ~2.2 μm.

Figure 4.27 - Comparison of an emulsion generated by co-injection at 5850 s^{-1} (left) to an emulsion stabilized by sonification (right). 40× magnification.

A second co-injection experiment was carried out using fly ash particles from batch C, which had a smaller average particles size and low carbon content. The fly ash dispersion to be injected was prepared by diluting the fly ash dispersion in DI water to 0.25 wt%. A new beadpack was prepared for this experiment. The fly ash dispersion and dodecane were then co-injected into the beadpack at an increasing flow rate. A phase ratio of 1:1.5 fly ash dispersion to dodecane was used in this experiment, except for the last flow rate tested, which was run at a phase ratio of 1:1 due to pump flow rate limitation. The effluent was inspected for the presence of emulsion to determine the critical shear rate. No emulsion was observed in the effluent until 5,200 s^{-1}, as shown in Figure 4.28. The observed emulsion was not stable, and broke in less than half an hour.

| Phase ratio (FA: Dodecane) | 1:1.5 | 1:1.5 | 1:1.5 | 1:1.5 | 1:1 |

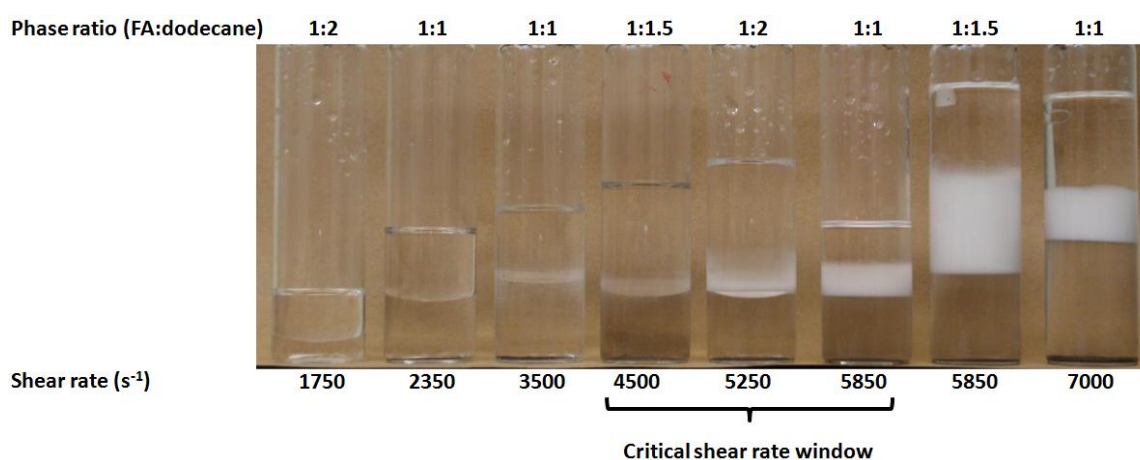| Shear rate (s^{-1}) | 1600 | 2700 | 3200 | 4300 | 5200 |

Critical shear rate window
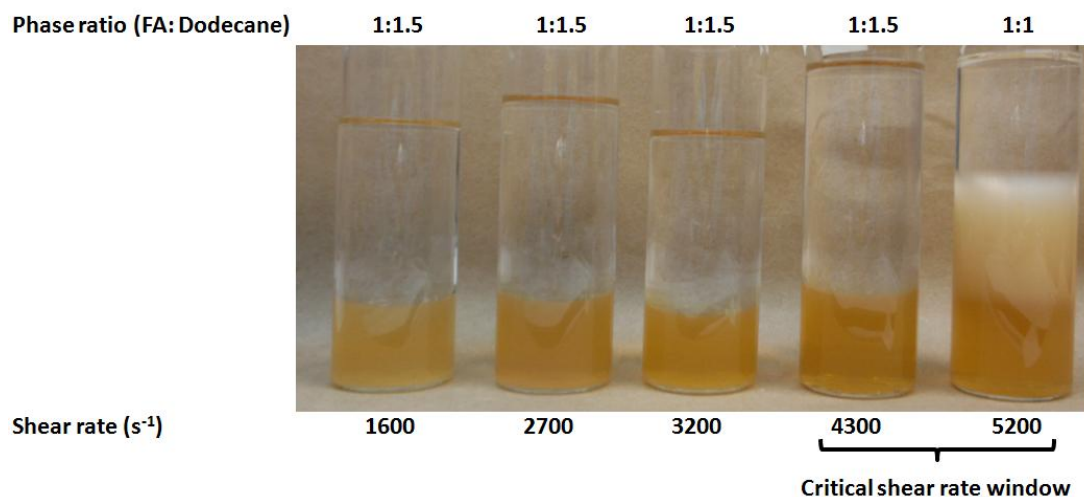
Figure 4.28 - Effluent collected from a co-injection experiment suggests the presence of a critical shear rate for emulsifying fly ash dispersion of 0.25 wt% and dodecane.

A sample of the emulsion was extracted and examined under a microscope before the emulsion completely broke. Figure 4.29 compares the emulsion sample from the co-injection experiment (left) to an emulsion stabilized by sonification (right). Both emulsions shown are at 40× magnification and both emulsions were prepared using the same fly ash dispersion and concentration. The average droplet size of the emulsion prepared by co-injection was 54 µm, while that of the stable sonified emulsion was 2.7 µm.
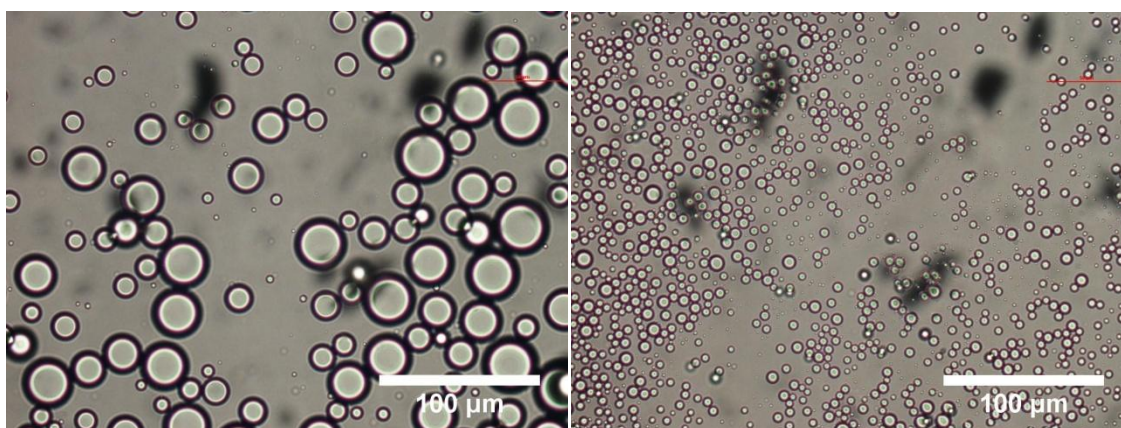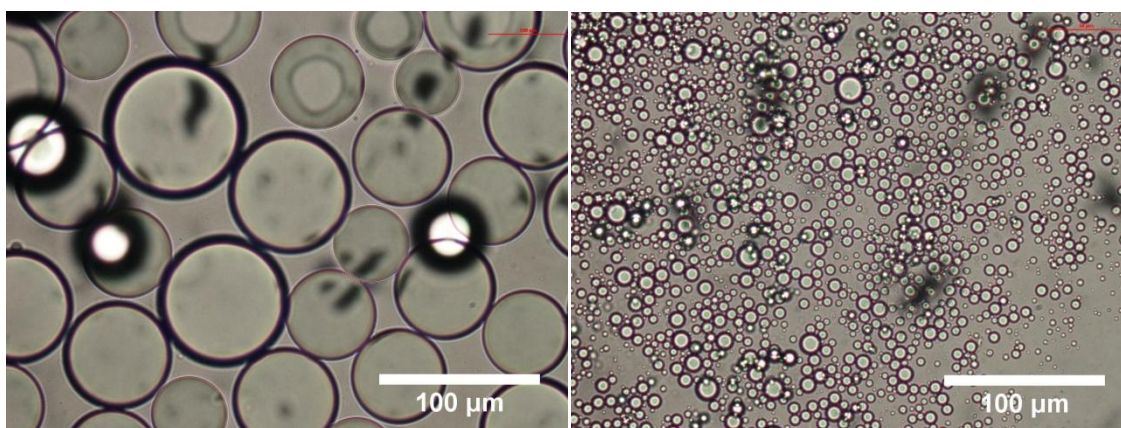
Figure 4.29 - Comparison of an emulsion generated by co-injection at 5,200 s^{-1} (left) to an emulsion stabilized by sonification (right). 40× magnification.

4.4.3 Fly Ash Foam Stabilization

Fly ash particles were shown to be able to generate o/w emulsions by sonification and co-injection through a beadpack. The ability of fly ash particles to stabilize c/w foams was then investigated by both co-injection through a beadpack and by mixing in a pressure cell.

4.4.3.1 Co-injection through Beadpack

Three experiments were run by co-injecting a fly ash dispersion and CO_2 through a beadpack filled with 180 μm glass beads at supercritical CO_2 conditions. The apparatus description and procedure used for these experiments are described in Section 3.2. The three experiments were run at similar conditions, which are summarized in Table 4.10. A temperature of 70 °C, and a pressure of 1,400 psia were used for these experiments. A volumetric phase ratio of 5:1 (CO_2:fly ash) at accumulator conditions (ambient T, 1,400 psia) was used. This translates to a phase ratio of 17.7:1at beadpack conditions (70 °C, 1,400 psia). The total injected flow rate used in these experiments was 6 mL/min at accumulator conditions, translating to 18.7 mL/min in the beadpack. At a flow rate of 18.7 mL/min through the beadpack, the shear rate is 11,000 s^{-1}. The volumetric conversion factor used is calculated based on the CO_2 density at 70 °C (0.233 g/mL), and at ambient temperature (0.825 g/mL). The three experiments were run using different fly ash dispersions in DI water, summarized in Table 4.11.

Table 4.10 - Experimental conditions of fly ash and CO_2 co-injection experiments.

Experimental conditions	
Beadpack temperature (°C)	70
Pressure (psia)	1,400
Vol. phase ratio* (CO_2:fly ash)	5
Vol. phase ratio at beadpack conditions (CO_2:fly ash)	17.7
Q_{total}* (mL/min)	6
Q_{total} (mL/min) at beadpack conditions	18.7
Shear rate at beadpack conditions (s^{-1})	11,000

* at accumulator conditions (ambient T, 1,400 psia)

Table 4.11 - Summary of CO_2 and fly ash co-injection experiments.

	Fly ash wt%	Batch	Preparation	Normalized Viscosity
FF1	N/A	A	Supernatant used after sonifying and centrifuging dispersion	1.07
FF2	0.2 wt%	C	Supernatant used after sonifying and centrifuging dispersion	1.23
FF3	1 wt%	D	Dispersed in DI water using stir bar	1.30

The first experiment was run using the supernatant extracted after sonifying and centrifuging a ~1 wt% fly ash sample from batch A. The exact fly ash concentration of the supernatant is unknown due to the method used to prepare the sample. The co-injection experiment did not result in foam stabilization; the normalized viscosity of the fluid mixture was calculated to be 1.07 with respect to the baseline experiment run at similar conditions. Figure 4.30 (left) is a photograph of the view cell during the co-injection experiment.

The second experiment was run using the supernatant extracted after sonifying a and centrifuging a ~0.5 wt% fly ash sample from batch C. The solid content of the supernatant was measured to be ~0.2 wt% by boiling away the liquid. The co-injection experiment did not result in foam stabilization; the normalized viscosity of the fluid mixture was calculated to be 1.23 with respect to the baseline experiment run at similar conditions. Figure 4.30 (center) shows a photograph of the view cell during the co-injection experiment.

The third experiment performed was run using a 1 wt% fly ash dispersion from batch D. This dispersion was prepared without any centrifuging or sonification. The co-injection experiment did not result in foam stabilization; the normalized viscosity was calculated to be 1.30 with respect to the baseline experiment run at similar conditions. Figure 4.30 (right) shows a photograph of the view cell during the co-injection experiment.
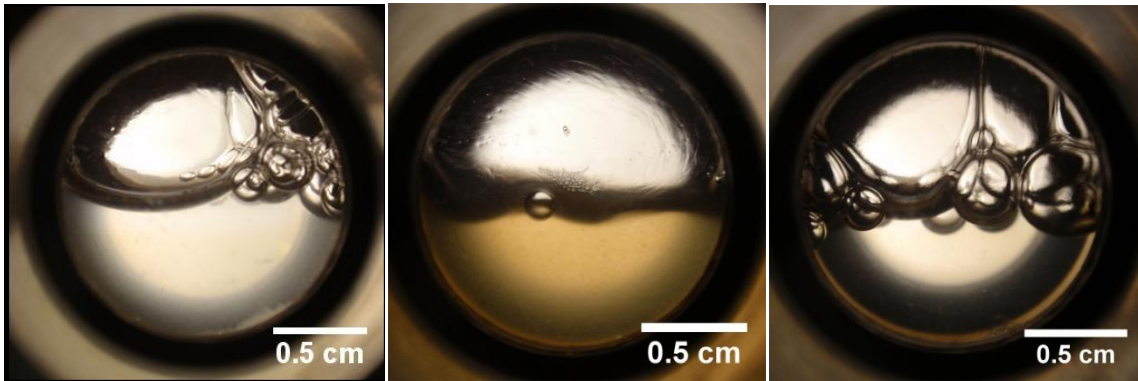
Figure 4.30 - View cell during fly ash/CO_2 co-injection experiments.

The greater than 1 normalized viscosities calculated may be caused by temperature differences between foam experiments and the baseline. Since the capillary tubing in the beadpack set up was only insulated and was not submerged in the water bath, the temperature might vary depending on the length of the experiment. Since temperature affects the viscosity of both water and CO_2 phases, this could affect the pressure drop reading across the capillary tubing. The large bubbles present in the view cell were formed as the fluid moved into the view cell and were not stable.

4.4.3.2 Batch Mixing

Since no foam was generated using fly ash by co-injection through a beadpack, a second method was tested. In this experiment, CO_2 and a fly ash dispersion are loaded into a high pressure view cell and mixed using a stir bar. A stable CO_2 foam was successfully generated using a 1 wt% fly ash dispersion from batch D and CO_2 at 2,500 psi and ambient temperature. The same fly ash dispersion did not generate a foam via the co-injection method at the conditions tested.

The experiment was run by first loading a high pressure view cell with equal volumes of CO_2 and fly ash (at 2,500 psi and room temperature). The contents of the cell were then stirred for approximately 30 minutes. Figure 4.31 shows the CO_2 foam generated immediately after mixing (left) and 18 hours later (right). The foam remained stable for at least 18 hours, before the cell was emptied. This experiment was run by Andrew Worthen (University of Texas at Austin- Dept. of Chemical Engineering).
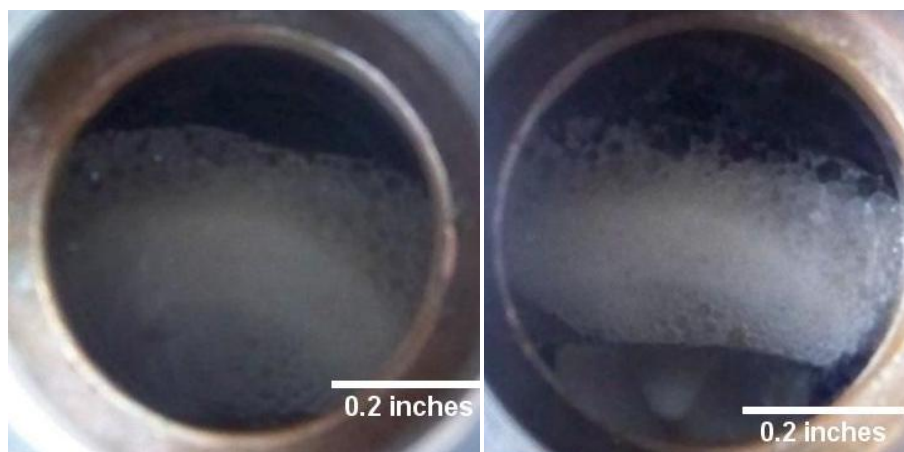

Figure 4.31 - CO_2 foam generated by mixing fly ash dispersion and CO_2 for 30 minutes using a stir bar. The pictures were taken immediately after mixing (left) and 18h after mixing (right).

Both untreated fly ash particles and NexSil 20 bare colloidal silica nanoparticles were unable to stabilize a c/w foam via co-injection through a beadpack. However, the same fly ash dispersion was able to stabilize a foam by mixing in the pressure cell. As a result of this observation, NexSil 20 uncoated silica nanoparticles were then tested using the batch mixing method. The experiment was run at similar conditions as the fly ash batch mixing experiment was. A pressurized cell was loaded with 5 mL of 1 wt% NexSil 20 dispersion in DI water, and 5 mL CO_2 (at 2,500 psi, ambient temperature). The contents of the cell were then stirred for 30 minutes using a stir bar inside the pressure cell. No foam was generated during the experiment. A photograph of the view cell (Figure 4.32) was taken immediately after mixing, however the poor lighting makes it difficult to clearly see the two separate phases present.
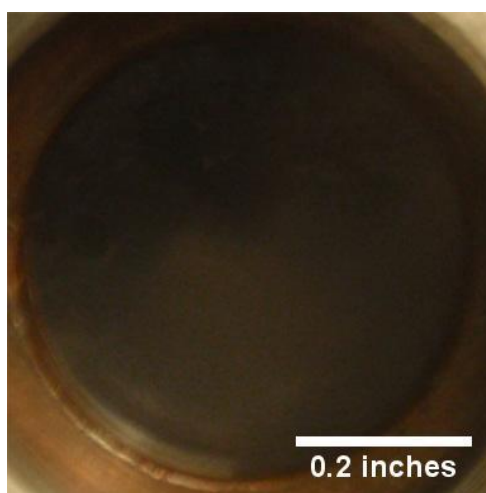
Figure 4.32 - Picture of view cell after mixing liquid CO_2 and 1 wt% NexSil 20 dispersion for 30min. No foam was generated during the experiment. The visible white item is the stir bar used.

At these conditions tested, fly ash particles without any surface treatment were able to stabilize a CO_2 foam, while NexSil 20 bare colloidal silica nanoparticles were not. The fly ash dispersion (batch D) used in this experiment is dispersed in DI water according to the source, and does not contain additives. The ability of the fly ash particles to stabilize a foam without surface treatment may suggest that the particles have some

affinity to the CO_2-water interface, and are less hydrophilic than the bare colloidal silica nanoparticles.

4.4.3.3 Comparing Methods

Since a stable c/w foam only was generated with fly ash particles by mixing in a cell but not by co-injection, the two foam generation methods used were compared. Table 4.12 highlights the key differences between the two methods used to test fly ash dispersions. Both experiments were run using fly ash dispersions of the same concentration and from batch D. A stable CO_2 foam was only generated using the batch mixing method. Possible causes behind this include:

- **Difference in CO_2 densities**: as mentioned in Chapter 2, a larger density difference between the two phases promotes emulsion destabilization, therefore a greater CO_2 density is desired. The batch mixing experiment was run with a CO_2 density greater than 4 times that of the co-injection experiment. As a result, the CO_2 density (0.9 g/mL) in the batch mixer is much closer to that of water.

- **Mixing/residence time**: increasing the amount of time the two phases are in contact and are being mixed might improve the likelihood of particles adsorbing onto the c/w interface. The batch mixing experiment was agitated using a stir bar for around 30 minutes, while the residence time of the fluids passing through the beadpack is less than 2 seconds at beadpack conditions.

- **Mixing method used**: the nature of mixing used is different for the two experiments. In the co-injection experiment, the fluid mixture is sheared through the pore throats and bodies of the beadpack. In the batch mixing experiment, the two fluids are agitated in a bulk vessel.

Table 4.12 - Comparison of co-injection and batch mixing experiments.

	Co-injection through beadpack	Mixing in cell
Pressure (psia)	1,400	2,500
Temperature (°C)	70	24
CO_2 density (g/mL)	0.23	0.90
Water density (g/mL)	0.98	1.0
Residence/ mixing time	1.6 seconds	30 minutes
	No stable foam generated	**Stable foam generated**

Chapter 5: Conclusions and Recommendations

5.1   CONCLUSIONS

- 5 nm PEG-coated silica nanoparticles were found to be able to stabilize CO_2-in-water foams by co-injection through non-fractured Boise sandstone cores. Results indicate the presence of a critical shear rate to generate foams, between core shear rates of 460 s^{-1} and 1,145 s^{-1} at the conditions tested.

- Stable CO_2-in-water foams were generated when dispersions of 5 nm PEG-coated silica nanoparticles and CO_2 were co-injected through fractured sandstone cores. Results suggest the presence of a critical shear rate, although the value was not established.

- Stable CO_2-in-water foams were generated by co-injecting 5 nm PEG-coated silica nanoparticles and CO_2 through fractured cement cores at shear rates as low as 3,360 s^{-1} through the fracture. The presence of a critical shear rate for foam generation by co-injection through a fracture is still unknown.

- The coating of nanoparticles was found to be critical to foam stabilization. Bare silica nanoparticles did not stabilize a foam either by co-injection or by mixing in a pressure cell. Silica nanoparticles with an in-house PEG polymer coating did not perform as well as 3M's 5 nm PEG-coated nanoparticles.

- Fly ash particles without surface treatment were found to stabilize o/w emulsions with concentrations as low as 500 ppm by sonification. Fly ash dispersions and emulsions were stable at temperatures up to 85 °C, but not stable in the presence of salt.

- Fly ash particles without surface treatment were able to generate an o/w emulsion by co-injection through a beadpack. A critical shear rate for emulsification was found to be around 5,000 s^{-1}. However, the emulsions generated were found to be unstable and the droplets coalesced within an hour.

- Fly ash particles without surface treatment were found to be able to stabilize CO_2-in-water foams by mixing in a batch reactor at liquid CO_2 conditions. The same fly ash particles were unable to stabilize a CO_2 foam by co-injection through a beadpack at supercritical CO_2 conditions.

5.2 FUTURE WORK

Critical shear rate through a fracture

The work done in this thesis shows that it is possible to generate a CO_2-in-water foam using PEG-coated silica nanoparticles by co-injection through fractured Boise and fractured cement cores. Whether a critical shear rate exists for foam generation in a fracture remains unknown.

Potential work that can be done to investigate the presence of a critical shear rate is to run numerous fractured cement corefloods to test behavior in a range of fracture apertures. There is some difficulty in maintaining the same fracture aperture between the baseline and foam experiments using the same core. It may be possible to preserve the fracture aperture by maintaining the system pressure at the end of the baseline experiment. Since the confining pressure and pore pressure are kept constant, and the core is not moved, the fracture aperture should ideally remain the same size. In order to run this experiment, an extra 2-way valve must be added at the outlet of the nanoparticle injection pump. This isolates the fractured core system from the pump, allowing the replacement of the DI water in the pump with a nanoparticle dispersion, thus without disturbing the pressure state of the fracture. Once the nanoparticles have been loaded, the pump should be operated to pressurize the line upstream of the valve before resuming the experiment. A check valve should also be added at the ISCO pump's outlet and

downstream of the CO_2 accumulator. In order for this experiment to be successful, the larger waste accumulator should be used. This procedure should only be done using a cement core, since it is not necessary to vacuum and re-saturate it between experiments.

Another method to characterize foams in a fracture would be to use an artificial fractured core made of steel, or aluminum. A 12" or 6" long core can be machined out of stainless steel or aluminum in the machine shop, as shown in Figure 5.1. For a given fracture aperture, there is a range of shear rates achievable by changing the injection flow rate. However, it may be possible to modify the artificial fracture's aperture by layering thin pieces of steel or aluminum over the machined down area. The added pieces will have to be epoxied or glued to prevent fluids from flowing through it. Some agitation may also be introduced to the artificial fracture in the form of beads or sand to evaluate the benefit of having some tortuosity in the flow path.
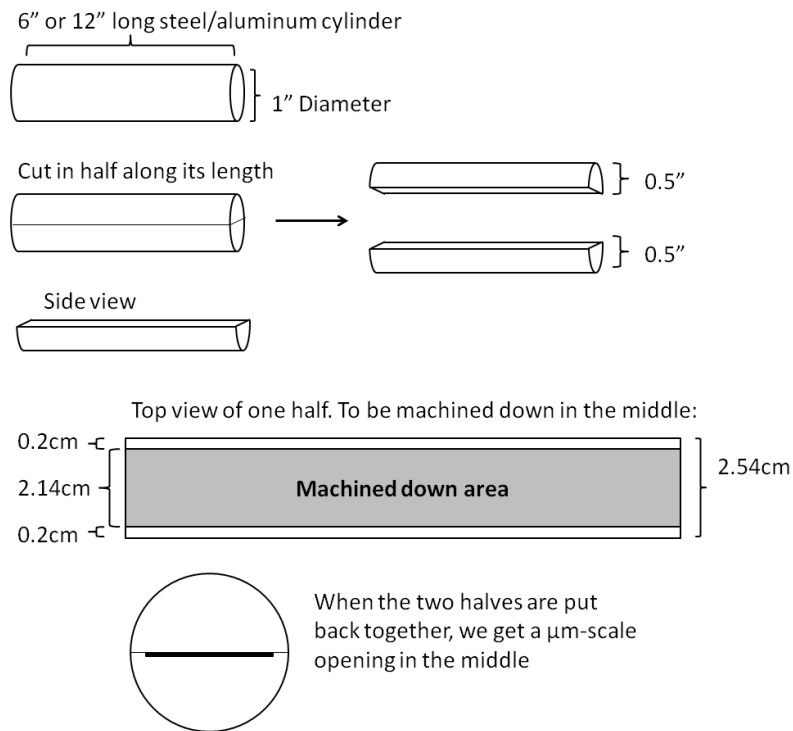

Figure 5.1 - Artificial fractured core schematic.

Critical shear rates of other rock types

Using Boise sandstone cores, this work demonstrated the generation of a stable foam above a certain shear rate range. It would be useful to know whether the shear rate found for Boise sandstone is applicable to other rock types, such as Berea sandstone (~120 mD) or Texas cream limestone (~10 mD). Because of the low permeability of Texas cream limestone, some modifications to the experimental set up may be necessary. The pressure transducers will have to be recalibrated to read a higher pressure drop. Since high shear rates will be achievable with low injection flow rates, it may be necessary to replace the spring loaded back pressure relief valve with a nitrogen dome loaded back pressure regulator. The N_2 BPR works better for low flow rates, and may eliminate the need for a waste accumulator with the installation of an inline filter.

The use of pressure taps along the core's length

The current experimental set up allows us to only measure the pressure drop across the entire length of the core. It would be useful to have pressure drop measurements along the length of the core to provide some insight on how the foam is generated within the core. It could provide information on how fast a foam is stabilized and whether residence time has an effect on the foam generated.

Injecting pre-generated foam into core

The use of a beadpack as a foam generator upstream of the core holder would help us understand how nanoparticle-stabilized foams behave in both rock matrix and fractures. Combined with the use of pressure taps, it would also provide information on whether a pre-generated foam would deteriorate, improve, or remain unchanged as it flows through rock matrix or a fracture.

Foam optimization

The work done in this thesis did not attempt to optimize conditions for foam viscosification. The effects of phase ratio, temperature, nanoparticle concentration, and

salinity were investigated for beadpack experiments by Espinosa (Espinosa 2011). However, it is unknown whether the effects of these parameters on foam generation still apply to foam generation within cores or fractures.

The use of other foaming agents

This work and the work by Espinosa (2011) have focused primarily on the use of PEG-coated silica nanoparticles for foam generation. The ability of other foaming agents to stabilize CO_2 foams should also be investigated. The use of nanoparticles-surfactant mixtures has been shown to generate stable CO_2 foams by Binks et al. (2008). Silica nanoparticles on their own were found to be too hydrophilic for foam stabilization, and surfactant stabilized foams were found to be unstable over time (less than a day at all concentrations tested). In these nanoparticle-surfactant mixtures, the synergism leads to improved foam stability at intermediate surfactant concentrations. The adsorption of surfactants onto the nanoparticle surface makes them interfacially active, resulting in the generation of stable foams.

Appendix

A.1   PREPARING NON-FRACTURED CORES (NON-CEMENT)

To prepare non-fractured cores, the core is first aligned with the core holder end platens. If a 6" core were used, then two 3" long aluminum spacers are placed in line with the core and the end platens. The core, spacers (if necessary), and end platens are then loaded into a heat shrinkable FEP tube that is slightly larger than 1" in diameter. The heat shrink tubing should only extend ~1/4" onto the machined-down portion of platens.

A heat gun or oven (200 °C) can then be used to shrink the tubing until becomes completely tight. Any excess heat shrink tubing extending over the non-machined down portions of the end platens are then cut off. The end platens were then pulled out of the heat shrink tubing. The prepared core was then vacuumed for a day to remove any trapped air. DI water was then introduced into the vacuumed vessel until the core was submerged by switching a 3-way valve. The vessel containing the submerged core was then vacuumed for 6 hours to ensure there is no trapped air left. Note that it is important to heat shrink wrap the cores before saturating them with water, otherwise the presence of water vapor due to heating results in a non-uniform heat shrink tubing.

A.2   PREPARING FRACTURED CORES (NON-CEMENT)

The following procedure should be used in preparing fractured sandstone or carbonate cores. Due to the size of the load frame plate and difficulties in fracturing cores, it is recommended to use a 6" long or shorter core. After baking the core and cutting it to the desired length, the core is then loaded into a heat shrink tubing of its length. The heat shrink tubing provides confining pressure which helps prevent crumbling and crushing while fracturing the rock.

Figure A.1 - Boise sandstone core in FEP heat shrink tubing.

The core and heat shrink tubing are then placed in the oven at ~200 °C to activate the heat shrink tubing. Note that if the core is not completely dry, water vapor may cause the heat shrink tubing to be uneven.

Figure A.2 - Boise sandstone core in FEP heat shrink tubing after placing in oven at 200 °C to activate heat shrink tubing.

A conventional load frame was used to fracture the cores by providing an axial force causing failure under tension along the length of the core. This provides a more natural, rough-faced fracture compared to cutting or sawing the core along its length.

Figure A.3 - Load frame used to fracture cores.

The wrapped core can then be placed in the load frame, ensuring that the entire length of the core is under the top load frame plate.
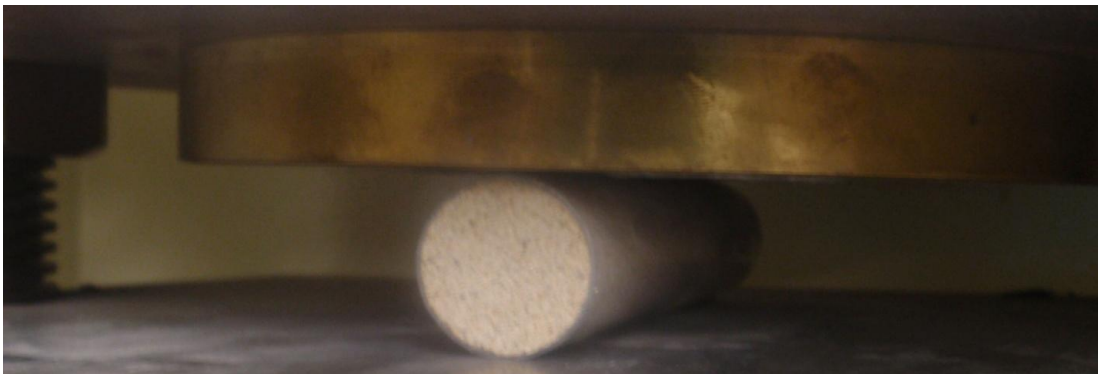

Figure A.4 - Boise sandstone core with heat shrink tubing placed in load frame.

The load frame should be set to run on high compressive load, with a loading rate of 1,000 psi/min. Run the load frame using the 'set' button to raise the bottom plate until the core makes contact with the top plate. Then run the load frame using the 'run' button until the core fails in compression. The 'run' button should be released the instant the core is fractured to prevent further crushing. Boise sandstone cores fail at approximately 20 kN of load.
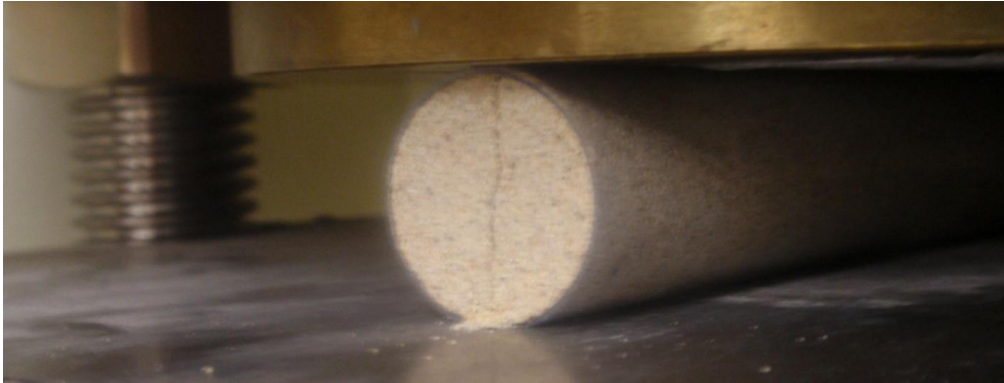

Figure A.5 - Boise sandstone core with heat shrink tubing after fracturing in load frame.

After fracturing the core, the load frame should be run on 'release' until the core can safely be removed from the load frame. A scalpel is then used to carefully cut the heat shrink tubing and the fractured core can be extracted. The fractured core must be handled with care to prevent crumbling.

Figure A.6 - Boise sandstone core after fracturing showing rough walled fracture.

The two core halves should then be fitted back together and coated with PTFE tape. This makes handling the core easier and prevents the cores from offsetting while loading into the core holder.

Figure A.7 - Both ends of a fractured sandstone core wrapped with PTFE tape.

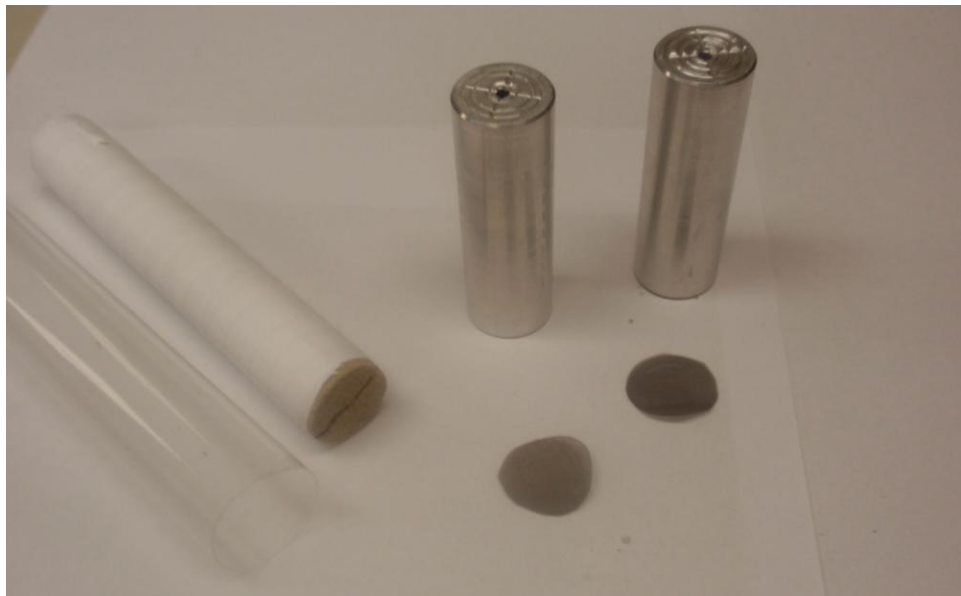Two circular pieces of mesh are used to prevent sand from flowing into the system.

Figure A.8 - Fractured core, spacers, mesh pieces, and shrink wrap tubing used to prepare core before loading into core holder.

The fractured core is then aligned with the spacers and placed in heat shrink tubing, with the pieces of mesh sandwiched between the core and spacer at both ends. The heat shrink tubing used should be ~0.5" longer than the length of the core and spacers to accommodate the core holder end cap platens. In order to prevent the extended ends of the shrink wrap from shrinking, a spacer (such as a 0.5" long core) should be placed at both ends when loading into an oven.

Figure A.9 - Fractured core is placed between the two spacers, and the pieces of mesh are sandwiched between the core and spacer on both sides. The segment is then placed inside heat shrink tubing of slightly greater length.

The prepared core (and spacers) is then placed in the oven at ~200 °C to activate the heat shrink tubing.

Figure A.10 - Fractured core and spacers after placing in oven to activate heat shrink tubing.

After the heat shrink tubing has been completely tightened, the core will have to be vacuumed overnight to remove trapped air. After vacuuming, the vacuum container is

then filled with water until the core is completely submerged. The vacuum pump is then run for an additional 6 hours until no more air bubbles are seen.

While loading the core into the core holder, the platens of both core holder end caps must be fitted into the extensions of the heat shrink tubing as shown in the following picture. This prevents the injected CO_2 from contacting the rubber sleeve.

Figure A.11 - Fractured core and spacers connected to the core holder end caps before loading into core holder.

A.3   PREPARING FRACTURED CEMENT CORES

Some experiments were carried out using fractured cement cores. Cement cores were prepared using class H Portland cement in the cement laboratory, courtesy of Dr. Paul Bommer. The procedure used is as follows:

1. Measure 1 parts tap water, and 2.63 parts class H Portland cement by mass. Make sure the total volume is not larger than the mixer container.
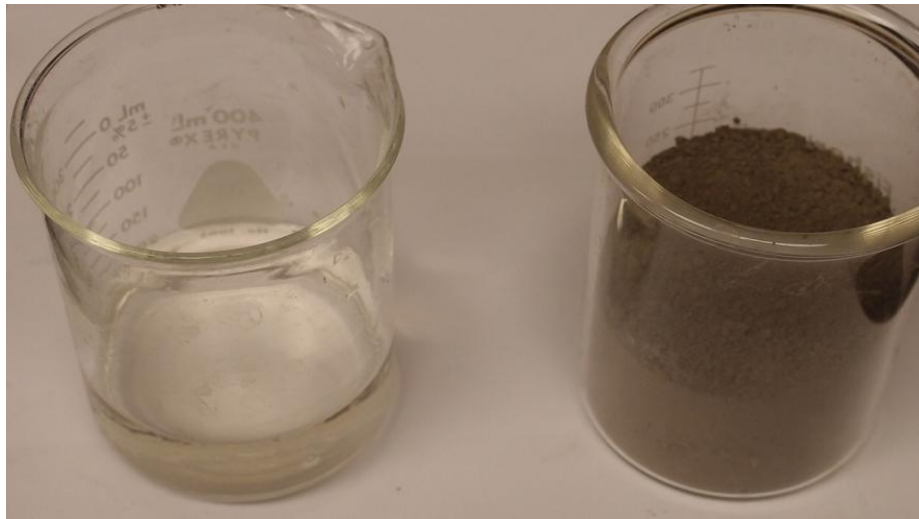
Figure A.12 - Tap water (left) and Portland cement (right) before mixing.

2. Place water in the mixer, cover the top, and run at 4,000 rpm (Figure A.13L).

3. Slowly pour the cement into the running mixer containing water.

4. Cover the top, and increase mixing rate to 12,000 rpm.

5. Run at 12,000 rpm for approximately one minute, and then turn the mixer off.

6. Pour cement mixture into plastic molds and cap (Figure A.13R).

Figure A.13 - Industrial mixer used to mix cement (left). Cement mixture poured into plastic tube molds (right).

7. Allow cement cores to cure for two days at room temperature.

8. Carefully remove the plastic mold using a box cutter.

9. Cure the cement core in the oven for another day at 60 °C. The plastic tube mold should not be placed in the oven. This step is done to speed up the curing process; the cores can be cured at room temperature for several days instead.

Figure A.14 - Cement core after curing in an oven at 60 °C for a day.

10. Place cement core in heat shrink tubing, and activate the heat shrink tubing by baking in an oven at 200°C for around 10 minutes.
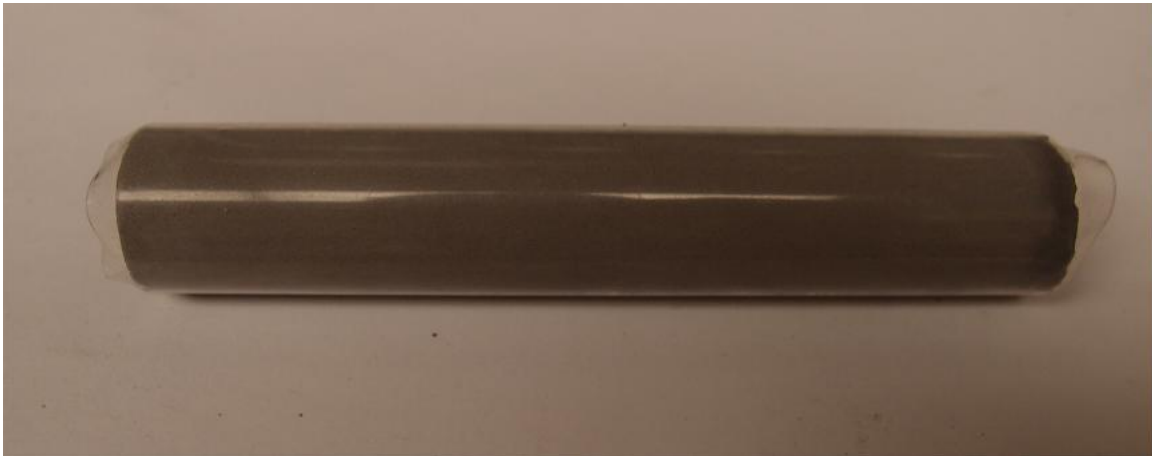
Figure A.15 - Cured cement core in heat shrink tubing after activating heat shrink tubing in oven at 200 °C.

11. Fracture cement core using the load frame; cement cores were found to fracture with approximately ~14 kN of force. Detailed description of operating the load frame can be found in appendix A.2.

Figure A.16 - Cured cement core before (left) and after (right) fracturing using conventional load frame.

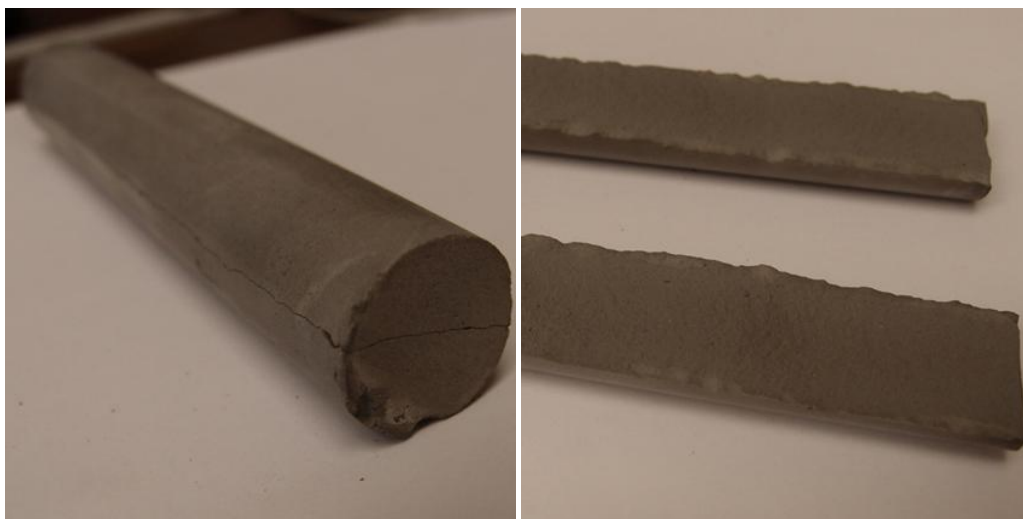12. Carefully cut heat shrink tubing and extract the fractured cement core.

Figure A.17 - Fractured cement core showing the rough walls of the fracture.

13. Offset the fractured core halves vertically by approximately 0.25". Mark the protruding ends of the core halves to be filed or sawed off. Rubber bands were used to make the core easier to handle.

Figure A.18 - Fractured cement core halves offset vertically by ~0.25".

14. Cut or file off the extended ends of the fractured core to get a smooth, flat core end.

Figure A.19 - Fractured cement core with protruding ends filed off. Both core halves are of the same length.

15. Wrap the fractured cement core with PTFE tape to hold the core halves together.

Figure A.20 - Fractured cement core held together by wrapping with PTFE tape.

16. Place fractured core and aluminum spacers inside heat shrink tubing, with circular pieces of mesh sandwiched between the spacer and core at both ends.

Figure A.21 - Fractured cement core, aluminum spacers, pieces of mesh, and FEP shrink wrap tubing used to prepare the core to be loaded.
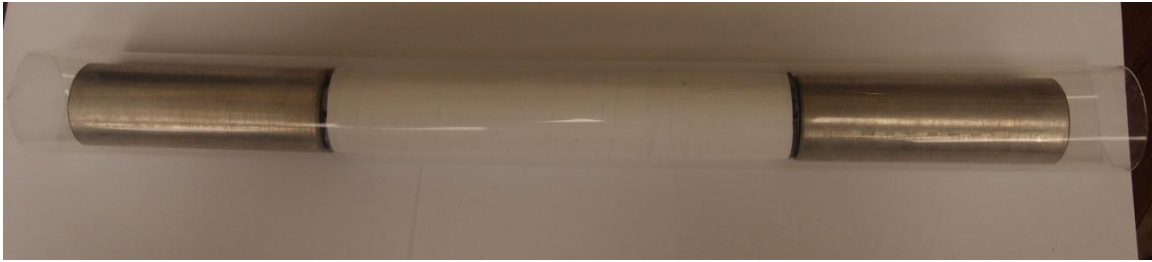
Figure A.22 - Fractured cement core, mesh, and spacers placed in heat shrink tubing.

17. Activate heat shrink tubing by baking in an oven at 200°C for around 10 minutes.
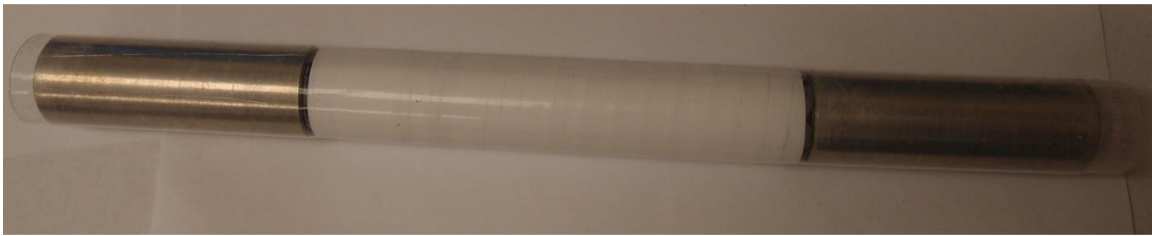
Figure A.23 - Fractured cement core, mesh, and spacers after activating heat shrink
tubing in an oven at 200 °C.

18. Core holder end platens can then be inserted into the protruding ends of the heat
shrink tubing so that the excess tubing can be cut off.
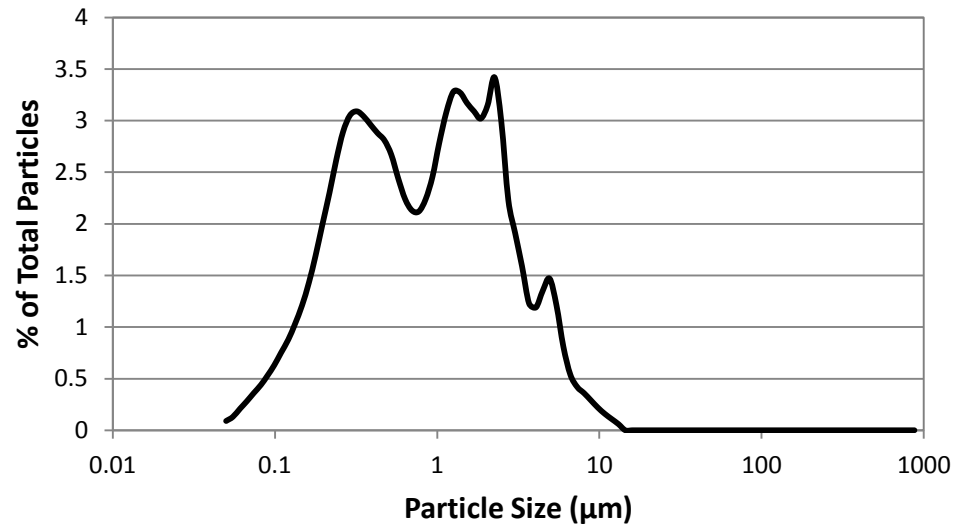
Figure B.1 - Particle size distribution for fly ash batch A.
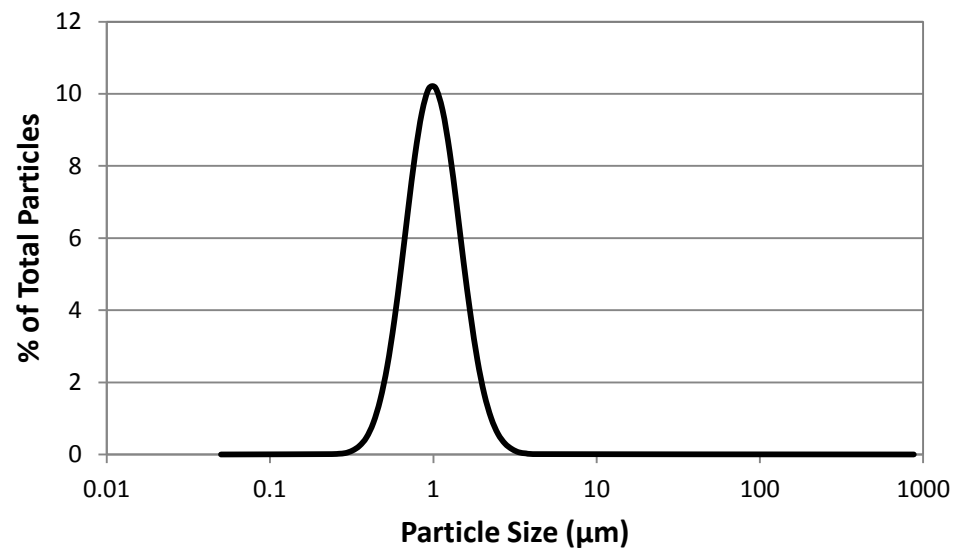
Figure B.2 - Particle size distribution for fly ash batch B.
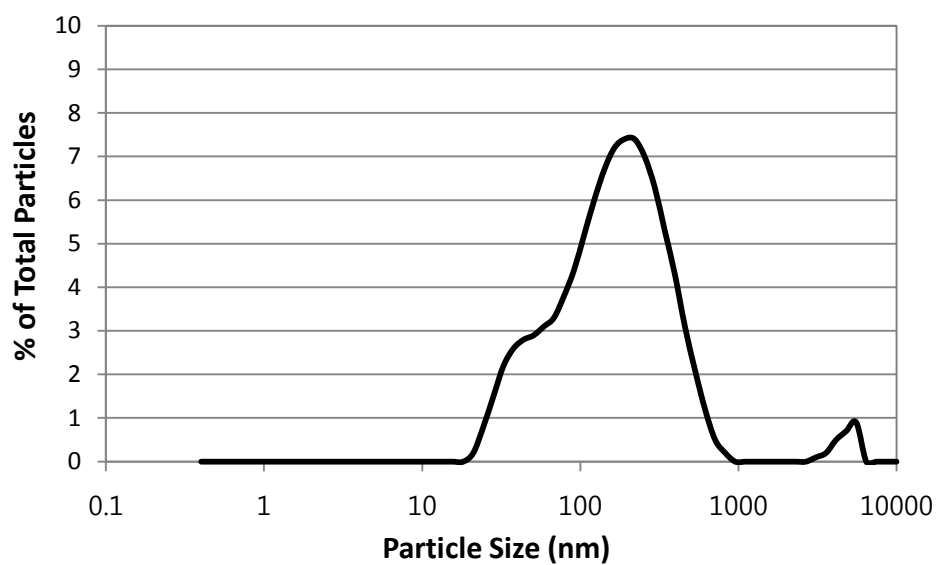
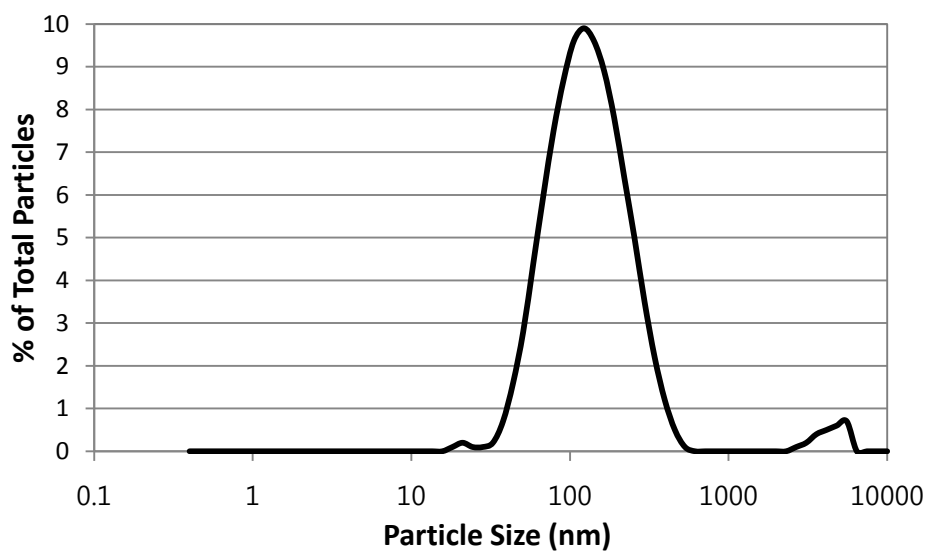Figure B.3 - Particle size distribution for fly ash batch C.

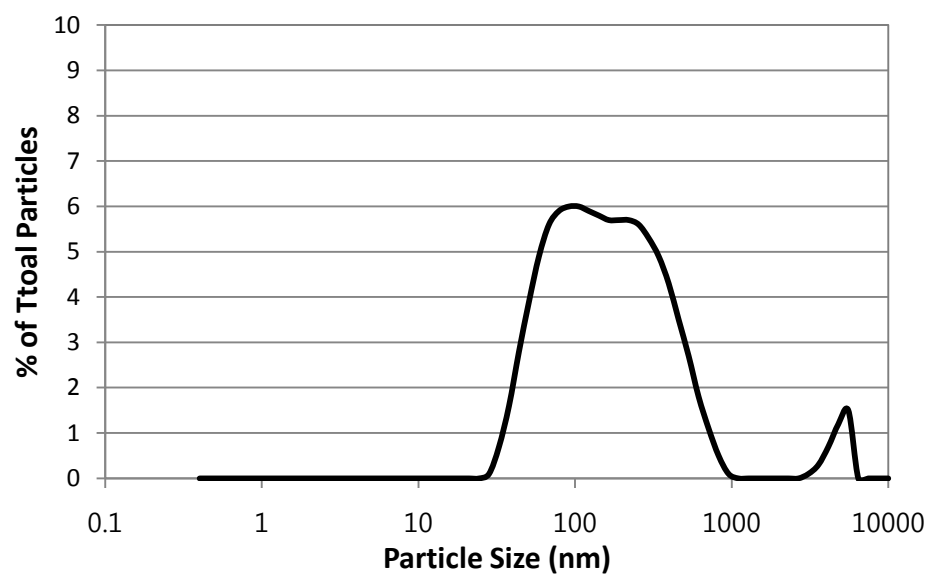Figure B.4 - Particle size distribution for fly ash batch D.

Figure B.5 - Particle size distribution for fly ash batch E.

C.   COREFLOOD EXPERIMENTS

Coreflood B1

A baseline experiment and a foam experiment were run using an 11.8" long non-fractured Boise sandstone core at ambient temperature and a pressure of ~2,000 psia. The foam experiment was run using a 1 wt% dispersion of 5 nm PEG-coated silica nanoparticles in DI water. The pressure drop measurements across the core and capillary tubing for both experiments are plotted in Figures C.1 and C.2, respectively.
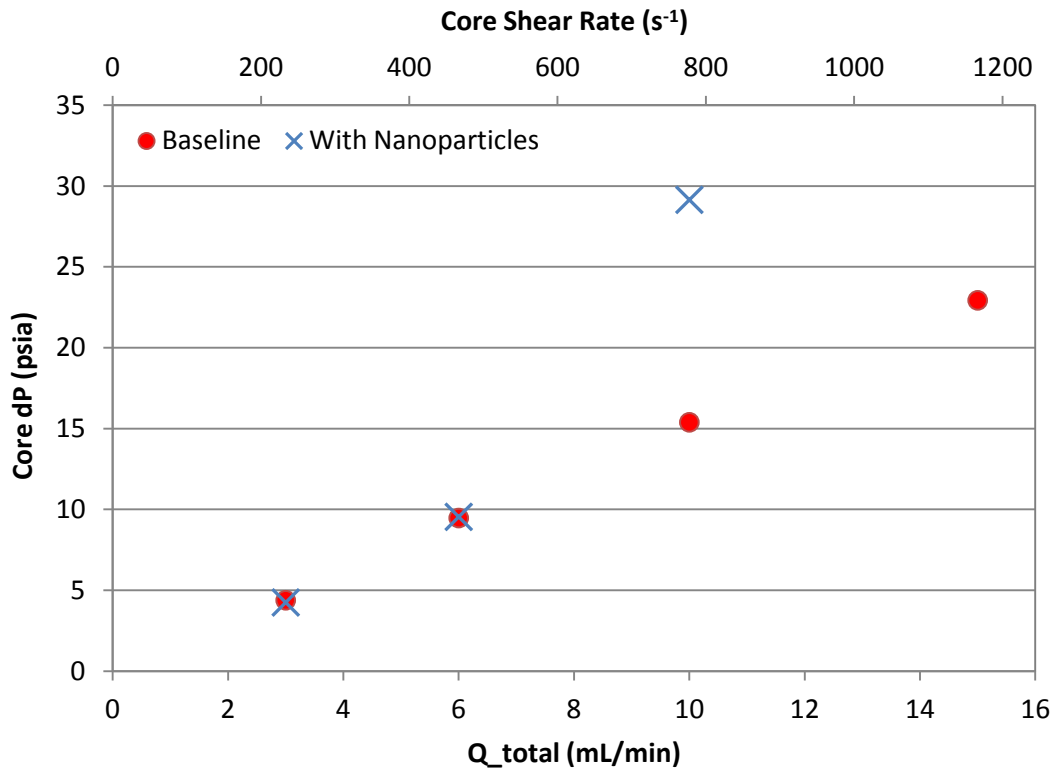

Figure C.1 - Pressure drop across the core for the baseline experiment and the foam experiment run using an 11.8" long non-fractured Boise sandstone core (coreflood B1).
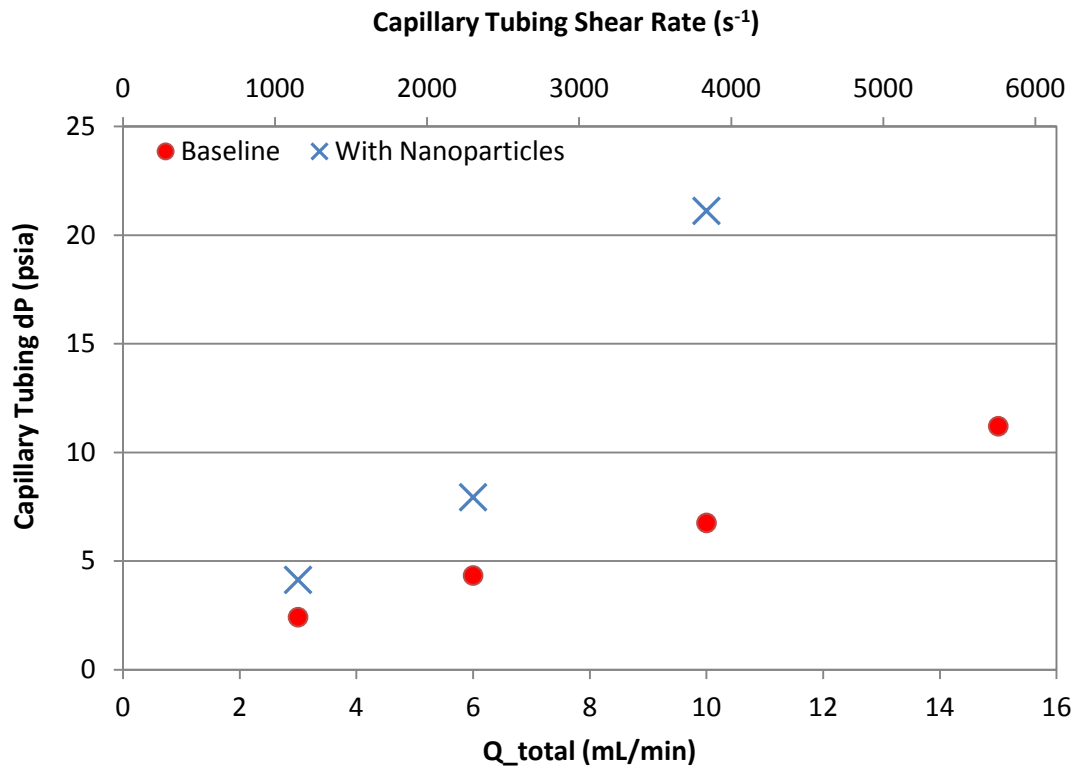
Figure C.2 - Pressure drop across the capillary tubing for the baseline experiment and the foam experiment run using an 11.8" long non-fractured Boise sandstone core (coreflood B1).

Figure C.3 shows the apparent viscosity of the fluid mixture in the presence of nanoparticles at different flow rates. The apparent viscosity is calculated using the pressure drop measurement across the capillary tubing, see 3.1.4.6.
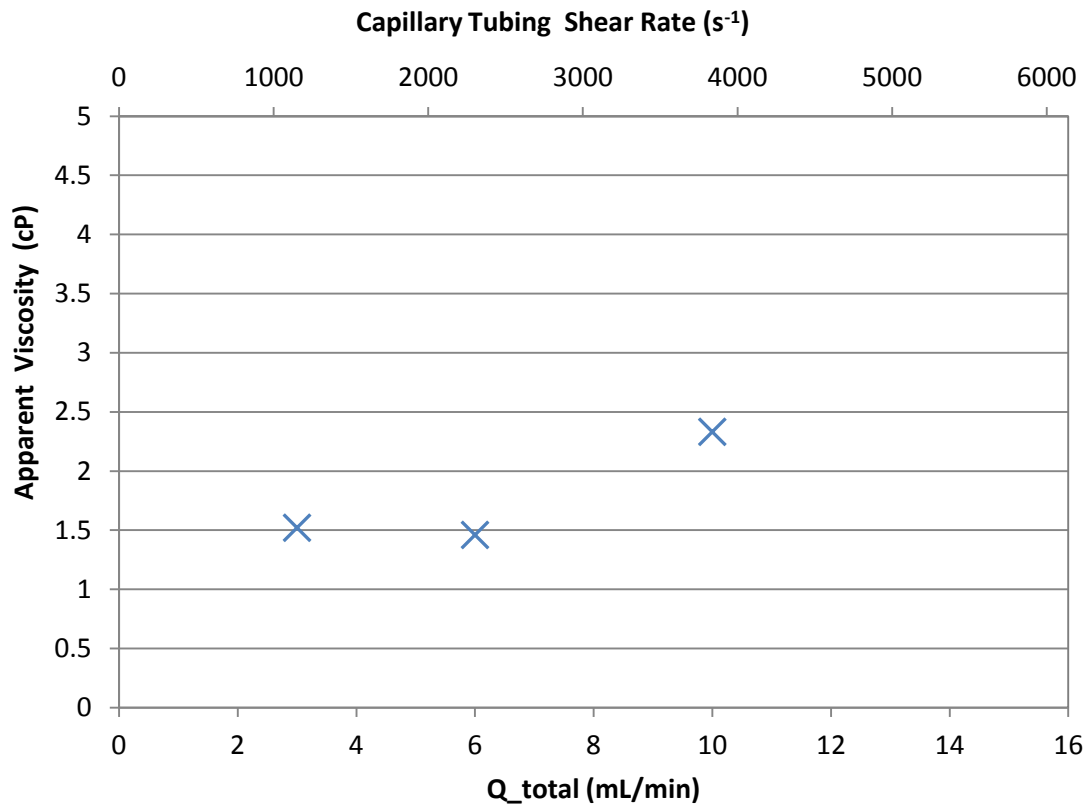
Capillary Tubing Shear Rate (s^{-1})

Figure C.3 - Apparent viscosity of the fluid mixture in the presence of nanoparticles calculated using the pressure drop measurement across the capillary tubing (coreflood B1).

Coreflood B2

        A baseline experiment and a foam experiment were run using an 5.9" long non-fractured Boise sandstone core at ambient temperature and a pressure of ~2,000 psia. The foam experiment was run using a 1 wt% dispersion of 5 nm PEG-coated silica nanoparticles in DI water. The pressure drop measurements across the core and capillary tubing for both experiments are plotted in Figures C.4 and C.5, respectively.
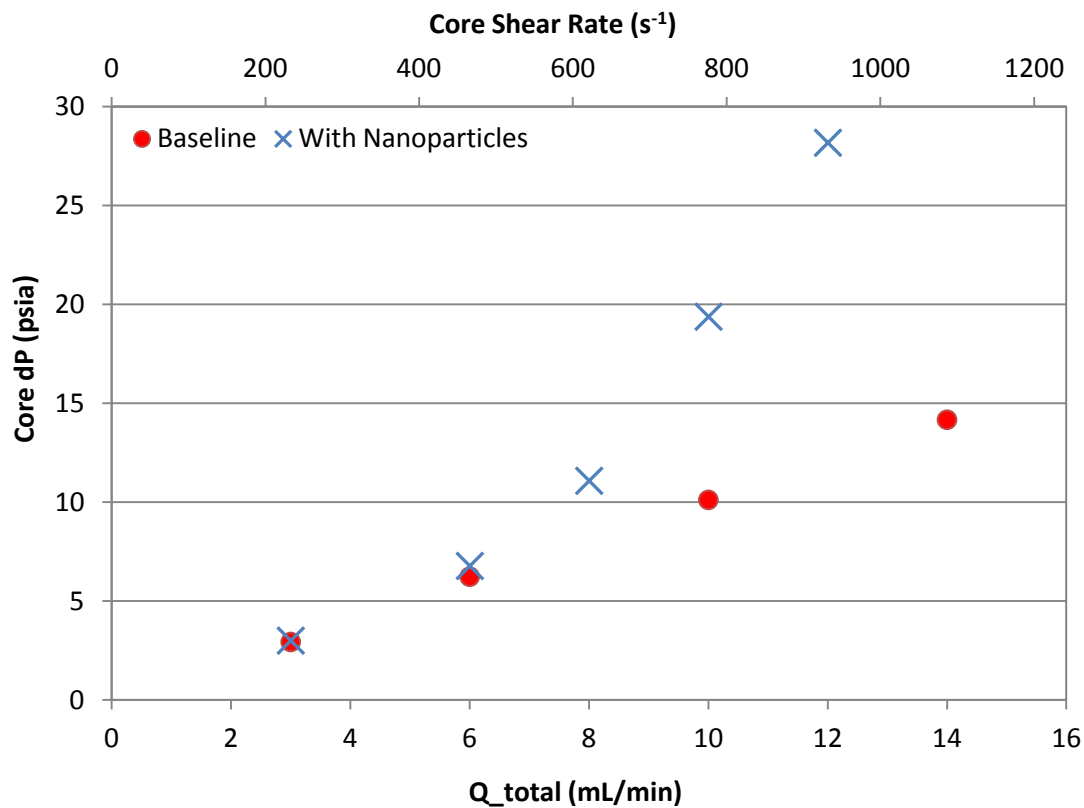

Figure C.4 - Pressure drop across the core for the baseline experiment and the foam experiment run using a 5.9" long non-fractured Boise sandstone core (coreflood B2).
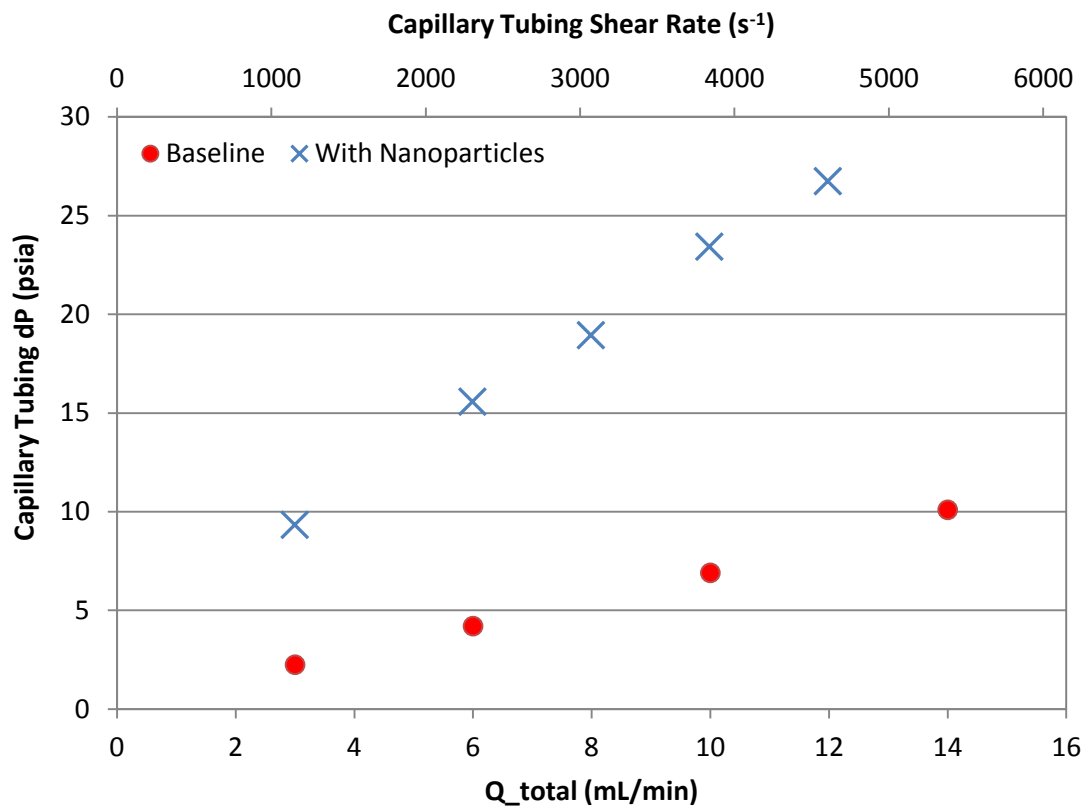
Figure C.5 - Pressure drop across the capillary tubing for the baseline experiment and the foam experiment run using a 5.9" long non-fractured Boise sandstone core (coreflood B2).

Figure C.6 shows the apparent viscosity of the fluid mixture in the presence of nanoparticles at different flow rates. The apparent viscosity is calculated using the pressure drop measurement across the capillary tubing, see 3.1.4.6.
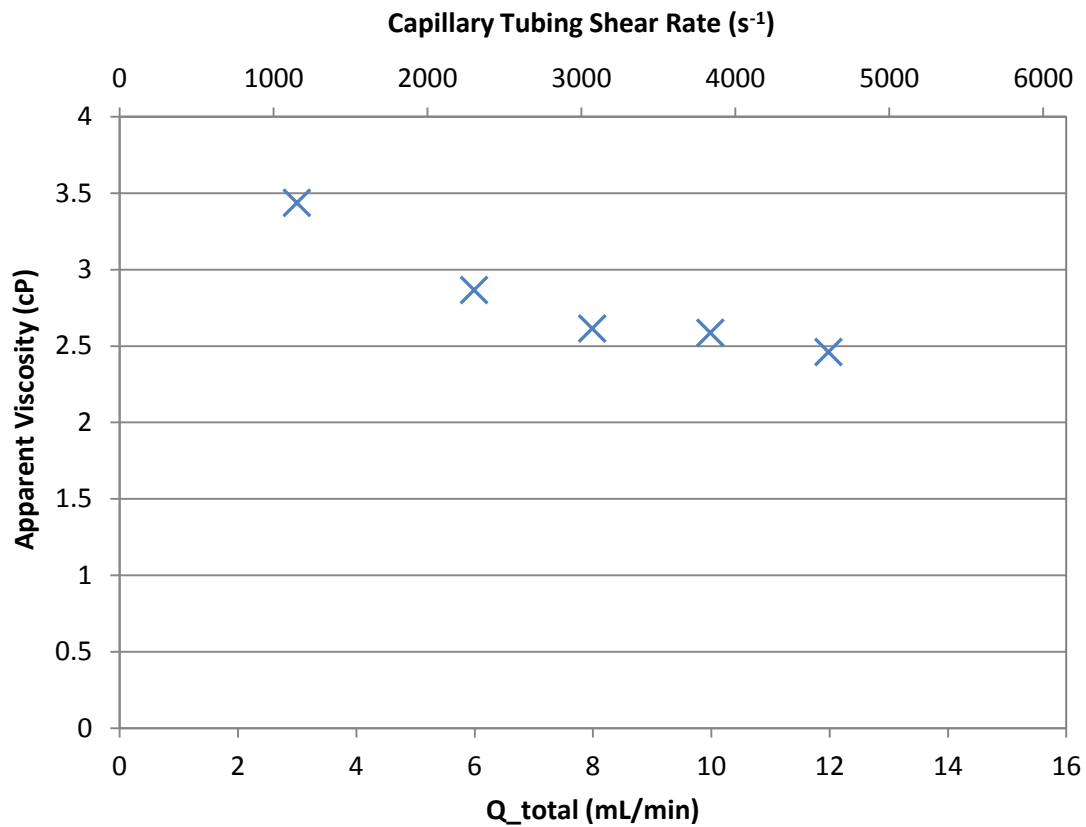

Figure C.6 - Apparent viscosity of the fluid mixture in the presence of nanoparticles calculated using the pressure drop measurement across the capillary tubing (coreflood B2).

Coreflood B3

A baseline experiment and a foam experiment were run using a 6" long non-fractured Boise sandstone core at ambient temperature and a pressure of ~2,000 psia. The foam experiment was run using a 1 wt% dispersion of 5 nm PEG-coated silica nanoparticles in DI water. The pressure drop measurements across the core and capillary tubing for both experiments are plotted in Figures C.7 and C.8, respectively.
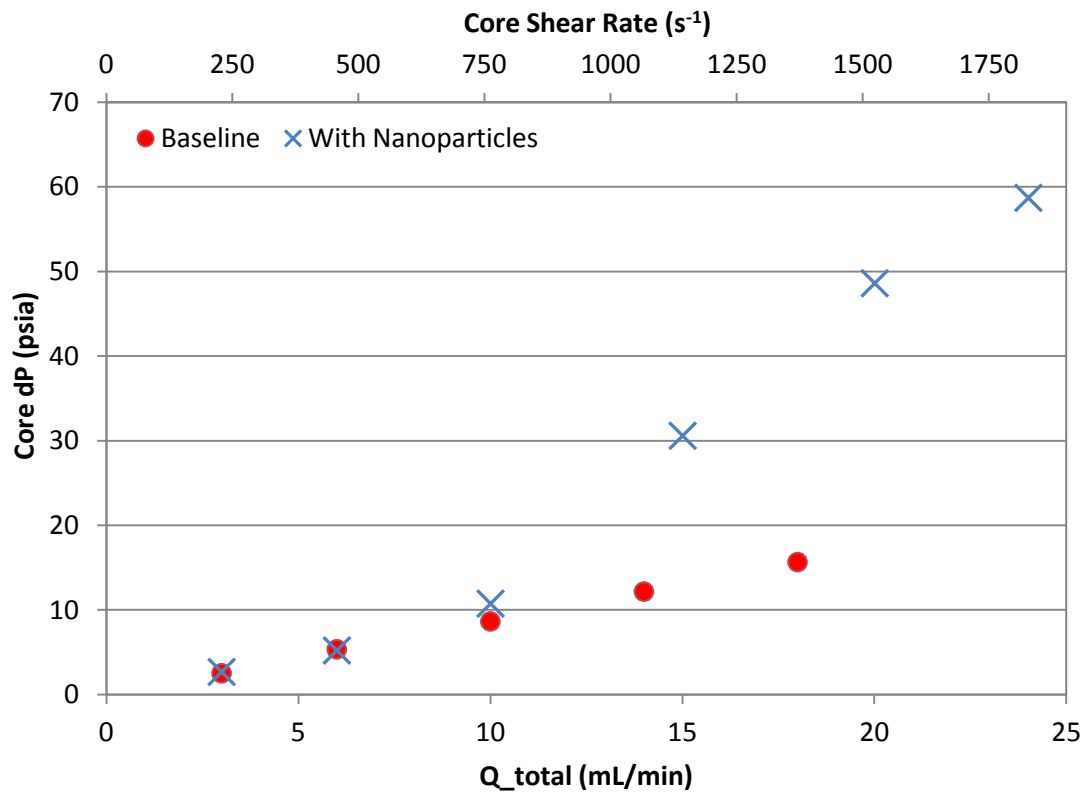

Figure C.7 - Pressure drop across the core for the baseline experiment and the foam experiment run using a 6" long non-fractured Boise sandstone core (coreflood B3).
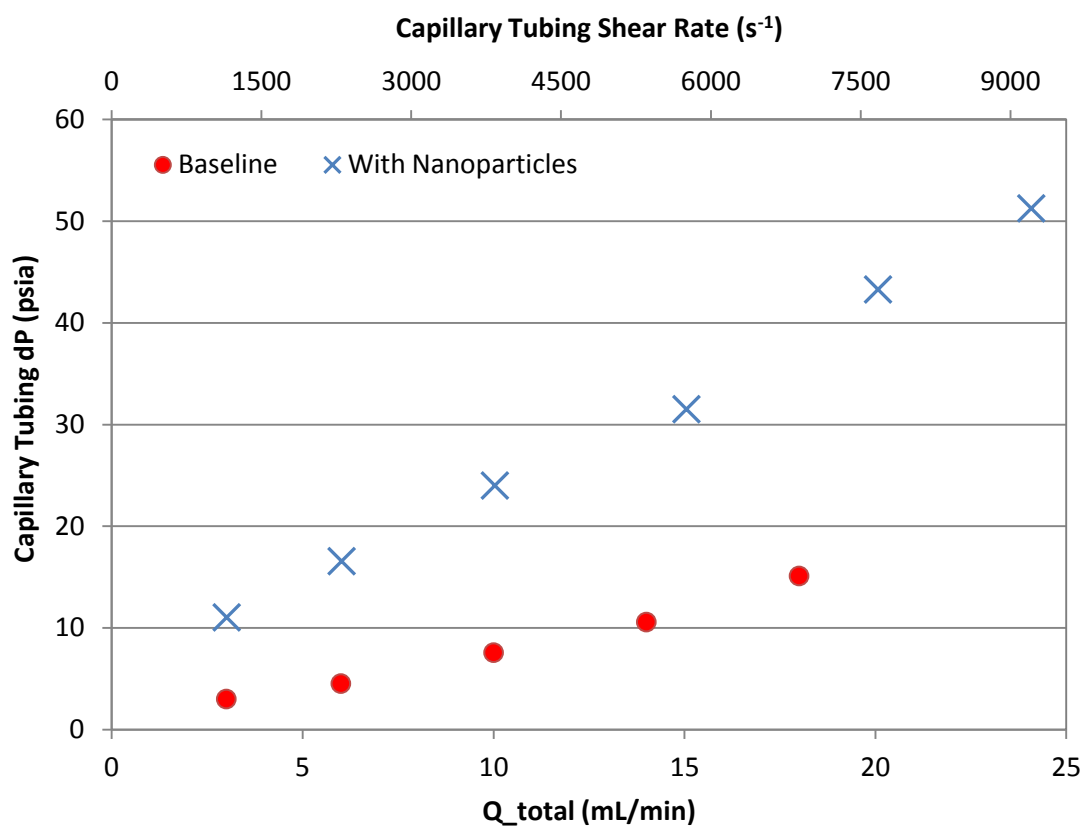
Figure C.8 - Pressure drop across the capillary tubing for the baseline experiment and the foam experiment run using a 6" long non-fractured Boise sandstone core (coreflood B3).

Figure C.9 shows the apparent viscosity of the fluid mixture in the presence of nanoparticles at different flow rates. The apparent viscosity is calculated using the pressure drop measurement across the capillary tubing, see 3.1.4.6.
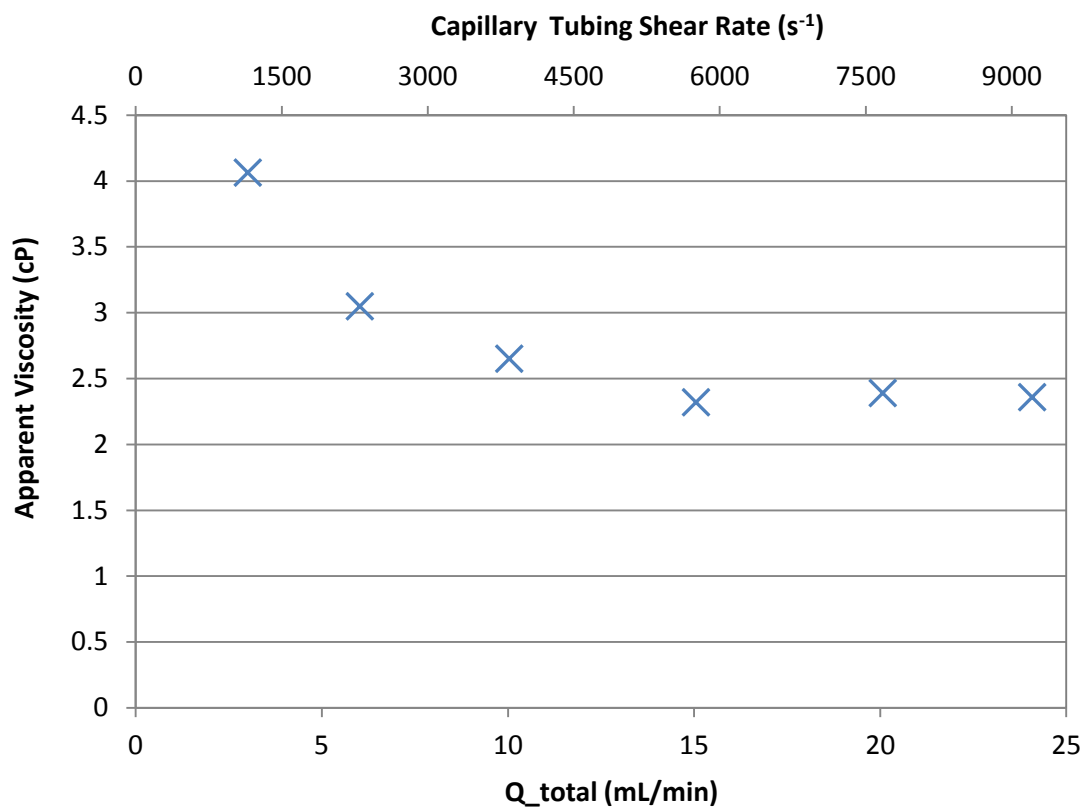

Figure C.9 - Apparent viscosity of the fluid mixture in the presence of nanoparticles calculated using the pressure drop measurement across the capillary tubing (coreflood B3).

Coreflood F1

A baseline experiment and a foam experiment were run using a 6" long fractured Boise sandstone core at ambient temperature and a pressure of ~2,000 psia. The foam experiment was run using a 1 wt% dispersion of 5 nm PEG-coated silica nanoparticles in DI water. During the foam experiment, the fracture aperture was estimated to be 105 μm, see 3.1.4.10. The pressure drop measurement across the core for the foam experiment is plotted against injection flow rate in Figure C.10. The pressure drop measurements across the capillary tubing for both the foam and baseline experiments are plotted in Figure C.11.
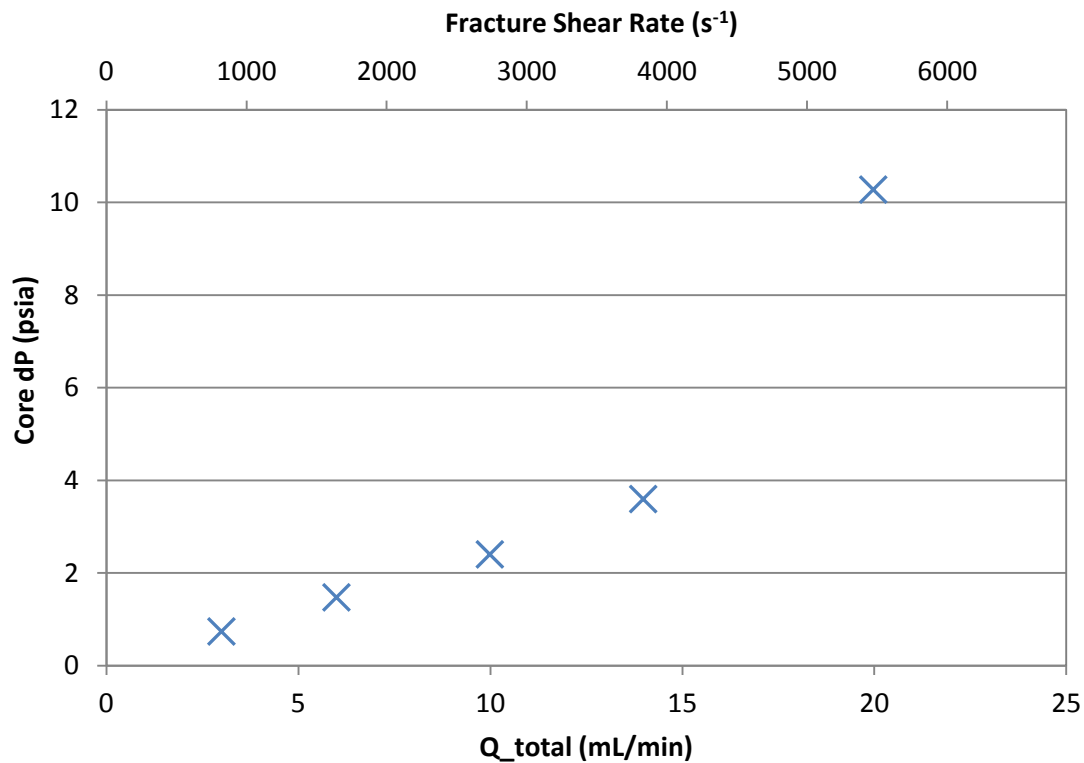

Figure C.10 - Pressure drop across the core for the foam experiment run using a 6" long fractured Boise sandstone core with a 105 μm fracture aperture (coreflood F1).

Figure C.11 - Pressure drop across the capillary tubing for the baseline experiment and the foam experiment run using a 6" long fractured Boise sandstone core with a 105 μm fracture aperture (coreflood F1).

Figure C.12 shows the apparent viscosity of the fluid mixture in the presence of nanoparticles at different flow rates. The apparent viscosity is calculated using the pressure drop measurement across the capillary tubing, see 3.1.4.6.

Figure C.12 - Apparent viscosity of the fluid mixture in the presence of nanoparticles calculated using the pressure drop measurement across the capillary tubing (coreflood F1).

Coreflood F2

A baseline experiment and a foam experiment were run using a 6" long fractured Boise sandstone core at ambient temperature and a pressure of ~2,000 psia. The foam experiment was run using a 1 wt% dispersion of 5 nm PEG-coated silica nanoparticles in DI water. During the foam experiment, the fracture aperture was estimated to be 66 μm, see 3.1.4.10. The pressure drop measurement across the core for the foam experiment is plotted against injection flow rate in Figure C.13. The pressure drop measurements across the capillary tubing for both the foam and baseline experiments are plotted in Figure C.14.

Figure C.13 - Pressure drop across the core for the foam experiment run using a 6" long fractured Boise sandstone core with a 66 μm fracture aperture (coreflood F2).
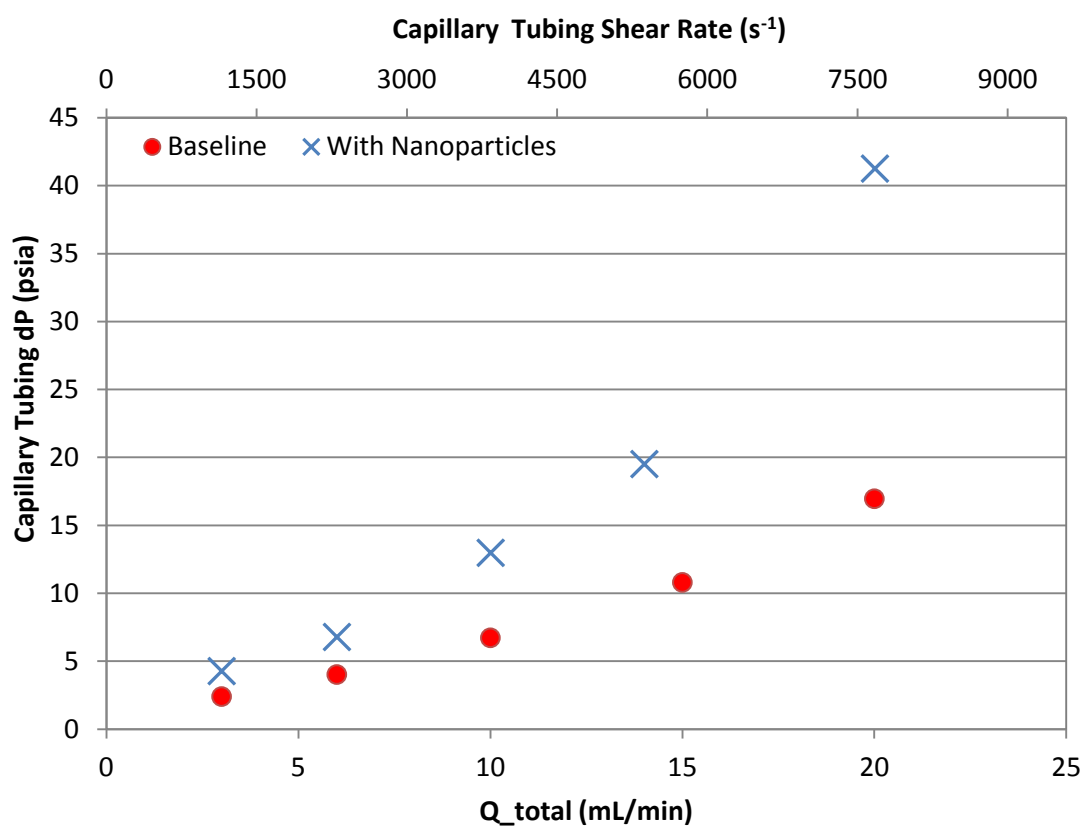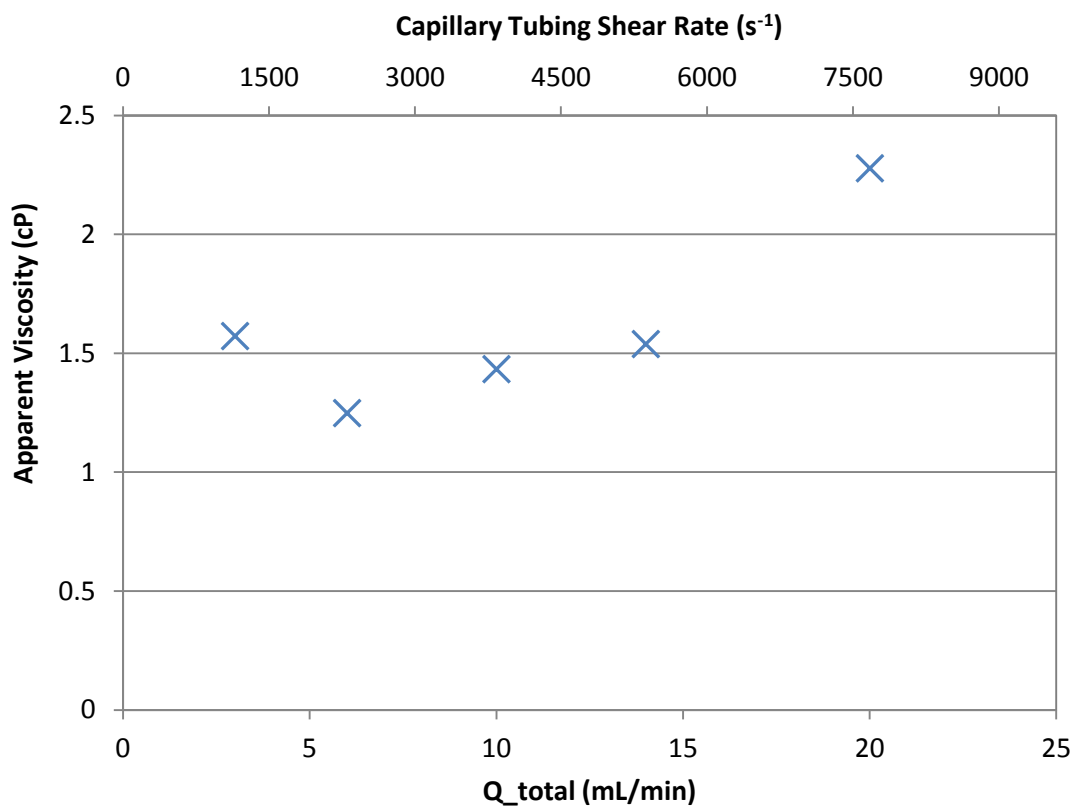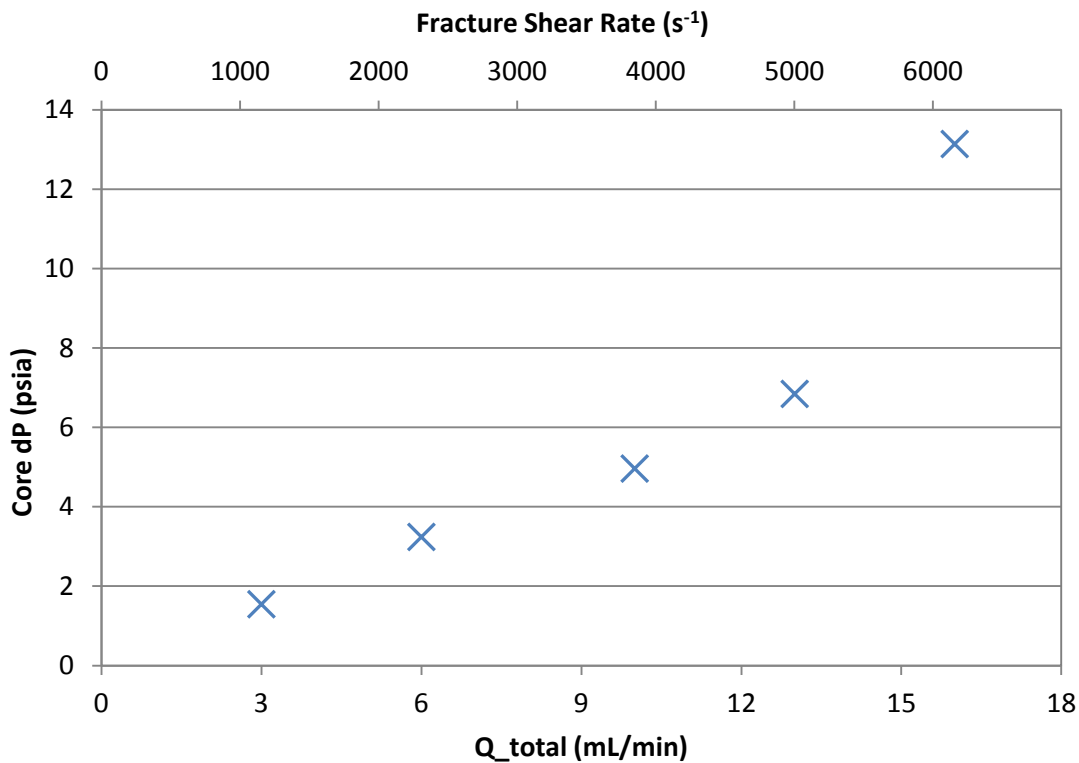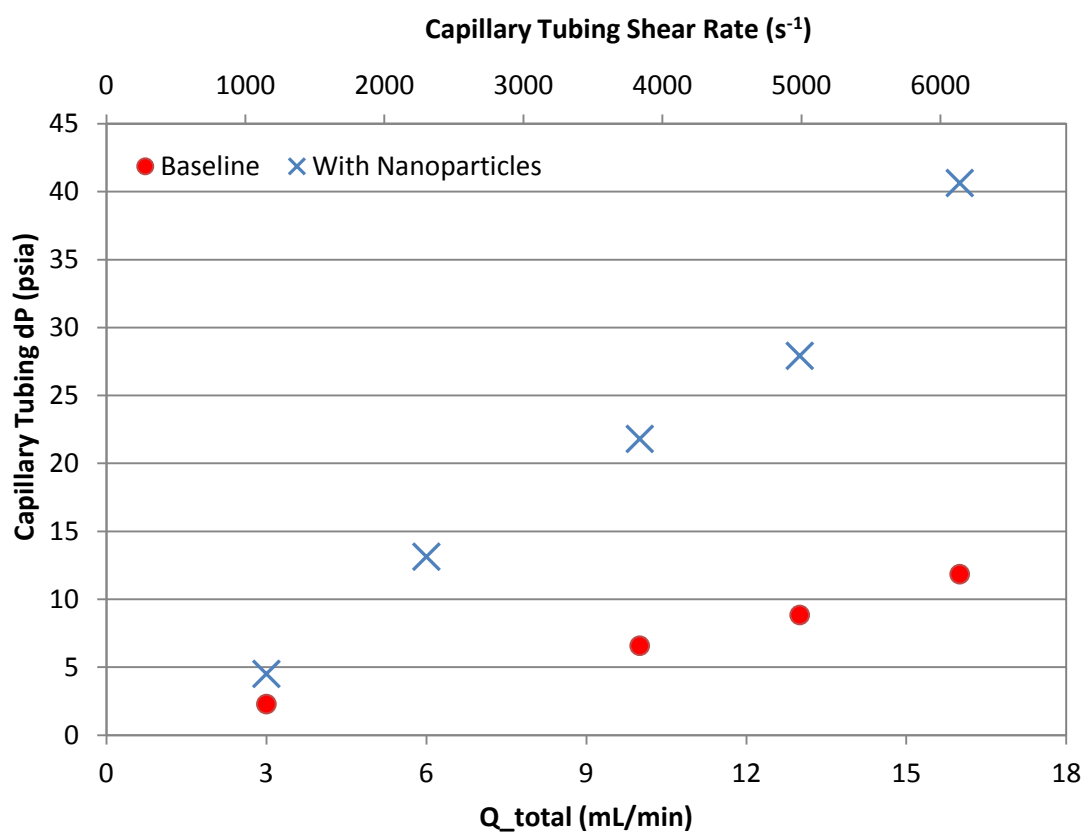
Figure C.14 - Pressure drop across the capillary tubing for the baseline experiment and the foam experiment run using a 6" long fractured Boise sandstone core with a 66 μm fracture aperture (coreflood F2).

Figure C.15 shows the apparent viscosity of the fluid mixture in the presence of nanoparticles at different flow rates. The apparent viscosity is calculated using the pressure drop measurement across the capillary tubing, see 3.1.4.6.

Figure C.15 - Apparent viscosity of the fluid mixture in the presence of nanoparticles calculated using the pressure drop measurement across the capillary tubing (coreflood F2).

Coreflood C1

A baseline experiment and a foam experiment were run using a 5.24" long fractured cement core at ambient temperature and a pressure of ~2,040 psia. The foam experiment was run using a 1 wt% dispersion of 5 nm PEG-coated silica nanoparticles in DI water. During the foam experiment, the fracture aperture was estimated to be 60.5 μm, see 3.1.4.10. The baseline experiment (CO_2 and DI water co-injection) did not have the same fracture aperture, therefore the core pressure drop data from the baseline was not used. Instead, the core pressure drop data from injecting only the nanoparticle dispersion was used in calculating the normalized viscosities shown in Figure 4.11. During the foam experiment, the nanoparticle dispersion is initially injected without CO_2 in order to estimate the fracture aperture. After obtaining pressure drop measurements at different flow rates, CO_2 injection is started. The fracture aperture should remain the same for the nanoparticle dispersion injection and for the CO_2 and nanoparticle dispersion co-injection since the pressures acting on the fracture remain the same. The pressure drop measurement across the core for both the nanoparticle dispersion injection and the foam experiment are plotted against injection flow rate in Figure C.16. Since different flow rates were used in the nanoparticle dispersion injection and the nanoparticle and CO_2 co-injection, some data points were extrapolated to calculate the normalized apparent viscosity.

Figure C.16 - Pressure drop across the core for the nanoparticle dispersion injection and the foam experiment run using a 5.24" long fractured cement core with a 60.5 μm fracture aperture (coreflood C1).

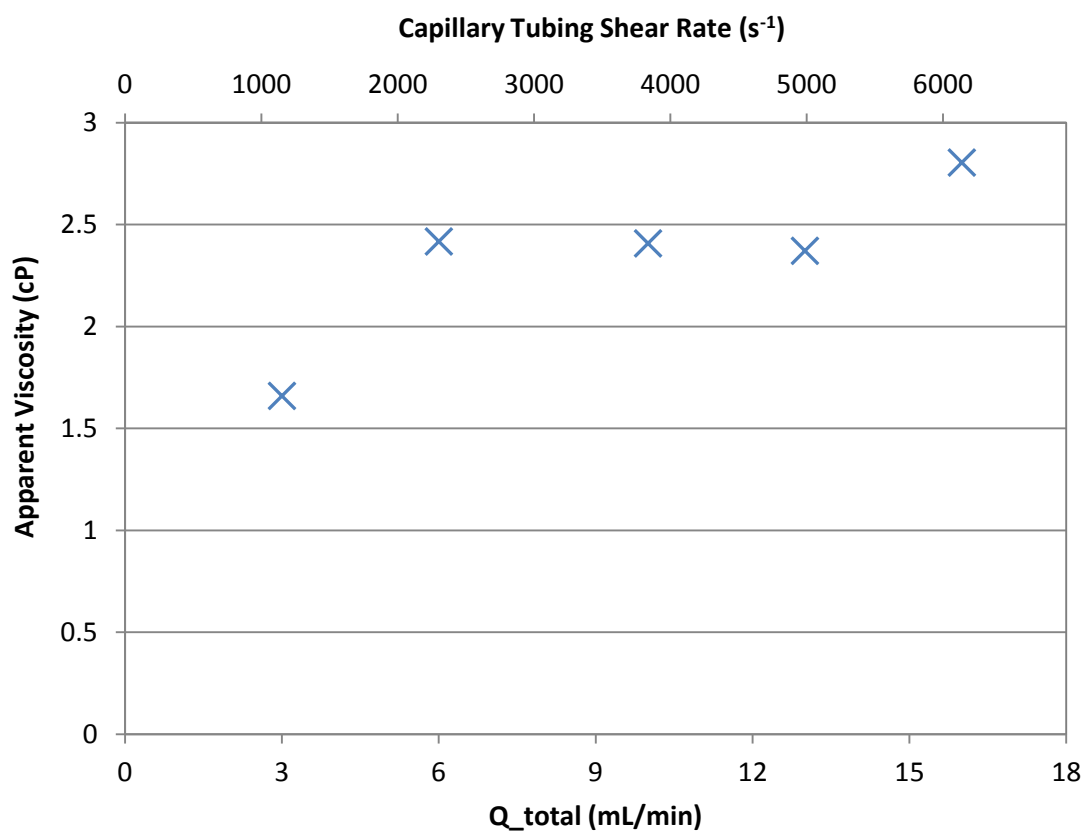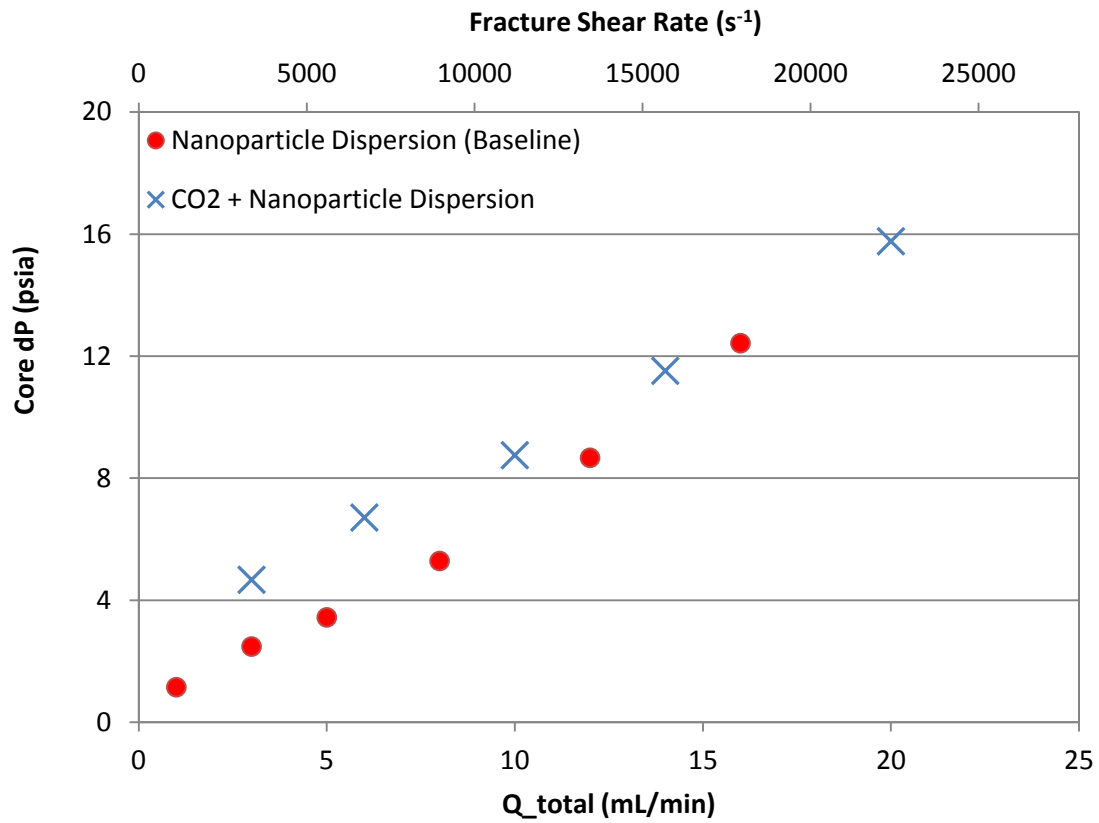The fracture aperture should not affect the pressure drop measurement across the capillary tubing of the DI water and CO_2 fluid mixture. Therefore, the capillary tubing pressure drop data from the CO_2 and DI water co-injection baseline can be used in calculating the normalized apparent viscosity of the CO_2 and nanoparticle dispersion fluid mixture. Figure C.17 shows the pressure drop measurements across the capillary tubing for both the foam and baseline experiments.
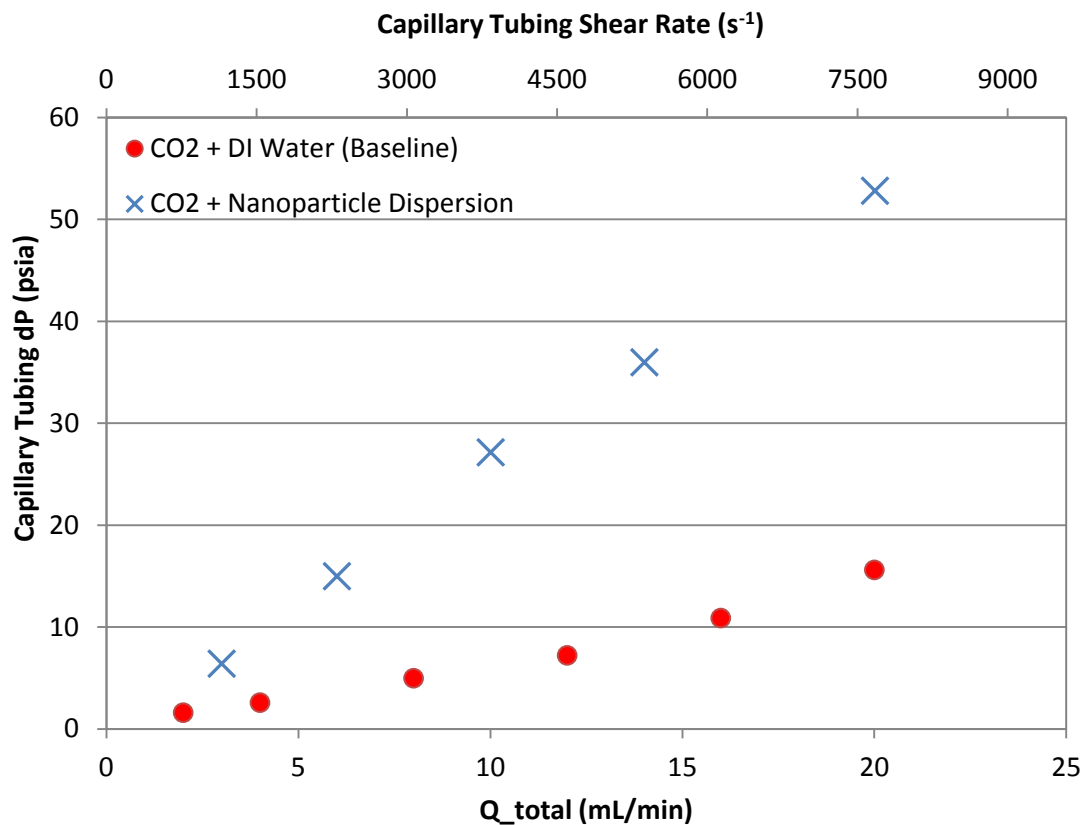
Figure C.17 - Pressure drop across the capillary tubing for the baseline experiment and the foam experiment run using a 5.24" long fractured cement core with a 66 μm fracture aperture (coreflood C1).

Figure C.18 shows the apparent viscosity of the fluid mixture in the presence of nanoparticles at different flow rates. The apparent viscosity is calculated using the pressure drop measurement across the capillary tubing, see 3.1.4.6.

Figure C.18 - Apparent viscosity of the fluid mixture in the presence of nanoparticles calculated using the pressure drop measurement across the capillary tubing (coreflood C1).

References

Abdallah, W., Zhao, W., Gmira, A., Negara, A., and Buiting, J. 2011. Sensitivity Analysis of Interfacial Tension on Saturation and Relative Permeability Model Predictions. 2011 SPE Saudi Arabia Section Annual Technical Symposium and Exhibition, 15-18 May 2011, Al-Khobar, Saudi Arabia. (SPE 149038)
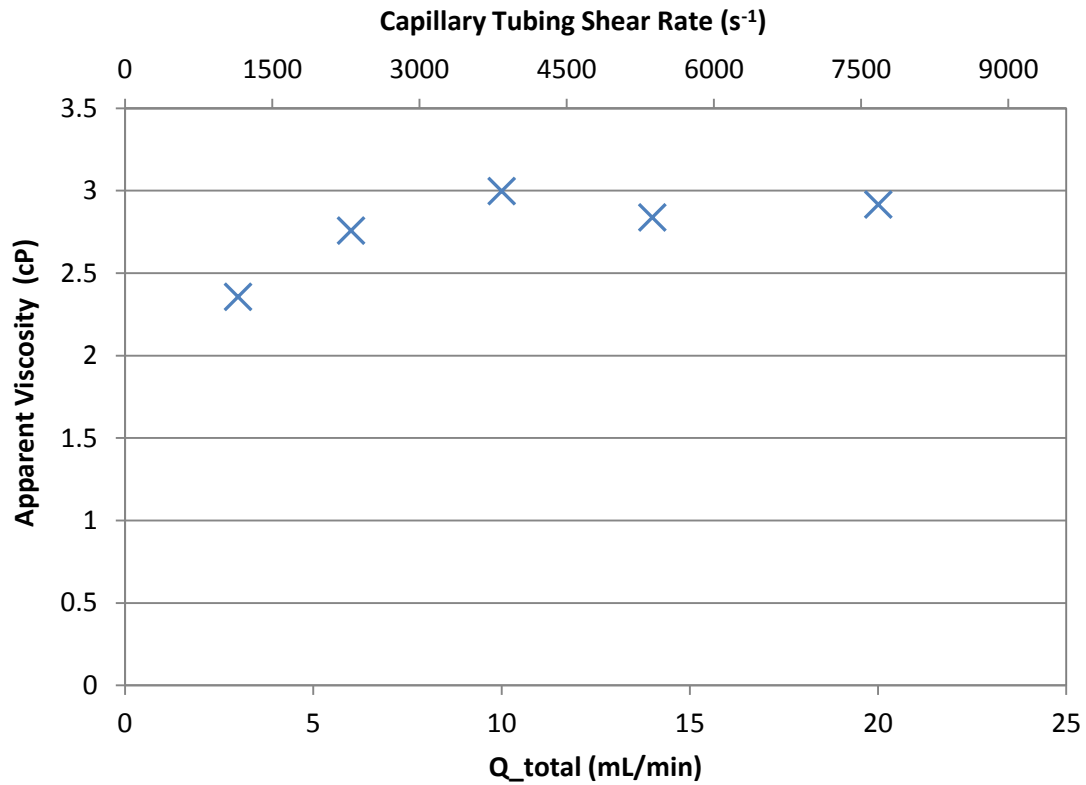
ACAA. 2009a. 2008 Coal Combustion Product (CCP) Production and Use Survey Report. Aurora, CO: American Coal Ash Association.

Bachu, S. and Bennion, B. 2009. Interfacial Tension between CO_2, Freshwater, and Brine in the Range of Pressure from (2 to 27) MPa, Temperature from (20 to 125) °C, and Water Salinity from (0 to 334 000) mg/L. Journal of Chem. Eng. Data, 2009, 54(3).

Bennion, B. and Bachu, S. 2005. Relative Permeability Characteristics for Supercritical CO_2 Displacing Water in a Variety of Potential Sequestration Zones in the Western Canada Sedimentary Basin. 2005 SPE Annual Technical Conference and Exhibition, 9-12 October 2005, Dallas, TX. (SPE 95547)

Benson, S.M. and Cole, D.R. 2008. CO_2 Sequestration in Deep Sedimentary Formations. Elements, Vol. 4, pp. 325-331, doi:10.2113/gselements.4.5.325.

Binks, B.P. 2002. Particles as Surfactants - Similarities and Differences. Current Opinion in Colloid and Interface Science, 7: 21-41.

Binks, B.P., Kirkland, M., Rodrigues, J.A. 2008. Origin of Stabilization of Aqueous Foams in Nanoparticle-Surfactant Mixtures. *Soft Matter*, **4**, 2373-2382 (2008).

Center for Applied Energy Research, University of Kentucky. Fly Ash via SEM View. (http://www.caer.uky.edu/kyasheducation/images/ccbs/gallery-ccbs/pages/Class-F-fly-ash-1-600.html)

Cho, H., Oh, D., and Chon, H. 2001. Removal of Heavy Metals from Aqueous Solution by Fly Ash. Geosystem Eng., 4(3), 77-83, September 2001.

Dickson, J.L., Binks, B.P., and Johnston, K.P. 2004. Stabilization of Carbon Dioxide-in-Water Emulsions Using Silica Particles. Langmuir, 20: 7976-7983.

Enick, R.M. and Olsen, D.K. 2011. Mobility and Conformance Control for Carbon Dioxide Enhanced Oil Recovery via Thickeners, Foams, and Gels – A Detailed Literature Review of 40 Years of Research. DOE/NETL-2012/1540, Activity 4003.200.01.

Espinosa, D., Caldelas, F., Johnston, K., Bryant, S., and Huh, C. 2010. Nanoparticle-Stabilized Supercritical CO_2 Foams for Potential Mobility Control Applications. 2010 SPE Improved Oil Recovery Symposium, 24-28 April 2010, Tulsa, OK. (SPE 129925)

Espinosa, D. 2011. Nanoparticle Stabilized Supercritical CO_2 Foams for Potential Mobility Control Applications. M.S.E. Thesis, The University of Texas at Austin, (May 2011).

Ettinger, R.A. and Radke, C.J. 1989. The Influence of Texture on Steady Foam Flow in Berea Sandstone. SPE Annual Technical Conference, 8-11 October 1989, San Antonio, TX. (SPE 19688)

Friedmann, F., Chen, W., and Gauglitz, P. 1988. Experimental and Simulation Study of High-Temperature Foam Displacement in Porous Media. SPE/DOE Fifth Symposium of Enhanced Oil Recovery, 17-20 April 1988, Tulsa, OK. (SPE/DOE 17357)

Friedmann, F., Chen, W., and Gauglitz, P. 1991. Experimental and Simulation Study of High-Temperature Foam Displacement in Porous Media. SPE Reservoir Engineering, February 1991, pp. 37 – 45.

Golomb, D., Barry, E., Ryan, D., Swett P., and Duan, H. 2006. Macroemulsions of Liquid and Supercritical CO_2-in-Water and Water-in-Liquid CO_2 Stabilized by Fine Particles. Ind. Eng. Chem. Res., 45(8), pp 2728 – 2733.

Habermann, B. 1960. The Efficiency of Miscible Displacement as Function of Mobility Ratio. Trans. AIME 219, 264.

Hirasaki, G.J., and Lawson, J.B. 1985. Mechanisms of Foam Flow in Porous Media: Apparent Viscosity in Smooth Capillaries. SPEJ, Apr. 1985, Vol. 25, No.2, 176-190. (SPE 12129)

IPCC (Intergovernmental Panel on Climate Change): Climate Change 2007: The Physical Science Basis. Cambridge University Press, Cambridge.

Kutchko, B.G. and Kim, A.G. 2006. Fly Ash Characterization by SEM-EDS. Fuel, Vol. 85 (17-18), pp. 2537-2544.

Kvamme, B., Kuznetsova, T., Hebach, A., Oberhof, A., and Lunde, E. 2007. Measurements and Modeling of Interfacial Tension for Water + Carbon Dioxide Systems at Elevated Pressures. Comput. Mater. Sci. 38, 506-513.

Lake, Larry. 1989. *Enhanced Oil Recovery*. Englewood Cliffs, NJ: Prentice Hall.

Li, R.F., Yan, W., Liu, S., Hirasaki, G.J., and Miller, C.A. 2010. Foam Mobility Control for Surfactant Enhanced Oil Recovery. SPE J.15, 2010, (4): 928-942. (SPE-113910)

Mo, D., Yu, J., Liu, N., and Lee, R. 2012. Study of the Effect of Different Factors on Nanoparticle-Stabilized CO_2 Foam for Mobility Control. 2012 SPE Annual Technical Conference and Exhibition, 8-10 October 2012, San Antonio, TX. (SPE 159282)

NIST (National Institute of Standards and Technology). Thermophysical Properties of Fluid Systems. http://webbook.nist.gov/chemistry/fluid/ (Accessed 29 October 2012).

Okwen, R.T., Stewart, M.T., and Cunningham, J.A. 2010. Analytical Solution for Estimating Storage Efficiency of Geologic Sequestration of CO_2. International Journal of Greenhouse Gas Control, 4, 102–107. doi:10.1016/j.ijggc.2009.11.002.

Parrish, D.R. 1963. Fluid Flow in Rough Fractures. Proceedings SPE-AIME, Proc. Res. Symp., Norman, OK, 1963, April 29-30, SPE 563, 9p.

Pickering, S.U. 1907. Emulsions. Journal of the Chemical Society, Transactions. Issue 91, pages 2001-2021.

Radke, C.J. and Ransohoff, T.C. 1986. Mechanisms of Foam Generation in Glass Bead Packs. (SPE 15441)

Renkema, W.J. and Rossen, W.R. 2007. Success of SAG Foam Processes in Heterogeneous Reservoirs. SPE Annual Technical Conference and Exhibition, 11-14 November 2007, Anaheim, CA. (SPE 110408)

Roberts, M.R. 2011. Shear-Induced Emulsions Stabilized with Surface-Modified Silica Nanoparticles. M.S.E. Thesis, The University of Texas at Austin, (May 2011).

Rossen, W.R. 1996. Foams in Enhanced Oil Recovery. Foams: Theory, Measurements, and Applications. R. K. Prudhomme and S. A. Khan. New York, Marcel Dekker.

Son, Y. 2007. Determination of Shear Viscosity and Shear Rate from Pressure Drop and Flow Rate Relationship in a Rectangular Channel. Polymer, vol. 48, pp. 632-637.

Tambe, D.E, and Sharma, M.M. 1994. The Effect of Colloidal Particles on Fluid-Fluid Interfacial Properties and Emulsion Stability. Adv. Colloid Interface Sci. 52, 1.

Worthen, A.J., Bagaria, H.G., Chen, Y., Bryant, S.L., Huh, C., and Johnston, K.P. 2013. Nanoparticle-Stabilized Carbon Dioxide-in-Water Foams with Fine Texture, Journal of Colloid and Interface Science, Volume 391, 1 February 2013, Pages 142-151, ISSN 0021-9797.

Yan, W., Miller, C.A., Hirasaki, G.J. 2006. Foam Sweep in Fractures for Enhanced Oil Recovery. Colloids and Surfaces A: Physicochemical and Engineering Aspects, Volumes 282–283, 20 July 2006, Pages 348-359, ISSN 0927-7757.

Zhang, T., Roberts, M.R., Bryant, S.L., and Huh, C. 2009. Foams and Emulsions Stabilized with Nanoparticles for Potential Conformance Control Applications. SPE International Symposium on Oilfield Chemistry, Woodlands, TX. (SPE 121744)

Zhang, T., Davidson, A., Bryant, S.L, and Huh, C. 2010. Nanoparticle-Stabilized Emulsions for Applications in Enhanced Oil Recovery. SPE Improved Oil Recovery Symposium, Tulsa, OK. (SPE 129885)

Vita

Tarek Rafic Hariz grew up in Lagos, Nigeria, before moving to Beirut, Lebanon for high school. After graduating from high school, he attended the American University of Beirut for a year before transferring to Rice University in 2007. He graduated with his Bachelor of Science degree in Chemical Engineering in 2010. After graduation, he worked at Rice University as a research assistant for 5 months. In January 2011, he started his pursuit of a Master of Science in Petroleum Engineering at the University of Texas at Austin, and graduated in December 2012.

Permanent email address: tarek.hariz@gmail.com

This thesis was typed by the author.